

Development of a new microscopy method:  
Optical Photon Reassignment  
Microscopy

kumulative  
DISSERTATION

zur Erlangung des akademischen Grades  
*doctor rerum naturalium (Dr. rer. nat)*



---

seit 1558

vorgelegt dem Rat der  
Chemisch-Geowissenschaftlichen Fakultät der  
Friedrich-Schiller-Universität Jena

von Dipl. Phys. Stephan Roth  
geboren am 29. Februar 1984 in Weimar

1. Gutachter: Prof. Dr. Rainer Heintzmann, IPC, FSU Jena
2. Gutachter: apl. Prof. Dr. Michael Schmitt, IPC, FSU Jena

Tag der öffentlichen Verteidigung: 29.03.2017

# Contents

List of Figures . . . . .	iii
List of Abbreviations . . . . .	iv
<b>1 Zusammenfassung</b>	<b>1</b>
<b>2 Summary</b>	<b>6</b>
<b>3 Introduction</b>	<b>9</b>
3.1 Fluorescent microscopy . . . . .	9
3.2 Superresolution microscopy . . . . .	11
3.3 The confocal microscope . . . . .	13
3.3.1 The scanning system in confocal microscopy . . . . .	15
<b>4 The reassignment principle</b>	<b>17</b>
4.1 The general concept . . . . .	17
4.2 Development of an idea . . . . .	19
4.3 Computational methods . . . . .	20
4.4 Optical methods . . . . .	21
<b>5 Optical Photon Reassignment Microscopy</b>	<b>24</b>
5.1 All-optical realization of the reassignment principle . . . . .	24
5.1.1 The scanning system in OPRA . . . . .	28
5.2 Superconcentration of light . . . . .	30
5.3 OPRA in three dimensions . . . . .	34
5.3.1 The influence of a detection pinhole in OPRA . . . . .	35
5.3.2 Resolution enhancement by structured illumination . . . . .	37
5.4 Conclusion and outlook . . . . .	41
<b>6 Publications</b>	<b>44</b>
6.1 Optical Photon Reassignment Microscopy (OPRA) [SR1] . . . . .	44
6.2 Superconcentration of light: Circumventing the classical limit to achievable irradiance [SR2] . . . . .	51
6.3 Optical Photon Reassignment with increased axial resolution by structured illumination [SR3] . . . . .	56
6.4 Interpretation of the optical transfer function: Significance for image scanning microscopy [SR4] . . . . .	66
<b>7 Appendix</b>	<b>74</b>
7.1 Peer reviewed publications . . . . .	74
7.2 Oral presentations . . . . .	75
7.3 Poster presentations . . . . .	76
7.4 Curriculum vitae . . . . .	77
7.5 Acknowledgement . . . . .	78
<b>References</b>	<b>81</b>

## List of Figures

1.1	Wechselbeziehungen in der Mikroskopie . . . . .	5
2.2	Trade-offs in fluorescent microscopy . . . . .	8
3.3	Jablonski diagram for fluorescent emission . . . . .	10
3.4	Principle of confocal microscopy . . . . .	14
4.5	Principle of photon reassignment . . . . .	18
4.6	Optical realization principle of photon reassignment . . . . .	22
5.7	Minimal extent of $\text{PSF}_{\text{OPRA}}$ for different Stokes shift . . . . .	26
5.8	Comparison of the resolution of a confocal microscope and OPRA . . . . .	27
5.9	Optical setup of OPRA with a 15kHz resonant beam scanner . . . . .	30
5.10	Optical setup of OPRA with a 2D beam-scanner for precise beam control and high numerical aperture measurements . . . . .	31
5.11	Comparison of the resolution of a confocal microscope and OPRA with respect to the absolute intensity . . . . .	33
5.12	Signal intensity in OPRA as function of the pinhole diameter . . . . .	35
5.13	Comparison of the PSF of OPRA and confocal microscopy . . . . .	36
5.14	Principle of OPRA with structured illumination . . . . .	38
5.15	3D-PSF of OPRA with structured illumination obtained by different reconstruction methods . . . . .	39
5.16	Mean intensity as function of the distance along the optical axis for OPRA with structured illumination . . . . .	40

## List of Abbreviations

AU	Airy unit: $1\text{AU}=1.22\cdot\lambda/\text{NA}$
BFP	back focal plane
CLSM	confocal laser scanning microscope
CSD-ISM	confocal spinning disk image scanning microscopy
FED	fluorescence emission difference
FOV	field of view
iSIM	instant structured illumination microscopy
ISM	image scanning microscopy
LSM	laser scanning microscope
MSIM	multifocal structured illumination microscopy
NA	numerical aperture
OPRA	optical photon reassignment
OTF	optical transfer function
PAINT	point accumulation for imaging in nanoscale topography
PALM	photoactivated localisation microscopy
PSF	point spread function
RSC	re-scan confocal
SD-OPR	spinning disk optical photon reassignment
SIM	structured illumination microscopy
HR-SIM	high-resolution structured illumination microscopy
STED	stimulated emission depletion
STORM	stochastic optical reconstruction microscopy

# 1 Zusammenfassung

Etwas Unsichtbares sichtbar werden lassen, stellt die Versinnbildlichung der Erfüllung des Forscherdrangs dar und übt daher schon immer eine Faszination auf die Menschheit aus. Diesen Menschheitstraum zu erfüllen ist Aufgabe der Mikroskopie. Schon eine der ersten Mikroskope von A. Leeuwenhoek wurden benutzt um biologische Proben und Zellbestandteile zu studieren. In diesem Sinn ist die Mikroskopie schon immer mit der biomedizinischen Bildgebung und dem Bedürfnis, biologische Prozesse zu verstehen und zu beobachten, verknüpft. Die Weiterentwicklung der mikroskopischen Geräte machte eine Steigerung der erzielten Auflösung möglich. Doch durch die theoretische Beschreibung der Auflösungsgrenze für Lichtmikroskopie durch E. Abbe im Jahre 1873 [1] schien der weiteren Verbesserung der Auflösung eine Grenze gesetzt zu sein. Auch wenn damals nur von Durchlicht-Mikroskopen ausgegangen wurde, besitzt diese Formel für beugungsbegrenzte Mikroskopiemethoden im Fernfeld auch heute noch ihre Gültigkeit. Raster-Mikroskopiemethoden im Nahfeld, bei denen verschiedene Wechselwirkungen zwischen der Probe und einer sehr nah darüber positionierten Spitze beobachtet werden, sind hingegen anderen Gesetzmäßigkeiten unterworfen. Abbe's Formel beschreibt, dass die kleinste auflösbare Periode eines Gitters,  $d_{\min}$ , nur von der numerischen Apertur  $NA = n \sin \alpha$ , mit dem Brechungsindex  $n$  des umgebenden Mediums und dem Sinus des Öffnungswinkels des benutzten Objektivs,  $\sin \alpha$ , sowie der Wellenlänge des verwendeten Lichts  $\lambda$  abhängig ist:

$$d_{\min} = \frac{\lambda}{2n \sin \alpha}. \quad (1.1)$$

Die Gleichung (1.1) beschreibt damit drei Parameter, anhand welcher die Auflösung im Rahmen der Abbe'schen Auflösungsgrenze verbessert werden kann und welche auch für mikroskopische Konzepte verwendet wurden. Beschränkt man sich nicht nur auf Photonen als Informationsträger, können durch die wesentlich kürzere De-Broglie-Wellenlänge von Teilchen (für Elektronen mit der kinetischen Energie von 200 keV beträgt die Wellenlänge etwa 2.5pm) kleinste Strukturen aufgelöst werden - dies führte zur Entwicklung der Elektronenmikroskopie. Durch die aufwendige Präparation der Proben und eine Beobachtung im Vakuum ist eine Anwendung für die Erforschung biologischer Prozesse jedoch fast nicht möglich. Für die Bildgebung in biologischen Proben sind Photonen von daher besser geeignet. Eine weitere Möglichkeit, stellt das Vergrößern der numerischen Apertur dar. Durch die Verwendung von hoch-brechenden Einbettungsmedien und entsprechenden, dem refraktiven Index des Mediums angepassten, Ölen kann eine verbesserte Bildqualität erreicht werden. Für

die Bildgebung von lebenden Zellen sollten die Objektive allerdings auf den refraktiven Index der Zellen angepasst werden. Aber auch der Öffnungswinkel konnte durch immer komplexere optische Konstruktionen der Objektive stetig verbessert werden. Bei dem Konzept der 4-Pi-Mikroskopie werden zum Beispiel zwei, sich gegenüberliegende Objektive, verwendet und damit der zur Verfügung stehende Öffnungswinkel vergrößert. Dies führt hauptsächlich zu einer verbesserten axialen Auflösung [2]. Die aufwendige Justierung eines solchen Mikroskopes und die speziellen Anforderungen an die Probenpräparation erzeugen allerdings große Probleme bei der Verwendung dieser Methode in der Praxis, was zu einer Verdrängung dieses Konzepts führte. Die Diskussion macht deutlich, dass in der Mikroskopie nicht nur die maximal mögliche Auflösung wichtig ist, sondern vor allem die Eigenschaften hinsichtlich einer einfachen, schnellen und universell einsetzbaren Methode eine herausragende Bedeutung besitzen.

Neben den beschriebenen Methoden wurden diverse "superauflösende" Techniken entwickelt. Dabei beschreibt der Begriff der "Superauflösung" ein Auflösungsvermögen, welches unter dem des in Gleichung (1.1) beschriebenen Abbe'schen Auflösungslimit liegt. Das Forschungsfeld der superaflösenden Fluoreszenz-Mikroskopie gilt als zukunftsweisende optische Schlüsseltechnologie um die Funktions- und Wirkungsprinzipien komplexer biologischer Prozesse zu analysieren und zu verstehen. Diese Bedeutung wurde auch durch das Nobel-Preis-Komitee im Jahre 2014 gewürdigt [3]. So wurde der Nobel Preis für Chemie an drei Forscher, welche sich mit superaflösenden Techniken der Fluoreszenz-Mikroskopie beschäftigten, verliehen. Die Unterschreitung des Abbe-Limits ist wesentlich, da viele Zellbestandteile im Größenbereich einiger weniger hundert Nanometer liegen und somit die Beobachtung von Funktion und Wechselwirkungsmechanismen nur mit hoch aufgelösten Bildern möglich ist. Durch Markierungstechniken ist es möglich, fluoreszente Farbstoffe an spezifische Moleküle der Zellbestandteile zu binden, um so ihre Funktion während verschiedener biochemischer Prozesse orts- und zeitaufgelöst analysieren zu können. Die superaflösenden Fluoreszenz-Mikroskopie-Verfahren zur Beobachtung aktiver, lebender Zellen und den darin stattfindenden Prozessen besitzen ein enormes Potential um komplexe, biochemische Fragestellungen zu beantworten.

Im Wesentlichen können drei superaflösende Techniken unterschieden werden. Die mit dem Nobel-Preis gewürdigte Laser-Scanning-Methode der "stimulierten Emissions-Auslöschung" (stimulated emission depletion microscopy, STED) beruht dabei auf dem Prinzip der Überlagerung zweier verschieden geformter Laserfoki mit

unterschiedlicher Wellenlänge (Anregungs- und Auslöschungslicht). Überlagern sich Anregungs- und Auslöschungslicht, wird die spontane fluoreszente Emission durch die stimulierte Emission (Auslöschungslicht) verhindert, so dass der Detektionsbereich auf die Region mit nicht vorhandenem Auslöschungslicht verkleinert werden kann [4–8]. Ebenfalls mit dem Nobel-Preis geehrt wurden die Methoden, welche auf der Detektion einzelner Fluorophore beruhen [9–11]. Dabei wird mittels verschiedener Verfahren ein gleichzeitiges Aufleuchten eng benachbarter Fluorophore verhindert, und so eine präzise Bestimmung der Position einzelner Farbstoffe ermöglicht. Da es viele spezifische Verfahren zur zeitlichen Trennung der Fluoreszenzemission gibt, werden diese Methoden (STORM, dSTORM, PALM, PAINT etc.) - in Anlehnung an den aus der Kunst bekannten Pointillismus - als pointillistische Methoden bezeichnet. Die dritte weit verbreitete supraauflösende Mikroskopiemethode ist die Methode der strukturierten Beleuchtung (structured illumination microscopy, SIM). Dabei ist es möglich, Bildinformation der Probe durch Beleuchtung mit einem periodischen Muster zu modulieren und so zu detektieren. Werden alle Probenbereiche durch verschiedene Modulationsrichtungen beleuchtet, ist es möglich diese Bildinformation durch nachträgliche Demodulation zurück zugewinnen [12–16].

Die hier vorgelegte Arbeit beschäftigt sich mit einem neu entwickelten supraauflösenden Verfahren der Fluoreszenz-Mikroskopie. Das Prinzip der optischen Photonen-Zuweisung (Optical Photon Reassignment, OPRA) macht es möglich auf der Basis von Laser-Scanning-Mikroskopen (LSM) in Kombination mit einem orts aufgelösten Detektor supraauflösende Bilder zu erhalten [SR1]. Die OPRA-Methode basiert auf dem Prinzip der computergestützten Pixelzuweisung, welches erstmals 1988 von C. Sheppard beschrieben wurde [17]. Viel Aufmerksamkeit erlangte dieses Mikroskopie-Konzept 2010 unter dem Namen “Image Scanning Microscopy (ISM)“, als mit Hilfe moderner Kameras hoch auflösende Bilder fluoreszierender Polymerkugeln aufgenommen wurden. In OPRA wird dieses computerbasierte Reassignment-Verfahren optisch realisiert, so dass es möglich ist, vollständig auf die Verwendung aufwendiger Rechenverfahren zu verzichten. Anhand der Messung von fluoreszenten Proben konnte gezeigt werden, dass es mit diesem neu entwickelten Konzept möglich ist, in nur einer einzigen Kamerabelichtung Bilder mit einer, im Vergleich zum Abbe-Limit, deutlich verbesserten Auflösung aufzunehmen. Zudem konnte gezeigt werden, dass dabei kein Fluoreszenzsignal verloren geht und somit das Licht besser auf der Kamera konzentriert wird, als es das Gesetz der Étendue-Erhaltung vorherzusagen scheint. Diese Eigenschaft wurde in Anlehnung an der etablierten



Begriff der ‘‘Superauflösung‘‘ als ‘‘Superkonzentration‘‘ bezeichnet [SR2]. In [SR3] wurde das Verfahren auf die dritte Dimension erweitert. Dabei wurden verschiedene Ansätze zur Verbesserung der axialen Auflösung mit Hilfe einer Detektionsapertur und strukturierter Beleuchtung unter Berücksichtigung der ‘‘Superkonzentration‘‘ diskutiert und experimentell evaluiert. Zudem konnte dieses Konzept in [SR4] verwendet werden um ein allgemeines Konzept zur Beurteilung von Mikroskopietechniken zu entwickeln. Dieses Konzept der normierten optischen Transferfunktionen (OTF) wurde am Beispiel der rechnergestützten Pixelzuweisung eingeführt. Diese Ergebnisse unterstreichen das Potenzial der Methode für die biomedizinische Bildgebung, da sie in vorher nicht bekannter Weise wichtige Eigenschaften hochauflösender Mikroskopie wie Sensitivität (was zu einer Verringerung der erforderlichen Beleuchtungsintensität führt) und Auflösung miteinander verbindet. Dabei schaffen es die Methoden, welche auf dem Prinzip der optischen Photonen-Zuweisung beruhen, zweifache laterale Auflösungserhöhung (in Bezug auf die Grenzfrequenz der Weitfeld-Mikroskopie) mit erhöhter Sensitivität bei nur einer benötigten Kamerabelichtung zu verbinden ohne dabei spezielle Anforderungen an die Probenpräparation zu stellen. Aufgrund der, im Vergleich zu herkömmlichen Laser-Scanning-Verfahren, erhöhten Sensitivität ist es möglich, die Beleuchtungsintensitäten zu verringern. Damit eignen sich die Konzepte, welche auf der optischen Photonen-Zuweisung beruhen, besonders für die Untersuchung biologischer Prozesse in lebenden Zellen.

Der Zusammenhang zwischen wichtigen Eigenschaften optischer Mikroskopiemethoden ist in Abbildung (1.1) dargestellt. Es ist leicht verständlich, dass erhöhte (zeitliche und räumliche) Auflösung immer mit erhöhter Beleuchtungsdichte einhergeht, weshalb die Eigenschaft der ‘‘Superkonzentration‘‘ ein entscheidender Parameter in der praktischen Anwendung von OPRA ist. Der Probenpräparation kommt aufgrund der Vielfalt an Markierungstechniken und entsprechenden Fluorophoren eine besondere Bedeutung zu. Gerade die pointillistischen Methoden und STED stellen an die verwendeten Fluorophore hohe spezifische Anforderungen [18, 19]. Hier besitzt OPRA als generelles Konzept eine deutlich vergrößerte Vielseitigkeit. Zudem ist das Prinzip der Pixelzuweisung nicht auf den Prozess der Fluoreszenz beschränkt und lässt sich auch auf andere Scanning-Verfahren, wie z.B. konfokale Raman-Mikroskopie, erweitern [20].

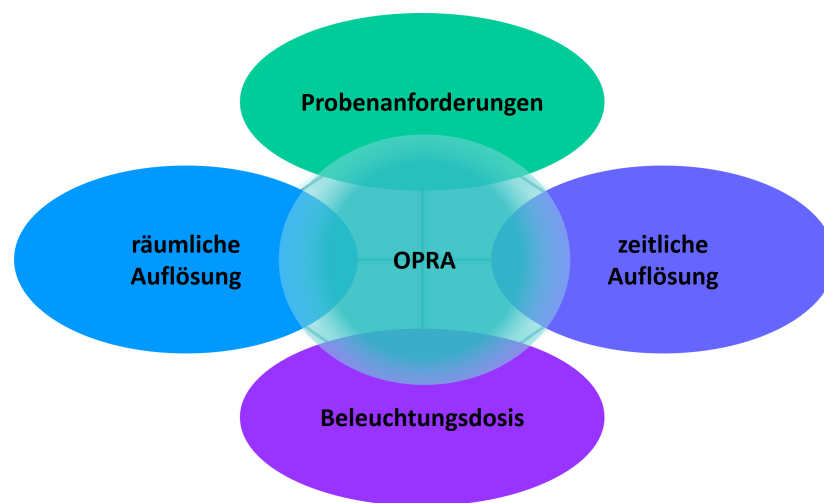


**Abbildung 1.1:** Stark vereinfachtes Schema über Wechselbeziehungen sich gegenseitig beeinflussender Mikroskopie-Eigenschaften. Dabei ist es gerade hinsichtlich der Beobachtung an lebenden Zellen sehr wichtig, dass alle Eigenschaften in einem ausgewogenen Verhältnis zueinander stehen. Die räumliche und zeitliche Auflösung sind zwei sich oftmals gegensätzlich gegenüberstehende Eigenschaften. Hier schafft es OPRA als instantane supraauflösende Methode gerade in einer Vielstrahl-Realisierung hochauflösende Bilder in extrem kurzer Zeit aufzunehmen. Das es zudem möglich ist, diese hohe Auflösung prinzipiell ohne den Verlust von emittierten Photonen zu erzielen, zeigt der als "Superkonzentration" bezeichnete Effekt. Auch stellt OPRA keine spezifischen Anforderungen an die verwendeten Farbstoffe und Probenpräparation, sodass mit einer einfachen Anwendung im Feld der biomedizinischen Bildgebung zurechnen ist. Diese Ausgeglichenheit der Eigenschaften von OPRA macht diese Methode zu einem vielversprechenden mikroskopischen Konzept mit dem Potenzial die konfokale Mikroskopie als Standardmethode abzulösen.

## 2 Summary

To make the unseen visible is an age-old dream of mankind and microscopes are made to turn this dream into reality. The word microscopy comes from the Ancient Greek *mikrós* for "small" and *skopeîn* meaning "to see". It describes the technology of visualizing objects which are too small for the observation by bare eye. The first inventions on track towards the development of microscopes dates back to 2000 years BC where Chinese used the higher refractive index of water to produce the first kind of light collecting "lens-like" devices. With the development and fabrication of glass also lenses could be constructed and they were used to magnify small objects. The first modern optical devices consisting of two convex lenses was invented around 1590 by Dutch eye glass makers H. and Z. Jansson [21]. A. Leeuwenhoek was the first person who really used a microscope and he discovered and described bacteria in 1674 [22].

Even as the microscopes improved during this time, there are basic properties of light diffraction which has to be considered. E. Abbe wrote in the important work "Beiträge zur Theorie des Mikroskops und der mikroskopischen Wahrnehmung" in 1873 that the smallest resolvable feature observed by far field optics is limited [1]. The famous formula describes, that the minimal resolvable distance  $d_{\min}$ , depend on the objectives numerical aperture  $NA = n \sin \alpha$ , with the refractive index  $n$  of the media between the objective lens and the sample and  $\sin \alpha$  the sinus of the opening angle of the objective, and the wavelength  $\lambda$  of the observation light:

$$d_{\min} = \frac{\lambda}{2n \sin \alpha}. \quad (2.2)$$

This equation is in its fundamentalism remarkably, as it is also valid for light emitting samples as fluorescent stained probes, even besides the fact, that fluorescent labelling techniques has not been discovered at this time. To improve the resolution the numerical aperture of the objective lens can be increased. That means, that the opening angle of the objective should be enlarged and immersion oils with a high refractive index are used. Regarding the imaging of living cells, the limit of the refractive index is set by the cells. It is also possible to decrease the observation wavelength  $\lambda$ . If particles instead of electromagnetic waves are used for the observation of the sample, the associated de-Broglie wavelength is much shorter (for electrons with the kinetic energy of 200keV the wavelength is approximately 2.5pm). Particle-based microscopes as electron-microscopes can achieve a resolution of few nanometers. As the preparation of the samples is complicated and the measurements have to be

performed under vacuum conditions, this techniques are not suitable for the imaging of living cells and biological processes.

As the possibilities within Abbe's equation are limited, approaches to circumvent this diffraction limit have been developed. Also it is important to maintain the advantages of fluorescent imaging - the possibility to observe the interaction of specific labelled molecules in their natural biological environment. In the research field of superresolution microscopy, several methods with the ability to overcome this diffraction limit, have been introduced and are explained in detail in section 3.2. The importance of these methods for biological research has been honoured by the nobelprize committee in the year 2014 [3].

In this thesis a promising new superresolution technique called Optical Photon Reassignment (OPRA) microscopy is introduced and applied to the field of fluorescence microscopy. The method is a optical realization of the computer-based reassignment principle in confocal microscopy introduced by Sheppard in 1988 [17]. There, the spatial information in the pinhole plane is used to increase the resolution. In the year 2010 this method received a lot attention as Müller and Enderlein published the same principle including experimental data from fluorescent samples [23]. As in OPRA the computational reassignment process is done optically, any necessary processing is avoided and only one camera readout is required. The microscopy concept, together with proof-of-principle experiments and a mathematical framework, was published and patented in 2013 [24, SR1]. The method combines several important properties of fluorescent imaging towards non invasive live-cell imaging in a unique way. OPRA achieves two-fold resolution enhancement in the focal plane if compared with the cut-off frequency of standard widefield microscopy. As OPRA does not require any processing, it is suitable for extremely fast imaging, especially if the method is parallelized. The imaging speed of the method is mostly limited by the scan speed. This is a system inherent advantage to other superresolution techniques as SIM or the pointillistic methods as PALM and dSTORM where several camera readouts are necessary. In [SR2] the special property of OPRA named "superconcentration" is introduced and discussed. This property describes, that the peak-intensity, compared to widefield microscopy, is increased and therefore the light is better concentrated than classical limits predicts. The theoretical background of this measurement concept was used for a general comparison of the microscopes OTF [SR4]. As the reassignment of the photons occurs in the pinhole plane, it is in general a two dimensional process.

However, there is an effect along the optical axis as well. In [SR3] it could be shown, that it is possible to improve the axial resolution by more than 10% over the resolution of a confocal microscope for reasonable big pinholes if OPRA is combined with structured illumination. This combination has the advantage, that the relatively large pinhole maintains the high signal level of OPRA.

In figure 2.2 the interaction of several important properties in modern superresolving fluorescent microscopy are illustrated in a simplified scheme. OPRA is able to link several characteristics in a new, unrivalled way. The described properties of OPRA have the potential to replace the confocal microscope as standard technique for biomedical imaging. OPRA in the parallelized realization is suitable for imaging of fast processes in living cells and is therefore a promising method to help answering important biomedical questions in the coming years of research. These properties of the optical reassignment methods lead to the development of several commercial products as the Re-Scan Confocal [25, 26], the spinning-disk variant (SD-OPR) by Yokogawa Electric Corporation [27, 28] or the multi-beam realisation called Vt-SIM by Visitech Int. [29].

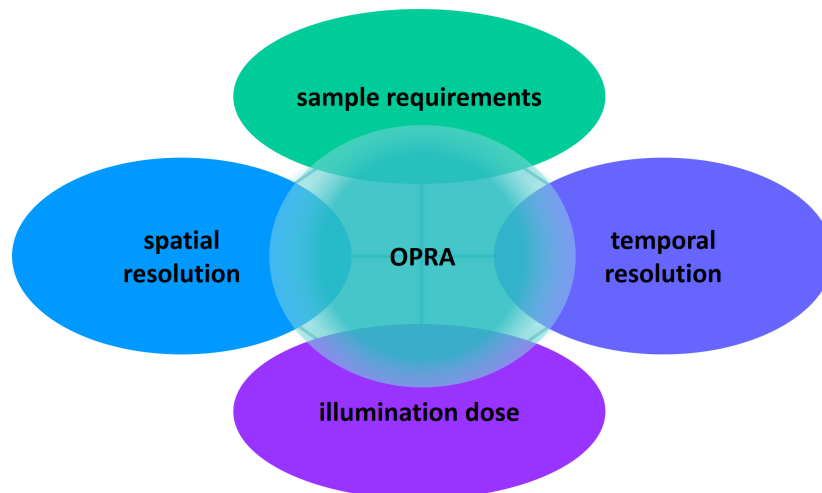


**Figure 2.2:** A versatile microscopic method is balanced in most of the specific properties of fluorescent microscopy. OPRA combines most of these properties in a unique way. As instant superresolution method it is possible to achieve high temporal and spatial resolution, especially if the method is parallelized. Also it is possible to achieve, due to the "superconcentration"-effect, very high sensitivity and therefore breaking the trade-off of high spatial resolution and illumination dose. This is an important property, as the illumination dose is limited towards imaging of fast biological processes in living cells. The method of optical reassignment is extremely versatile as no specific requirements for the sample preparation are necessary - the method works with all fluorophores. As OPRA can deal with all this properties in a well-adjusted way, the methods linked to the reassignment principle are suitable to replace confocal microscopy as the standard technique in fluorescent biomedical imaging.

## 3 Introduction

The presented work discusses a microscopic technique which can be classified in the field of superresolving fluorescent microscopy. Therefore the aim of this section is, to give a short overview over the underlying process of fluorescence and the field of research in superresolution fluorescent microscopy. As the concept of optical photon reassignment is based on laser scanning, the fundamentals in confocal microscopy are explained in this chapter as well.

### 3.1 Fluorescent microscopy

Fluorescence is the ability of a molecule to emit light after it gets excited by absorbing electromagnetic radiation. The excitation with light describes the difference to other forms of luminescence as chemiluminescence, where the molecules are excited by chemical reactions, or electroluminescence. The photon emission occurs if the molecular state switches from  $S_1$  to  $S_0$  whereas in phosphorescence the molecule has to be transferred to a triplet state before relaxation to the ground state  $S_0$ . As the phosphorescent emission takes significantly longer ( $\approx 10^{-4}$ s) than fluorescent emission, it is not suitable for fast imaging and will further not be considered. The fluorescent process can be split in several steps and is described also in figure 3.3. First, a photon is absorbed by the molecule ( $\approx 10^{-15}$ s) by converting its energy to excite the molecule from ground state  $S_0$  to excited state  $S_1$ . After a fast internal conversion ( $\approx 10^{-12}$ s), the molecule is in the lowest rotational and vibrational level of the excited state  $S_1$ , and then can spontaneously emit a photon ( $\approx 10^{-9}$ s). The probability for a transition between two energy levels is described by the overlap of their specific wave functions and their population and results in the named transition times. Therefore, the energy distance between the levels for excitation is normally larger than the distance between emission levels. This difference in excitation and emission wavelength is called Stokes shift. It is also used to separate emission and excitation light by dichromatic beamsplitters. As the emission process is spontaneous, there is no connection of phase for several fluorescent emitters and therefore fluorescent microscopy is incoherent.

For simplification the scheme in figure 3.3 doesn't show any triplet states. Also it has to be noted, that the Jablonski diagram is only valid for one specific molecule. If the chemical structure changes, which can also be triggered by light (for example in PALM), then also the molecular states changes, which leads to different absorption and emission properties.

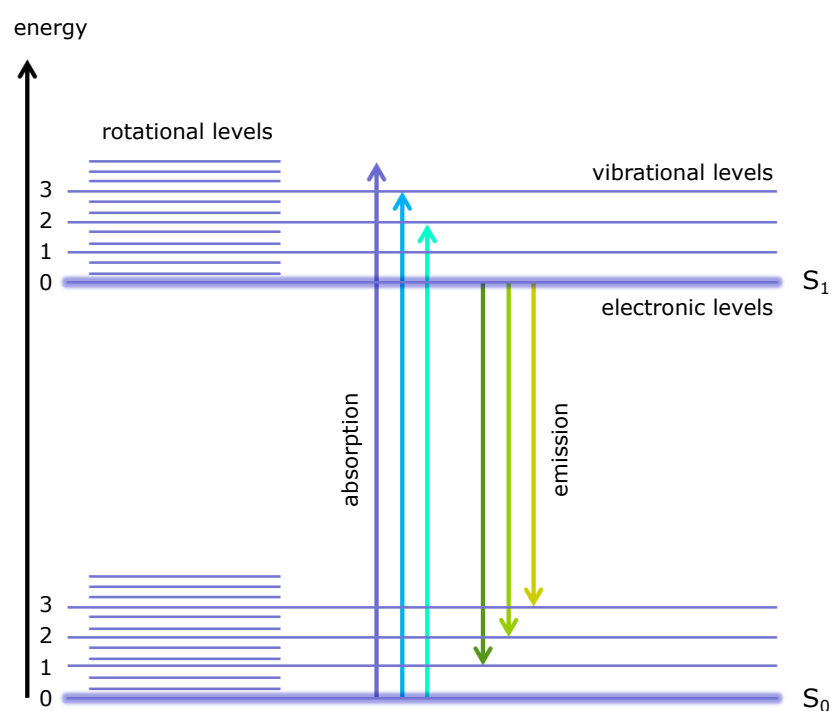


**Figure 3.3:** Schematic Jablonski diagram for fluorescent emission showing the different singlet states in a fluorophore for fluorescent emission. Different length of the arrows indicate different energy and therefore different wavelength (also indicated by different colour). The shape of absorption and emission spectrum (indicated by variable colours) depend on the different energy levels of the considered molecule. For a transition between two levels, the probability is represented by the overlap of their specific wave functions and their population. This illustration is adapted from [30].

As not the properties of the fluorophores itself are of main interest in microscopy, but the tissue they label, the development of fluorescent labelling techniques had a big impact on the field of biological imaging. The huge advantage in fluorescent microscopy is that the interesting parts of the sample can be labelled with a specific fluorophore and therefore identified while using the correct excitation wavelength even in living cells. In the development of fluorescent labelling techniques properties like fluorescent quantum efficiency, distance between label and target and labelling density are current fields of research [31, 32]. The advantage of labelling can also be seen as a disadvantage: except auto-fluorescence being present in some molecules, the specimen has to be prepared by labelling before they are suitable for fluorescence microscopy. This is where label-free techniques, based on elastic and inelastic scattering processes (e.g. Raman-scattering), give an alternative to observe the interaction between electromagnetic radiation and the biological specimen.

## 3.2 Superresolution microscopy

Superresolution microscopy techniques are always connected with "breaking the diffraction resolution limit" S. Hell and J. Wichmann wrote in their first paper about STED microscopy [4]. Circumventing this classical limit is a goal for modern microscope developers already a very long time. Superresolution fluorescence microscopy is defined as an increase of the incoherent spatial cut-off frequency supported by the optical system.

$$\nu_{\text{cut-off}} = \frac{2\text{NA}}{\lambda} \quad (3.3)$$

As a confocal microscope is capable to increase this frequency described by Abbe's formula (3.3), it is the first superresolving microscopic technique. Today there is a whole collection of techniques that are able to achieve superresolution and it is not the aim of this section to give a complete overview over this field of research as this is given in the literature [33–37]. Nevertheless, as the introduced method of Optical Photon Reassignment microscopy is a new superresolving method, important other techniques should be named. There will be an extended discussion about confocal microscopy as OPRA emerged from this technique.

There are several ways to classify the microscopic techniques, one is to separate them by the type of acquisition. There are on the one hand the scanning techniques such as



confocal microscopy, STED and the methods linked to reassignment principle (ISM, OPRA, Re-scan confocal (RSC), instant SIM (iSIM), SD-OPR etc.) and on the other hand the full-field techniques where the whole field of view (FOV) is illuminated and recorded at once, such as SIM and the pointillistic methods such as STORM, dSTORM, PALM etc. [5, 19, 38].

The scanning technique of STED uses the overlay of two different laser-foci in the sample. Where the first laser spot excites the fluorophores, the second, red-shifted laser spot, de-excites the fluorophores by stimulated emission. As the second, so called STED beam, has zero intensity in its centre, the region of possible fluorescent emission is, in dependency on the STED beam intensity, reduced on that small area. This technique can achieve very high resolution, if the sample can tolerate high laser intensities (up to 6nm resolution for nitrogen-vacancies) [39]. Also it is possible to parallelize the method to increase the imaging speed [7, 8]. As the powerful STED beam tends to bleach the fluorophores very fast, it is necessary to develop specific fluorophores which are not excited by the STED beam [40]. However, live-cell imaging is very challenging with this method.

The full-field technique SIM has the big advantage, that the illumination dose is not as high as in STED. Here, the sample is illuminated with a sinusoidal pattern, inducing a down-modulation of the high-frequency information into the region of support of the objective. As this information has to be reconstructed, several images of the sample illuminated with the shifted illumination pattern in several directions are necessary. The absolute resolution improvement is not as high as in STED, but the method needs significantly less illumination intensity and is able to acquire images up to 79fps [41]. The imaging speed is also an advantage compared to the pointillistic methods as STORM, dSTORM or PALM. Here the imaging conditions are set in that way, that only very few fluorophores emit at the same time, enabling fitting each separated fluorophore and precisely determination of its centre. As several thousand images are needed to achieve nicely resolved images, the imaging speed is limited. Also it is challenging to set the imaging conditions that way, that the fluorophores do not emit at the same time and therefore do not overlap. Here, it is also necessary to develop specific fluorophores to achieve the necessary blinking behaviour [42, 43].

### 3.3 The confocal microscope

The reassignment principle is based on confocal laser scanning microscopy (CLSM), which is a scanning system combined with a point detection unit. Therefore this section explains the fundamentals of confocal microscopy and a general scheme can be found in figure 3.4. The "confocal principle" is normally associated with detection after the signal is focused on a pinhole. This principle was invented in the year 1955 and patented in 1957 by Marvin Minsky [44]. To generate the signal in the observed sample a diffraction limited spot is used for excitation. Therefore the back focal plane (BFP) of the objective has to be fully illuminated with collimated light. To illuminate the whole sample, the excitation spot has to be moved over the field of view (FOV). This makes a very accurate scanning of the sample necessary. As the scanning is also very important in OPRA, this should be explained in more detail in a separate paragraph.

If the sample is excited at one scan position with the illumination spot, it generates a fluorescent signal in the sample which is detected via the objective. After descanning, meaning that the fluorescent signal passes the scanning system, the signal is split from the excitation light via the dichromatic beamsplitter. The key properties of CLSM arise as the signal is focused on a detection pinhole. Only the signal which passes this pinhole will hit the integrating detector and generate a signal corresponding to the scan position ( $\mathbf{s}$ ). As the pinhole suppresses fluorescent light from out-of-focus planes it generates the characteristic sectioning effect.

The point spread function (PSF) describes the intensity distribution of a point-like object if observed through the optical system of interest. For an ideal system, the PSF is only limited by diffraction. Therefore the PSF can be used to characterize different microscopic techniques. The PSF of the confocal technique can be found to be:

$$\text{PSF}_{\text{confocal}}(\mathbf{x}) = \text{PSF}_{\text{ex}}(\mathbf{x}) \cdot [\text{PSF}'_{\text{det}} \otimes \text{ph}](\mathbf{x}). \quad (3.4)$$

Here  $\text{PSF}'_{\text{det}}$  and  $\text{PSF}_{\text{ex}}$  describe the point-spread function of emission and excitation light, with the mirrored, symmetric detection point spread function  $\text{PSF}'_{\text{det}}(\mathbf{x}) = \text{PSF}_{\text{det}}(-\mathbf{x})$ . The three dimensional image coordinates are described by the vector ( $\mathbf{x}$ ). The pinhole is represented by the function  $\text{ph}$  and  $\otimes$  is the convolution operator. With (3.4) the two extreme cases for the pinhole function are nicely visible. If the pinhole is infinitely large, (3.4) simplifies to  $\text{PSF}_{\text{confocal}}(\mathbf{x}) = \text{PSF}_{\text{ex}}(\mathbf{x})$  which is

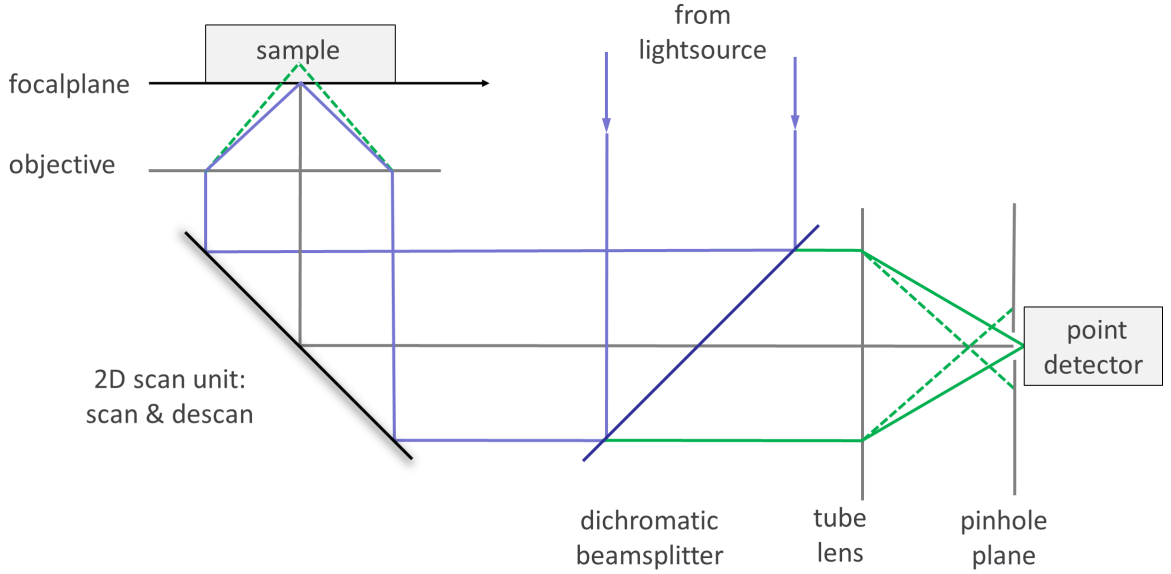


**Figure 3.4:** Principle of confocal microscopy. After passing a dichromatic beam splitter, the collimated light from the light source is directed to a beam scanning unit to create a moving diffraction limited spot in the focal plane of the objective to excite the fluorophores within the sample. The fluorescent light is collected with the same objective, directed to the scanning unit and split with the dichromatic beam splitter from the excitation light (due to the Stokes shift indicated with the green lines). For every scan position  $s$ , the light which passes the pinhole forms the intensity signal at the corresponding position. Fluorescent light from out-of-focus areas (dashed lines) will not pass the detection pinhole and therefore will not contribute to the confocal signal (for simplification the lines are only drawn near the focal planes).

known as the laser scanning limit. Interestingly the width of the PSF depends only on the width of the excitation function and can therefore be smaller than the width of a widefield  $\text{PSF}_{\text{em}}$ . On the other hand, for infinitely small pinhole (ph is approximated by a  $\delta$ -distribution), the confocal point spread function can be described by  $\text{PSF}_{\text{confocal}}(\mathbf{x}) = \text{PSF}_{\text{ex}}(\mathbf{x}) \cdot \text{PSF}_{\text{em}}(\mathbf{x})$ . The multiplication of emission and excitation PSF comes along with an improved resolution. If the PSF is approximated by a Gaussian of the form

$$f(\mathbf{x}) = \exp\left(-\frac{1}{2}\left(\frac{\mathbf{x}}{\sigma}\right)^2\right), \quad (3.5)$$

which is acceptable for imaging planes, but not for the axial direction, then this multiplication leads to the often cited  $\sqrt{2}$  smaller FWHM of  $\text{PSF}_{\text{confocal}}$  compared to  $\text{PSF}_{\text{em}}$ . It has to be noted, that this limit is a theoretical limit only, as a microscope with a closed pinhole, would not detect any light. Nevertheless this limit can be almost reached [45]. For biological samples the SNR is very important and a good compro-

trade-off between resolution and signal level has to be found. This results in an often used practical pinhole diameter of 1 AU even a diameter of approximately 0.62 AU seems to give the best SNR [46, 47]. Here the pinhole diameter is given in Airy units (AU)

$$1\text{AU} = 1.22 \frac{\lambda}{\text{NA}}, \quad (3.6)$$

which describes the diameter of the first dark ring with zero intensity for a far-field diffraction pattern of a circular aperture. In a real microscope the magnification at the pinhole plane has to be considered.

### 3.3.1 The scanning system in confocal microscopy

The scanning system in CLSM is a rather complex topic as many aspects such as scanning speed or linearity of the sample illumination have to be considered. The easiest way of scanning is by moving the sample [48]. This method has the advantage, that the optical setup is relatively easy as all optics are centred on the optical axis and the FOV is not limited by the optical elements. On the other hand this method is very slow as fast movement of the stage leads to vibrations of other components. In addition many biological samples do not tolerate these vibrations. It is also possible to scan the fast axes with a beam scanning mirror and step the slow axes with a motorized stage, but this solution is as well not suitable for fast scanning applications. In modern microscopes the illumination of the FOV is normally realized while using a two dimensional beam scanner in a conjugated plane of the BFP. For the acquisition of 3D data a piezo-driven stage or objective mount is normally used to capture images along the optical axes. In CLSM there are several ways to generate the illumination scanning [49]. Instead of using galvanometric mirrors, also acousto optic deflectors can be used [50]. The main problem in beam scanning is that the two imaging axes need to be placed in a conjugated plane of the BFP. It is possible to project this plane onto both scan mirrors by using concave mirrors between the two scan mirrors [51]. Alternatively it is possible to use some relay optics between the two mirrors. Also MEMS - scanning devices are available nowadays which can be very fast and small. As these scanning mirrors are very thin and light, the deformation of the mirrors while scanning causes aberrations [52].

In normal CLSM problems like not perfectly flat or axially displaced scanning mirrors are not that critical, as they only affect the excitation side of the microscopy setup. On the detection side the fluorescent beam passes the scanning device in the

other direction and is guided to an integrating detector. In most confocal scanning systems the conjugated BFP is placed halfway between of the x- and y-scan mirror, inducing a non perfect placements of both scanning planes. This findings change massively, when the integrating detector of an CLSM is replaced by a camera. As only one dimensional scanning is necessary for bilateral "direct-view" slit scanning confocal microscopes, imaging via the scan mirror is still perfectly possible [53, 54]. Here the illumination light forms a long line in one dimension and is scanned in the other. This has the advantage, that the rotational axis of the scanning mirror can be placed directly at a plane conjugated to the BFP. The emission light is re-scanned, directed to a slit for pinholing and re-scanned with the backside of the same scanning mirror again. The methods of instant SIM and MSIM use this approach of one dimensional scanning and de-scanning while using the backside of the mirror for re-scanning [55–57]. In the new developed method of Optical Photon Reassignment microscopy the specimen has to be scanned, de- and re-scanned in two dimensions which is a major challenge for the scanning system (see figure 5.9 and 5.10).

For further parallelization it is possible to extend the idea of confocal microscopy to many excitation foci while, instead scanning a conjugated plane of the BFP, the image plane is scanned. These so called confocal spinning disk (CSD) microscopes use the nipkow disk (which was invented already in 1884) to rotate pinholes on the excitation and emission side to generate spot-like illumination and pinholed detection [58, 59]. Due to the high amount of parallelization these microscopes have the ability to scan very fast. As the whole sample is illuminated while moving the pinhole plane, a fixed spatial resolved detector such as a camera or even the eye could be used in a CSD. This makes the usage of complicated pixel clocking and time consuming image calculation unnecessary. It has been shown, that these techniques can be expanded with the optical reassignment principle to SD-OPR [27].

## 4 The reassignment principle

The reassignment principle is a general concept in microscopy which uses the two dimensional spatial information of the emitted light in a descanned imaging plane of a laser scanning microscope (LSM) to improve the image resolution and quality. This principle was developed over the past decades and in the last two years even commercial products used this technique (Zeiss AiryScan use computational reassignment [60] and Vt-iSIM from VisiTech International Ltd. and the CSU-SR from Yokogawa reassigns the photons optically [28, 29]). As the microscopy technique we developed is based on the general frame of the reassignment principle, this section should give an overview over the underlying microscopic principles and show the history of most important findings. The concept in general, optical and computational realizations of the principle will be explained. In the end OPRA is put into the context of the other presented realizations.

### 4.1 The general concept

Already with the development of the confocal microscope, it became obvious that the pinhole plane information can be used to enhance the imaging properties of a microscope. The key-advantage of confocal microscopy is the improved sectioning ability by suppressing the out-of-plane fluorescence, for which a simple unit in the form of an iris diaphragm is sufficient. This can be explained with the low information content of out-of-focus fluorescence. To gain an improved in-plane resolution, the pinhole diameter should be significantly smaller than 1 AU (see figure 5.13). On the other hand also the signal level dramatically drops for such small pinholes [61–63]. The trade-off between signal intensity and resolution leads to a commonly chosen size of the pinhole of approximately 1 AU for biological application, maintaining the sectioning behaviour but losing nearly all of the in-plane resolution enhancement.

However, the capability of resolution enhancement in confocal microscopy relies on using position information in the pinhole plane. The idea is visualized in figure 4.5 showing one specific time point during a scanning process. Here a fluorophore, which is not centred at the optical axis, is illuminated and then detected at the pinhole-plane. For this off-centre fluorophore, with the two dimensional position  $\mathbf{r}$ , the detection  $\text{PSF}_{\text{det}}$  is imaged to a corresponding position  $\mathbf{r}$  into the pinhole plane. In contrast, the confocal microscope sums all signal from the pinhole plane and assigns the signal to the corresponding scan position  $\mathbf{s}$  in the image. However, the knowledge about

scan position  $\mathbf{s}$  and detection position  $\mathbf{r}$  gives the possibility to determine the most probable position of emission for the detected photons. This area,  $\text{PSF}_{\text{tot}}$ , is described by the product of  $\text{PSF}_{\text{det}}$  and  $\text{PSF}_{\text{ex}}$ . Assuming the same width for  $\text{PSF}_{\text{det}}$  and  $\text{PSF}_{\text{ex}}$ , this probability area  $\text{PSF}_{\text{tot}}$  has its centre exactly in between the positions  $\mathbf{r}$  and  $\mathbf{s}$ . Please note that figure 4.5 is not in scale as the maximum amplitude of  $\text{PSF}_{\text{det}}(\mathbf{r})$  is equal to the value of  $\text{PSF}_{\text{ex}}$  at position  $\mathbf{r}$  and therefore also the product  $\text{PSF}_{\text{tot}}$  of both functions has a smaller amplitude than shown. However, the positions of the PSFs are indicated correctly. The reassignment principle uses this knowledge about scan and emission position while moving the detected photons for every single scan position  $\mathbf{s}$  in the pinhole plane from position  $(\mathbf{s} - \mathbf{r})$  to  $(m \cdot (\mathbf{s} - \mathbf{r}))$ . If this reassignment is done for every single time point during the scan process, the narrowed overall  $\text{PSF}_{\text{OPRA}}$  is formed (see section 5). Normally the intermediate magnification factor is set to  $m = 0.5$  (meaning a demagnification of the pinhole plane) as this gives the best performance regarding resolution assuming identical detection and excitation PSF.

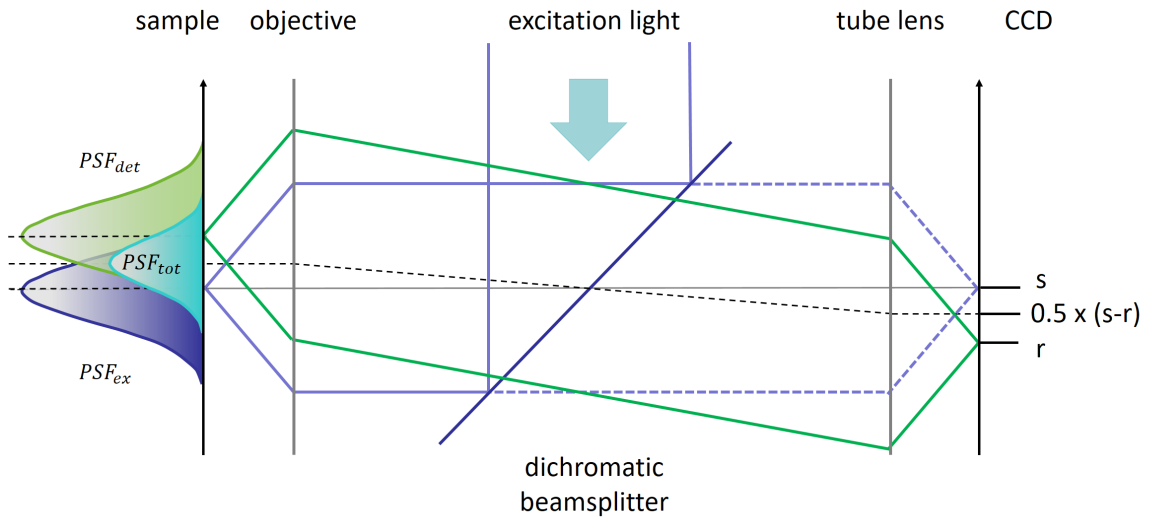


**Figure 4.5:** A schematic drawing of the reassignment principle. The illumination side (blue lines describing the excitation wavelength) of this setup is similar to a confocal illumination part shown in figure (3.4). The illumination  $\text{PSF}_{\text{ex}}$  is centred at scan position  $\mathbf{s}$ . For spatially resolved detection, the off-centred emitted fluorescent photons (green lines) are spread by  $\text{PSF}_{\text{det}}$  and centred at position  $\mathbf{r}$ . The most probable emission origin is described by  $\text{PSF}_{\text{tot}} = \text{PSF}_{\text{ex}} \cdot \text{PSF}_{\text{det}}$ . The reassignment principle uses this knowledge to reassign the emitted photons to this most probable emission origin. This reassignment can be done computationally or by optical means. If the reassignment process occurs for every scan position, the overall  $\text{PSF}_{\text{OPRA}}$  with reduced width is formed. Note that the intensity of the PSF are not drawn to scale, as the maximum amplitude of  $\text{PSF}_{\text{det}}$  is equal to the value  $\text{PSF}_{\text{ex}}$  at position  $r$  in the sample.

In the first realizations of the concept, the reassignment was done computationally

while acquiring one image of the pinhole plane for every scan position and demagnifying every pinhole image by the factor of two, giving a superresolved ISM image by the sum of all individual pixel reassigned pinhole images [23, 64].

The computational reassignment principle can also be explained by interpreting every camera pixel as a small pinhole and therefore approaching the theoretical limit of a confocal microscope with a pinhole described by a  $\delta$  - function. The reassignment of the photons can also be done optically while demagnifying the pinhole plane and subsequent rescanning - this method is known as Optical Photon Reassignment [SR1]. Also it is possible to interpret the laser spot in LSM as specific form of structured illumination [33]. As OPRA uses the cut-off frequency of illumination and detection PSF, the region of support is doubled. In that sense OPRA is a specific form of linear SIM with on-the-fly processing via time-multiplexing.

## 4.2 Development of an idea

The first discoveries linked to the reassignment principle happened, as quite often in science, by accident. Cox et al. reported in the year 1982 [65, 66] that the resolution of a CLSM improves, if the detection pinhole is slightly misaligned, meaning not precisely centred to the optical axes. This investigation was the first hint for a general concept using the spatial information in the pinhole plane. This general idea was published in the year 1988 by Colin Sheppard [17]. In this article he suggests instead of using a point detector to use a detector array and "instead of integrating directly ... such signal is reassigned to its particular image point". Sheppard also gives a formal theoretical description for reflective systems and mentioned that this "method is also applicable to fluorescent microscopy". Also other groups noticed the behaviour of the displaced detector [67, 68]. In 2003 Rainer Heintzmann brought this idea back to mind while giving a talk on the conference "Focus on microscopy" in Genova [69]. Also several methods were presented, which used different ways of subtracting pinhole plane information taking for different pinhole sizes and shapes [70, 71]. In 2010 the reassignment idea got a lot attention as C. B. Müller and J. Enderlein published "Image Scanning Microscopy (ISM)" [23]. Due to the development of sensitive cameras since 1988, they were able to detect the fluorescent signal for every single scanning position and to digitally reassign the detected signal to its most probable origin. This publication gained a lot of interest as it was also subject of a article review in Physics [64]. This article was the starting point for many research groups to



think about possible improvements of the reassignment principle. In 2012 York et al. published a multi beam implementation of ISM with the name multi-focal structured illumination microscopy (MSIM) in Nature Methods [57]. This publication included 3D data of living cells with a resolution improvement of  $\sqrt{2}$  for the in-plane FWHM of the PSF. In the year 2013, three all-optical realizations were published simultaneously, presenting three different ideas with the names Re-Scan confocal (RSC), iSIM and OPRA [25, 55, SR1]. Where York et al. (instant SIM) used a multi-beam variation, De Luca et al. (RSC) and Roth et al. (OPRA) showed single beam realizations of the principle. Both single beam methods are each covered by a patent, submitted by the authors of the article of the OPRA method [24]. These three publications mark the first all-optical realizations of the reassignment principle.

The further development of the principle can be split into the two fields of computational and optical reassignment methods and will be discussed in the next section.

### 4.3 Computational methods

The computational methods are all based on the reassignment approach published by Sheppard in 1988 and in 2010 by Enderlein (ISM) [17, 23]. In 2012 York et al. proofed in a very complicated setup, that it is possible to parallelize the method with the multi-focal spot variant MSIM [57]. Sheppard et al. published in 2013 a in depth analysis of the reassignment properties of ISM which forms a basis for the computational methods [72]. They showed simulations of the PSFs for different detector pixels and described properties as the enhanced peak intensity of the PSF in ISM. The group of J. Enderlein published in 2013 a spinning disk variant of ISM (CSD-ISM) where they were able to multiplex the ISM principle and therefore could improve the acquisition speed [73]. In 2014 the company Carl Zeiss Microscopy GmbH brought the LSM 880 with the AiryScan unit based on 32 GaAsP detectors to the market [74]. In the year 2015 Castello et al. simplified the method while theoretically showing, that it is already enough to use a quadrant detector instead of a normal confocal detector to gain resolution performance. McGregor et al. summed up various methods of calculating and post-reassigning two dimensional data acquired in the pinhole plane of a laser scanning microscope [75]. The group of Xu Liu used an AiryScan detector for photon reassignment to improve their method of fluorescence emission difference microscopy (FED) [76–78].

In general the computational reassignment methods have the drawback, that the calculation needs time and therefore they are not as fast as optical methods. Compared to OPRA, the synchronization is also more complex, as the recorded data has to be connected to the excitation position and therefore a precise pixel clock is necessary. As this synchronization challenges are similar to confocal microscopy, many technological solutions can be adapted. On the other hand, as published for example in the first realization of ISM [23] the optical setup is simpler than the optical reassignment realizations. This also helps to avoid signal loss in additional optical components. The drawback of processing time, comes with the advantage, that the collected data has a higher information content and gives the opportunity to further enhance the image quality with post-processing strategies as deconvolution methods or weighted averaging [75, 79]. Also it is possible to get different output images. It is for example possible to generate a fast, or nearly "live", non-reassigned image for adjustment and finding the right sample position, and, on the second, a reassigned image.

#### 4.4 Optical methods

This section presents an overview and a classification of existing optical realizations of the reassignment principle and arranges OPRA into this field. The optical methods have, compared to the computational methods, the advantage, that the reassignment of the photons takes place automatically and therefore no additional processing is necessary to achieve superresolved images. In this perspective the optical methods are really unique in the field of superresolution microscopy, as they achieve their resulting image in only one single camera frame without any necessary processing. This shows the huge potential of the optical methods for superresolved imaging of fast biological processes [33].

Similar to confocal microscopy (see section 3.3.1), optical reassignment methods can be classified on the basis of the scanning system. Interestingly all the three first inventions in this field use a different approach. The figure 4.6 shows a schematic drawing of the optical methods. Note that the beam diameter is not in scale. The systems of Roth et al. [SR1] and De Luca et al. [25] uses a single beam variant with two-dimensional beam scanning and are described in the patent by the authors of OPRA [24, SR1]. The Re-Scan confocal (RSC) uses two separate two-dimensional galvometric scanning units. After scanning and de-scanning, the fluorescent beam is directed to the pinhole and then re-scanned with the second scanning unit. This has

the advantage, that the optical setup is simplified as there are only rectangular angles in the beam path. The synchronisation of the two scanning units has to be precise but once the scanning units are in phase, the imaging performance can be adapted to the given Stokes shift of the fluorophores in the sample by changing the ratio of the two scanning amplitudes. The ratio of the scanning amplitudes in RSC corresponds to the intermediate magnification factor  $m$  in the description of OPRA (see equation 5.7).

The publication by York et al. uses a multi-beam variant [55] and 2015 Curd et al. published a step-by-step instruction of how to build an iSIM microscope [56]. The arrangement with a slightly tilted multi-lens array gives the opportunity to use a double sided mirror for one-dimensional scanning. As done in bilateral slit-scanning microscopy this mirror can be placed perfectly in the BFP [53, 54]. The parallelization of the concept has the big advantage of a faster imaging, which is important regarding live cell imaging of fast processes. The advantage that only a one-dimensional scanner can be used in iSIM comes with the prize, that the exact alignment of the multi-lens array for illumination and the combined multi-lens and multi-pinhole array is very challenging. The parallelization is limited by the channel crosstalk. As known from

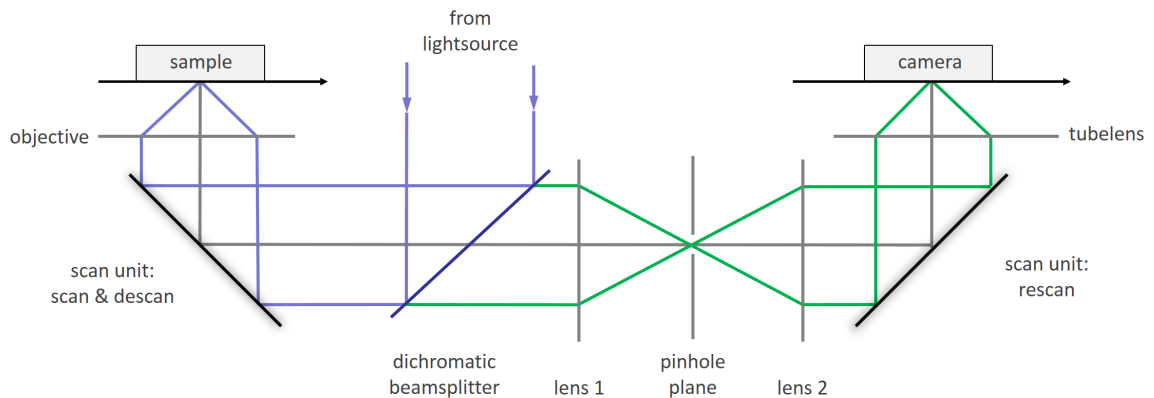


**Figure 4.6:** Optical realization principle of photon reassignment. This figure shows a general scheme of possible optical realizations of the reassignment principle. The confocal illumination side (see fig. 3.4) is combined with the optical reassigning unit. The emitted fluorescent light is collected with the objective lens and descanned via the beam-scanner. In OPRA the reassignment of the photons occurs while demagnifying the detection beam via the lenses 1 & 2 and rescanning with the same beam-scanner (note that for this case, the beam-diameter is not drawn to scale). In Re-Scan confocal (RSC) this reassignment is done by using two different beam-scanner and adjusting the scan-amplitude of the second scanner accordingly (lens 1 & 2 are only for background suppressing with the detection pinhole) [25]. For multi-beam realizations only one dimensional scanning is necessary, and therefore the backside of the beam-scanner can be utilized [55, 56].

---

confocal spinning disk microscopy, the background suppression for an out-of-focus fluorescent plane is connected to the distance of the individual micro-lenses [49]. Interestingly the same group used in 2014 for the two photon excitation variant of iSIM two separate two-dimensional beam scanners for scanning and re-scanning [80, 81]. In the two-photon variant no detection pinhole is integrated into the beam path.

In 2015 Takuya et al. from the Yokogawa Electric Corporation demonstrated that it is possible to design a spinning disk confocal microscope with optical reassignment and therefore realize a image scanning optical reassignment microscope with fixed pinhole diameter [27]. Their method of spinning disk optical photon reassignment (SD-OPR) gives promising results, but further investigation of known parallelization issues as channel cross-talk will show, how a potential commercial product will look like [28].

## 5 Optical Photon Reassignment Microscopy

### 5.1 All-optical realization of the reassignment principle

This section gives an overview about the new microscopic technique of Optical Photon Reassignment Microscopy (OPRA) which was invented and developed at the laboratories of the Leibniz Institute of Photonic Technologies. This method is one of the first presentations of an optical realization of the reassignment principle. Remarkably all three publications use a different way of optically reassigning the photons in the fluorescent beam path [25, 55, SR1]. The method used in Luca et al. with the technique they name "Re-Scan Confocal" (RSC) is also covered by the patent "Verfahren zum optisch hochaufgelösten Raster-scanning eines Objektes" which the authors of [SR1] published [24].

First the mathematical framework of reassignment microscopy is presented according to [SR1] and some main properties are discussed. The general framework of the optical and computational methods is identical, if there is no additional processing as digital pinholing, Fourier-filtering or multi-view deconvolution applied.

As the reassignment principle is based on the confocal microscope, the mathematical description in [SR1] is based on confocal point scanning microscopy. It is also possible to interpret the scanning of an diffraction limited spot as specific form of structured illumination and adapt the theoretical formalism of SIM to OPRA [23, 73]. Of course both ways of interpretation lead to same results. To interpret LSM as a specific form of structured illumination also explains why York et al. [55] called there method instant SIM and makes a multiplexing of the method via multi-beam approaches even more obvious.

The image formation in optical reassignment is discussed for an infinitely large detector. It could be found that the point spread function (PSF) of OPRA can be described as

$$\begin{aligned} \text{PSF}_{\text{OPRA}}(\mathbf{x}) &= \int \text{PSF}_{\text{ex}}(\mathbf{s}) \cdot \text{PSF}'_{\text{det}}\left(\frac{\mathbf{x}}{1-m} - \mathbf{s}\right) d\mathbf{s} \\ &= [\text{PSF}_{\text{ex}} \otimes \text{PSF}'_{\text{det}}]\left(\frac{\mathbf{x}}{1-m}\right). \end{aligned} \quad (5.7)$$

Here  $\text{PSF}'_{\text{det}}$  and  $\text{PSF}_{\text{ex}}$  are the symmetrical point spread functions of detection and

excitation wavelength (meaning  $\text{PSF}_{\text{ex}}(\mathbf{x}) = \text{PSF}_{\text{ex}}(-\mathbf{x})$ ),  $\otimes$  is the convolution operator and  $m$  the intermediate magnification. The image coordinates ( $\mathbf{x}$ ) and ( $\mathbf{s}$ ) are vectors in two dimensions. Also the modified detection point spread function  $\text{PSF}'_{\text{det}}(\mathbf{x}) = \text{PSF}_{\text{det}}\left(\frac{1-m}{m} \cdot \mathbf{x}\right)$  is used for the convolution in (5.7). If Gaussian shaped excitation and detection function of the form

$$f(x) = \exp\left(-\frac{1}{2}\left(\frac{\mathbf{x}}{\sigma}\right)^2\right) \quad (5.8)$$

are used for description, the standard deviation  $\sigma$  of  $\text{PSF}_{\text{OPRA}}$  could be found to be:

$$\sigma_{\text{OPRA}}^2 = \sigma_{\text{ex}}^2 m^2 + \sigma_{\text{det}}^2 (1-m)^2. \quad (5.9)$$

As the Stokes shift in most fluorophores is only small, the case with negligible discrepancy between the detection and excitation wavelength is often discussed. If  $\lambda_{\text{ex}} = \lambda_{\text{det}}$  is assumed, equation (5.9) shows, that the smallest width for the resulting PSF is expected for an intermediate magnification factor of  $m = 0.5$ . For this specific case ( $\text{PSF}_{\text{ex}} = \text{PSF}_{\text{det}}$  and  $m = 0.5$ ), equation (5.7) can be simplified to:

$$\text{PSF}_{\text{OPRA}}(\mathbf{x}) = [\text{PSF}_{\text{ex}} \otimes \text{PSF}_{\text{det}}](2\mathbf{x}). \quad (5.10)$$

Often this simplified equation is used and the intermediate magnification factor is set to  $m = 0.5$  [23, 27, 55]. With this assumption, equation (5.9) can be simplified to:

$$\sigma_{\text{OPRA}} = \frac{1}{\sqrt{2}} \sigma_{\text{det}}, \quad (5.11)$$

showing the  $\sqrt{2}$  resolution enhancement of OPRA if compared with  $\text{PSF}_{\text{det}}$ .

Nevertheless there are some cases where the assumption  $\text{PSF}_{\text{ex}} = \text{PSF}_{\text{det}}$  is not sufficient and a closer look on the minimal extent of  $\text{PSF}_{\text{OPRA}}$  is necessary. For example if OPRA is combined with STED microscopy, the excitation PSF in STED has a very small effective width and therefore the intermediate magnification factor should be adapted. Also in two-photon-microscopy the effective excitation PSF width differs from the assumption of equal detection and excitation wavelength. The best intermediate magnification factor  $m$  to achieve a minimal extend of the final  $\text{PSF}_{\text{OPRA}}$  can be determined to:

$$m = \frac{\sigma_{\text{det}}^2}{\sigma_{\text{ex}}^2 + \sigma_{\text{det}}^2}. \quad (5.12)$$

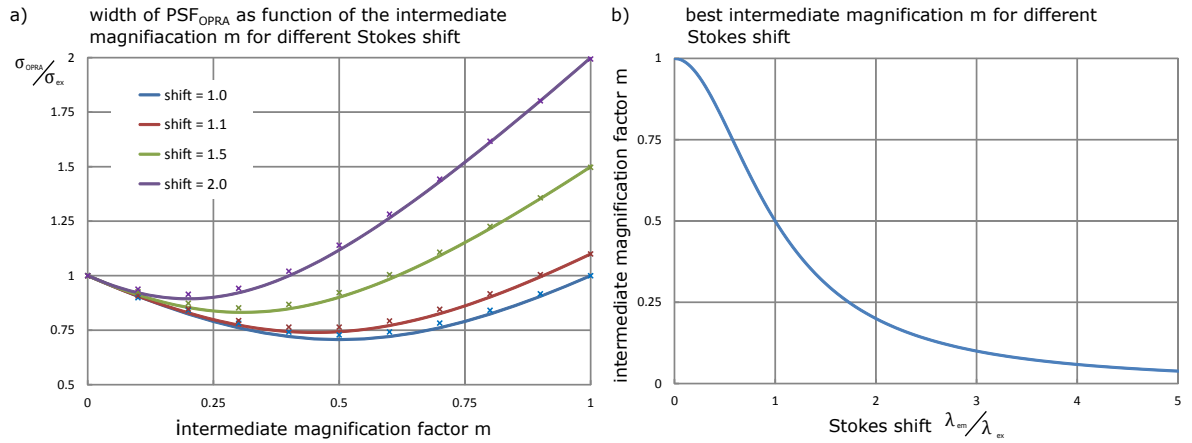


**Figure 5.7:** Correlation of the intermediate magnification factor  $m$ , Stokes shift and width of PSF<sub>OPRA</sub>. In a) the width of PSF<sub>OPRA</sub> relative to the width of the excitation function is displayed in dependence on the intermediate magnification factor  $m$  for different Stokes shift. The Stokes shift here is defined as the quotient of detection and excitation wavelength. The marks represent a full numerical simulation while the lines showing the simplified model (see equation 5.9) using Gaussian shaped PSFs (equation 5.8). In b) the best intermediate magnification, where  $\sigma_{\text{OPRA}}$  is minimal, is shown as function of the Stokes shift.

This correlation is shown in figure 5.7 b) where the best intermediate magnification factor  $m$ , achieving a minimal extent of PSF<sub>OPRA</sub>, is plotted as a function of the Stokes shift. In figure 5.7 a) the width of PSF<sub>OPRA</sub> is shown as function of  $m$  for different Stokes shift. The intermediate magnification of  $m = 0$  represents the confocal scanning with an open pinhole (all the light per scan point is focussed on the scan position  $s$ ). If no magnification is present ( $m = 1$ ), the resolution of OPRA is the same as in widefield microscopy, even though it is a laser scanning technique. The simplification  $m = 0.5$  is justified, as for a more realistic Stokes shift of 1.1 ( $525\text{nm}/475\text{nm} \approx 1.1$ ) the minimal extent of PSF<sub>OPRA</sub> is only marginally bigger than for  $m = 0.5$  (minimal extent for  $m = 0.45$ ,  $\sigma_{\text{OPRA}} \approx 0.74 \cdot \sigma_{\text{ex}}$ ). For larger Stokes shift, the intermediate magnification has to be adapted accordingly, but also the resolution improvement in relation to the excitation PSF<sub>ex</sub> is decreased.

Figure 5.8 shows a simulation of the resolution properties of OPRA compared to confocal microscopy. For better visualization a sample with separated fluorescent points (300nm in horizontal and 240nm in vertical direction) is imaged for different pinhole diameters. This simulation shows, that OPRA is able to achieve the resolution properties of a confocal microscope with a very small pinhole, even for a completely open pinhole. Where the confocal microscope shows a strong connection between pinhole diameter and resolution capability, there is nearly no dependency for the resolving

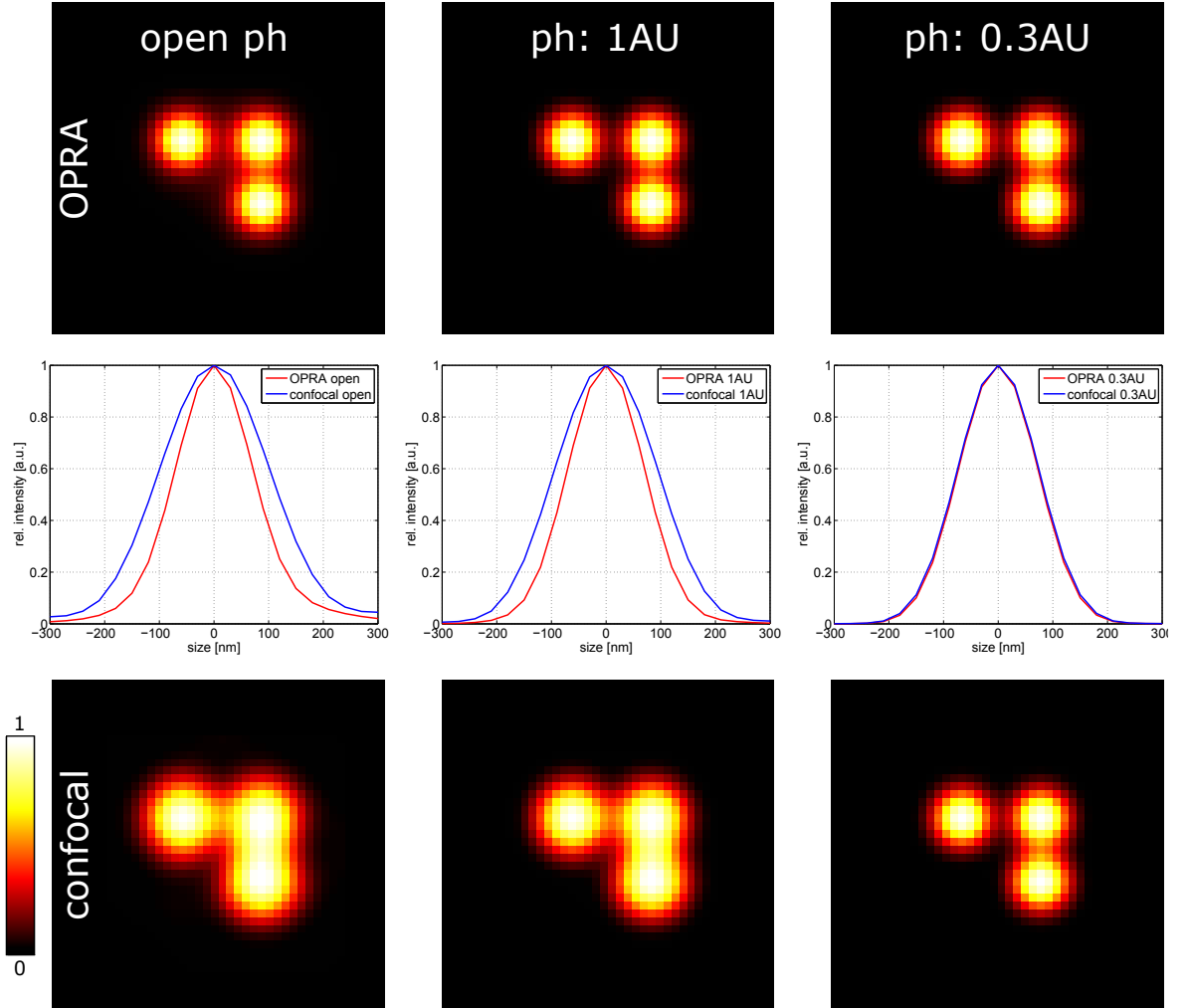


**Figure 5.8:** This numerical simulation compares the resolution of OPRA and a confocal microscope for different detection pinhole (ph) sizes on point objects. The line traces show the corresponding one-dimensional PSF. All images are normalized. Whereas OPRA shows nearly no dependency of the resolution on the pinhole diameter, the width of the PSF of a confocal microscope decreases from that of  $\text{PSF}_{\text{ex}}$  (if no pinhole is used) to roughly  $\sqrt{2}$  resolution enhancement for the case of a nearly closed pinhole (the resolution enhancement is exact  $\sqrt{2}$  for the assumptions of Gaussian PSF with the same wavelength for excitation and detection (no Stokes shift)). OPRA achieves this upper resolution limit in all the simulated cases. Simulation parameter:  $\text{NA}=1.2$ ,  $\lambda_{\text{ex}}=488\text{nm}$ ,  $\lambda_{\text{em}}=525\text{nm}$ , point distance: 300nm (horizontal) and 240nm (vertical).



power of OPRA in two lateral dimensions (see also figure 5.12). On the other hand the pinhole is important for the axial resolution as it is discussed in section 5.3. These findings are very important as the pinhole is responsible for most of the light losses in confocal microscopy. To visualize this behaviour, figure 5.11 shows the same settings as in figure 5.8, but normalized to the maximal intensity.

### 5.1.1 The scanning system in OPRA

As the reassignment of photons in OPRA takes place in between the processes of de-scanning and re-scanning, the scanning unit has a significant impact on the imaging properties. The scanning unit has to fulfil several properties, which are sometimes opposing each other. Some important properties are:

- Scan speed

As OPRA is a processing free method and there are cameras with frame rates in the MHz range available, the imaging speed mainly depends on the scanning. As long as the other properties as flatness and mirror size could be maintained, a faster scanner is preferable but the reduced pixel dwell time has to be considered. For same laser power, the illumination density decreases with increasing scan speed and associated camera frame rate (caused by reduced pixel dwell time). Therefore, it is possible to scan the FOV multiple times per camera frame to reduce read-out-noise and bleaching.

- Mirror properties: flatness

As the light is in total three times reflected by the scanning mirror in OPRA, optical properties as reflectivity and flatness are important. Especially the flatness is a crucial property, as very flat mirrors have to be very thick and therefore are relatively heavy which prevents them from fast scanning. As long as mirrors are used, always a compromise between scan speed and flatness has to be made. The use of mirror-free scanners as AODs for imaging, is not suitable as they don't have the quality regarding beam shape.

- Mirror properties: size

As the scan unit is placed in the parallel beam path of the point scanning microscope, the diameter of the beam is determined by the beam expander composed of scan and tube lens. In the aim of a relatively short optical beam path a bigger mirror is favourable. Also it has to be considered, that for Zeiss objectives the colour correction is made for specific tube-lenses with a fixed focal length.

- Position along conjugated planes

Especially for 2D-scanning units, it is very difficult to arrange the rotational axes of the scanning devices in a BFP. Due to multiple transits, the alignment in OPRA becomes more challenging. Compensating concave mirrors or additional optics between the two scan mirrors are complicated to use in OPRA, as the second transit of the fluorescent light is not directly on the optical axis any more.

- Scan shape

The very fast resonant scanners have the disadvantage of a sinusoidal scan shape, causing a longer illumination and pixel dwell time at the edge of the FOV. This can be compensated by pockels cells or acousto-optic modulators (AOM) which adapt the intensity of the excitation light to the pixel dwell time which results in a homogeneous illumination pattern [80]. For more advanced techniques as structured illumination in combination with OPRA a precise movement of the scanner is necessary.

This properties has to be considered while constructing an OPRA system [SR1, SR3]. The optical system which was published in 2013 [SR1] has the advantage of a very fast resonant scanner (15kHz) for the fast scan axis which allows image frames up to 120 frames per second with a relatively large FOV (250 lines for the slow axis). As seen in figure 5.9 the fast resonant scanners (SMX) works only in one scan direction and therefore a second 1D-scanning mirror for the slow axis has to be installed (SMY1). Here we used a second scanner (SMY2) for the slow scan axis to project the conjugated plane, which is placed on the rotational axis of the fast mirror (SMX), onto the slow axis scanner (SMY1). To achieve this projection, both slow axis scanner move in phase with different amplitudes. The ratio of the amplitude is constant, as only small angles has to be considered. Unfortunately the galvanometric scanners used in our setup (Cambridge Technologies Inc.) have not the required flatness for imaging and therefore causing aberrations in the resulting images.

A different approach for the scan unit is used in [SR2, SR3] where a optical beam scanner with two rotational axes (S-334.2SL with E-517 controller, Physik Instrumente GmbH, Germany) is used. This scan system is relatively slow but has the advantage, that both scanning axes are in the same plane with the BFP. Also the scan shape can be controlled precisely to avoid sinusoidal scan pattern and, as the slow axis can be moved step-wise, the generation of a structured illumination pattern is possible (see also chapter 5.3). Another big advantage of this system is the flatness and size of the mirror (mirror size of 1cm in diameter with specified flatness of  $\lambda/10$ ) which made this system applicable for high NA measurements. The optical system can be seen in figure

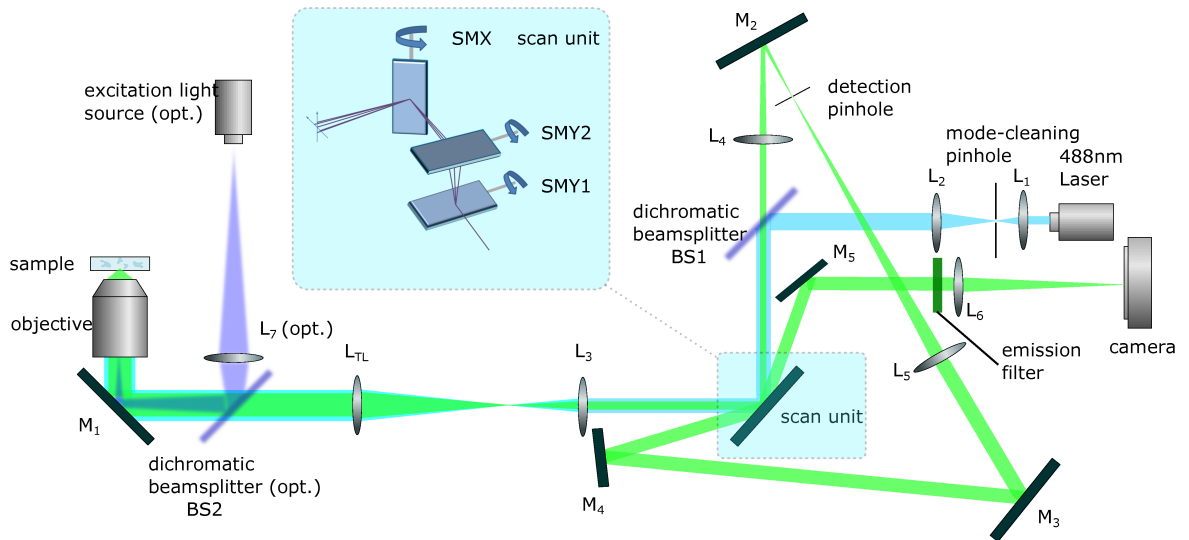


**Figure 5.9:** Optical setup of OPRA with a 15kHz resonant beam scanner allowing camera frame rates up to 120Hz. As the resonant scanner (SMX) scans only in one direction, the second scanner for the slow scan axis can't be placed into the conjugated plane. To avoid image distortion, a second slow scanning mirror (SMY2) is placed into the beam path to project the conjugated plane onto the slow axis scanner (SMY1). Extended description of the optical setup: The light from the 488nm laser passes a clean-up ( $f_1=50\text{mm}$ ;  $f_2=100\text{mm}$ ) and is reflected by the dichromatic beam splitter (BS) and directed to the scan unit. The second beam expander ( $f_3=60\text{mm}$ ;  $f_{\text{TL}}=400\text{mm}$ ) provides the over-illumination of the objective BFP. After descanning, the fluorescent beam is expanded by a factor of two realizing the reassignment of the photons in the pinhole plane ( $f_4=200\text{mm}$ ;  $f_5=400\text{mm}$ ). After the expansion the beam is rescanned and projected to the camera ( $f_6=200\text{mm}$ ). For comparison with widefield microscopy an excitation light source, the optional (opt.) lens  $L_7$ , and a dichromatic beam splitter (BS2) were added to the setup. This image is reprinted with permission and can be found in [SR1].

5.10 where a picture of the setup is shown besides the optical scheme.

## 5.2 Superconcentration of light

To achieve superresolved images, the density of fluorescent labels needs to be increased and the illumination and detection sampling has to be adapted. That means that the necessary energy density increases if the resolution is increased. This increased illumination density leads to unwanted bleaching and photo-toxic effects. Especially in live-cell-imaging it is very important to observe the biological processes without influencing them by laser radiation and therefore the illumination density has to be as small as possible. Other superresolution methods need either very high laser power (STED) or are very slow as they need a lot of camera frames per superresolved image (pointillistic methods like STORM, dSTORM, PALM etc.). SIM as widefield

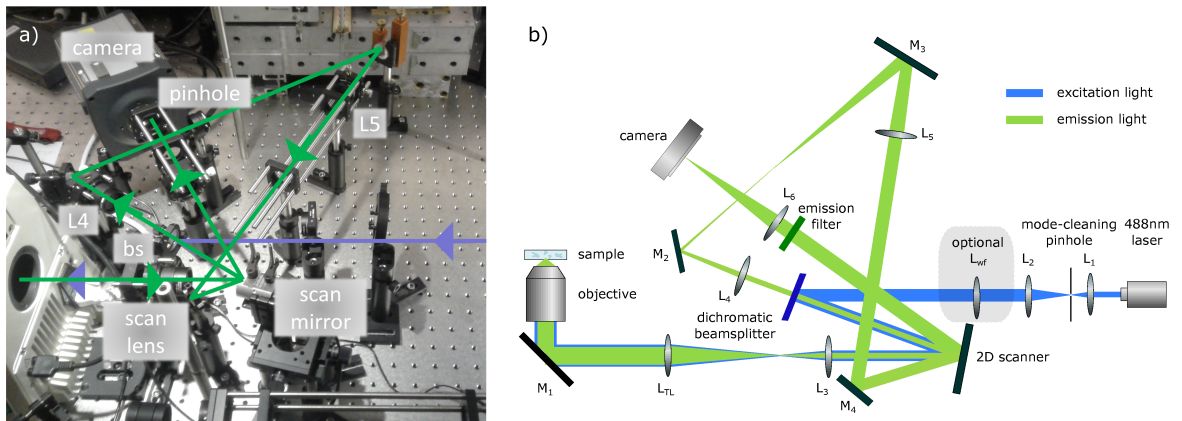


**Figure 5.10:** Setup of OPRA with a 2D scanner for precise beam control showing an optical realization of the reassignment principle. Lenses  $L_1$  and  $L_2$  (with respective focal lengths  $f_1=50\text{mm}$  and  $f_2=100\text{mm}$ ) are used as laser clean up. To properly over-illuminate the BFP of the objective, a second beam expander is used ( $f_3=60\text{mm}$ ,  $f_{TL}=400\text{mm}$ ). The fluorescent light is descanned and separated from the excitation light using the aforementioned dichromatic beam splitter. After descanning, the optical reassignment takes place by expanding the fluorescent beam by a factor of 2 ( $f_4=200\text{mm}$ ,  $f_5=400\text{mm}$ ) resulting in a demagnification of the resulting pinhole image on the detector ( $m = 0.5$ ). Using the 2D scanner again, the demagnified pinhole image is projected with the correspondent scan position via the lens  $L_6$  ( $f_6=200\text{mm}$ ) on the camera. The figure 5.10b) is reprinted with permission and can be found in [SR2].

technique needs at least 9 frames per slide to acquire highly resolved images. This gives a good compromise regarding number of image frames and low illumination density achieving up to 79 frames per second [41]. In this point of view OPRA is really unique in its properties as it acquires superresolved images in one camera frame without losing any light which is captured by the objective. Even if it is possible to construct a rescanned "direct-view" version of a STED microscope to acquire superresolved images in only one frame, it is in the fundamental principle of STED microscopy that most of the light, which is emitted by the fluorophore, is lost in the stimulated emission process and therefore does not contribute to the signal.

From this point of view, methods linked to the reassignment principle form a completely new approach in achieving superresolved images. Instead of losing fluorescent photons, all emitted photons contribute to the image performance. Already in the first publication on the Optical Photon Reassignment microscopy [SR1] this very promising and important effect of improved peak-intensity was mentioned. Sheppard et al. [72] conclude in their theoretical analysis of the reassignment technique, that a peak-intensity enhancement of 1.84 for the PSF can be expected. Also other authors in this field referred to the high photo-efficiency of optical realizations of the reassignment

principle [25, 56]. This is very remarkably, as confocal microscopy is normally known to be more photo-toxic than widefield microscopy and normally all the superresolution techniques are less photo-efficient [82, 83]. It has to be considered, that a better peak-intensity does not automatically lead to less photo-toxicity in the sample, but it is one of the most important properties for light-efficient microscopes. There is also a huge potential to reduce photo-damage and photo-toxicity by developing new fluorophores towards live-cell imaging. From the optical point of view good light collection and light concentration properties are a key aspect of research.

To study the light concentration of this fluorescent microscopy technique, the complex photo-chemical reactions in the sample has to be treated as linear process between fluorescence excitation and detection. Roth et al. analysed the enhanced photo-efficiency by developing a measurement scheme to verify the theoretical predictions made by Sheppard et al. [72, SR2]. It could be found, that the all-optical realization of the reassignment principle indeed leads to enhanced peak-intensities even though this seems to be prohibit by the fundamental optical law of étendue conversation. As the method of OPRA directly achieves superresolved images in only one single camera frame by simultaneously preserving all the emitted light supported by the objective's NA, it is possible to circumvent, the resolution barrier and simultaneously seemingly the concentration barrier of light. The étendue is defined as product of opening angle (in microscopy this is the NA) and the area which is crossed by a light-beam in an optical system (with the normal parallel to the beam's Poynting vector). This Lagrangian invariant is constant for ideal systems and increases for a real system. While in OPRA the active scanning system is used to generate the images, it is possible to circumvent these fundamental law in optics. A look in the literature shows that the étendue conversation is only valid for passive systems and is therefore consistent with our active scanning approach [84, 85]. While using the time as an information transporting channel, it is possible to circumvent this limit of light concentration. In [SR2] it is written: "The fundamental limit is still valid at every single time point, but overall it is circumvented, as our system, by design, integrates knowledge about localized sequential illumination and detection into a single scheme. The reason that the fundamental limit can be overcome in this case is time sequential scanning."

To quantify the absolute peak-intensity of a fluorescent bead captured by different imaging methods, is not straight-forward and many constraints have to be fulfilled.

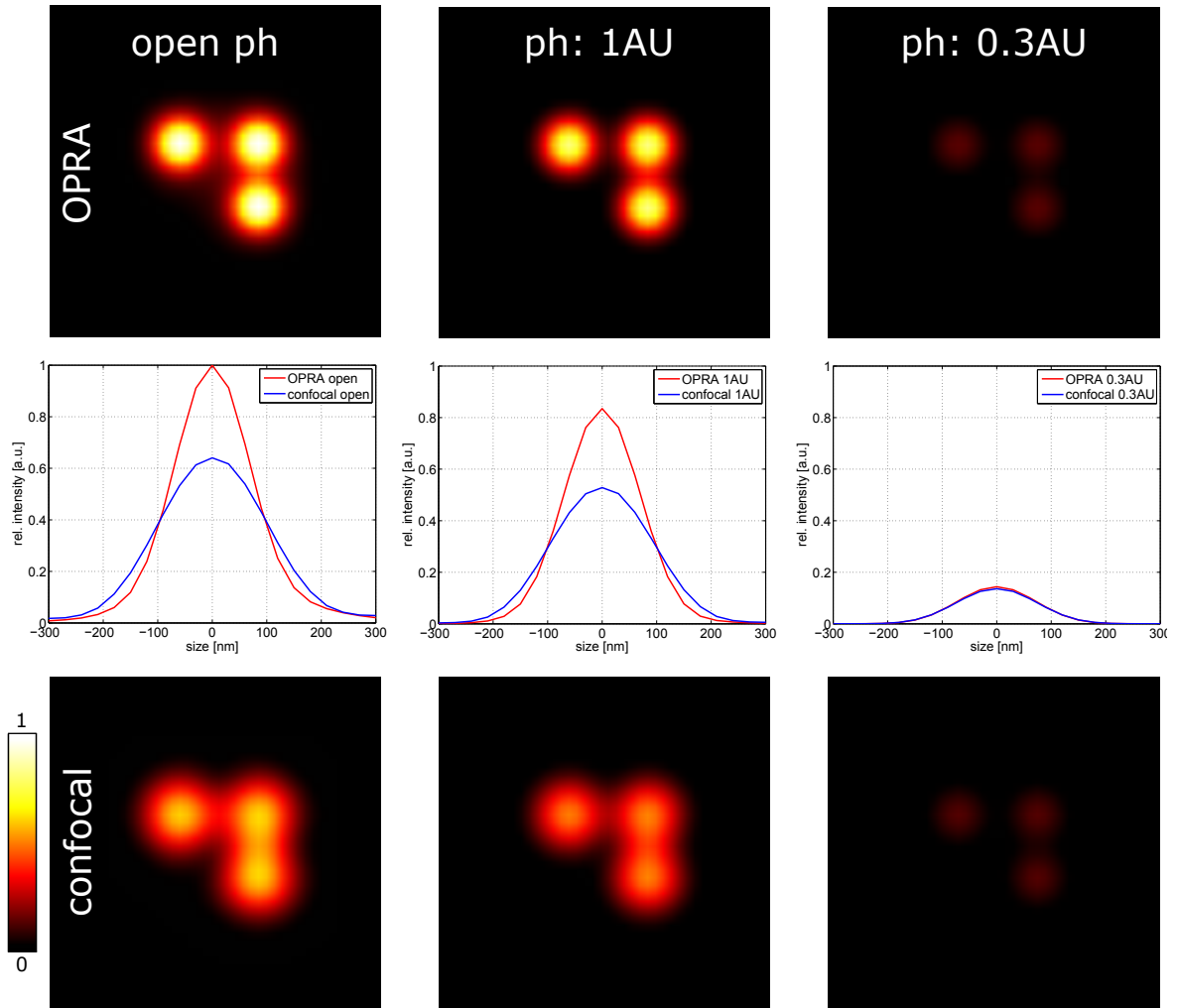


**Figure 5.11:** This numerical simulation compares the resolution of OPRA and confocal microscopy for different detection pinhole (ph) sizes on point objects. The line traces show the corresponding one-dimensional PSF. In contrast to figure 5.8 all images are normalized to the PSF of OPRA with no detection pinhole illustrating the enhanced signal. Besides the already discussed resolution behaviour, it has to be noted, that OPRA achieves enhanced peak intensity. This is remarkably, as the resolution of a confocal microscope increases if the pinhole diameter and therefore the signal level decreases. OPRA reaches the upper resolution limit of confocal microscopy while simultaneously increasing the peak intensity even if no detection pinhole is used. Simulation parameters:  $NA=1.2$ ,  $\lambda_{ex}=488\text{nm}$ ,  $\lambda_{em}=525\text{nm}$ , point distance:  $300\text{nm}$  (horizontal) and  $240\text{nm}$  (vertical).

The main goal of the measurements setup presented in [SR2] was to limit the number of constraints to a small number. To account for different parameters as illumination dose, sampling or absorption of optical components a normalization has to be done. It could be found that a normalization with a homogeneous fluorescent plane fulfils this requirements and only the linearity of the photo-response has to be guaranteed. This means, that the scanning for OPRA should be very slow, as the maximum illumination dose for LSM is relatively high compared to widefield microscopy. In [SR2] this general concept was supported by a setup which needs no changes in the imaging beam path while switching between the two imaging modes of widefield and OPRA microscopy. Only the illumination part has to be adapted while inserting a lens and the beam scanner has to be stopped. The use of a homogeneous fluorescent plane for normalization and quantification could be used for a theoretical analysis of different microscopy methods and was used in [SR4].

### 5.3 OPRA in three dimensions

The reassignment principle can be described as a two dimensional effect as the reassignment of the photons takes place in a image plane. However, as biological specimen are normally not restricted to two dimensions, a deep analysis of the imaging conditions of OPRA in three dimensions is required. There are many arguments why OPRA is very suitable for imaging in three dimensions. In contrast to widefield techniques ORPA features the advantage of laser scanning microscopes for three dimensional imaging as the illumination is not uniform along the axial axis. Corresponding to the excitation PSF, every single illumination spot excites dominantly in the focal plane, which gives less out-of-focus light for every single excitation position. However, the average out-of-focus illumination light in LSM is the same as in widefield microscopy. The possibility of inserting a detection pinhole in the beam path of OPRA gives the ability to transform OPRA into a confocal microscope with reassignment properties. The influence of the pinhole on the imaging performance of OPRA is analysed in the next section. Even if no detection pinhole is inserted, there are options to improve the resolution along the third dimension. In addition structured illumination together with digital image processing gives the chance to suppress unwanted out-of-plane fluorescence. A detailed analysis of the interaction of detection pinhole and structured illumination on the imaging properties of OPRA is presented in [SR3].

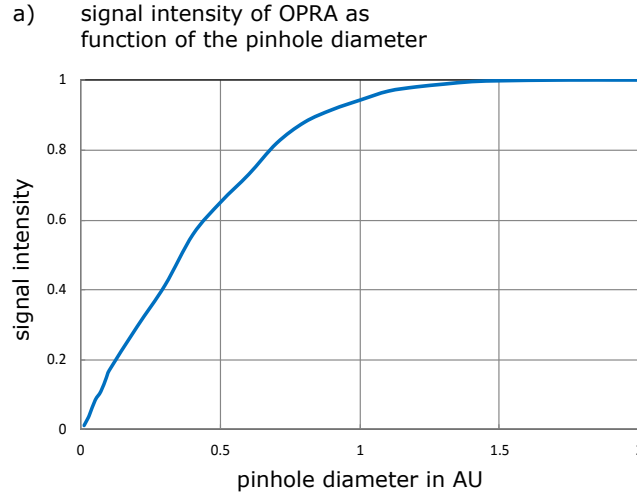


**Figure 5.12:** Signal intensity in OPRA as function of the pinhole diameter. The relative peak-intensity of OPRA with increasing pinhole diameter is shown. Only for pinhole diameters bigger than 1.5 Airy units the full signal level is achieved. Note that the full signal level of OPRA is equal to 1.84 the peak intensity of widefield emission. Simulation parameters:  $NA=1.4$ ,  $\lambda_{ex}=488nm$ ;  $\lambda_{em}=525nm$ .

### 5.3.1 The influence of a detection pinhole in OPRA

As in confocal microscopy the pinhole in OPRA can be used to suppress unwanted out-of-plane fluorescence. As seen in equation (3.4) the PSF of a standard confocal microscope can be described as:

$$\begin{aligned}
 \text{PSF}_{\text{confocal}}(\mathbf{x}) &= \int \text{PSF}_{\text{ex}}(\mathbf{x}) \cdot \text{PSF}_{\text{det}}(\mathbf{x} - \mathbf{s}) \cdot \text{ph}(\mathbf{s}) d\mathbf{s} \\
 &= \text{PSF}_{\text{ex}}(\mathbf{x}) \cdot \int \text{PSF}_{\text{det}}(\mathbf{x} - \mathbf{s}) \cdot \text{ph}(\mathbf{s}) d\mathbf{s} \\
 &= [\text{PSF}_{\text{ex}} \cdot (\text{PSF}_{\text{det}} \otimes \text{ph})](\mathbf{x}).
 \end{aligned} \tag{5.13}$$

Here  $\otimes$  describes the convolution operator,  $\text{ph}$  the pinhole function and  $(\mathbf{x})$  and  $(\mathbf{s})$  are the image coordinates in three dimensions. The best resolution is achieved for a  $\delta$ -distribution as pinhole function.

The image formation of OPRA including a pinhole can be described according to (5.7) with the integral:

$$\text{PSF}_{\text{OPRA}}(\mathbf{x}) = \int \text{PSF}_{\text{ex}}(\mathbf{s}) \cdot \text{PSF}'_{\text{det}}\left(\frac{\mathbf{x}}{1-m} - \mathbf{s}\right) \cdot \text{ph}'(\mathbf{x} - \mathbf{s}) d\mathbf{s}. \tag{5.14}$$

Here  $\text{ph}'$  is the magnified pinhole-function  $\text{ph}'(\mathbf{x}) = \text{ph}(\mathbf{x}/m)$ . Contrary to equation (5.7) it is not possible to convert this integral into a convolution integral and therefore



the analysis has to be done numerically.

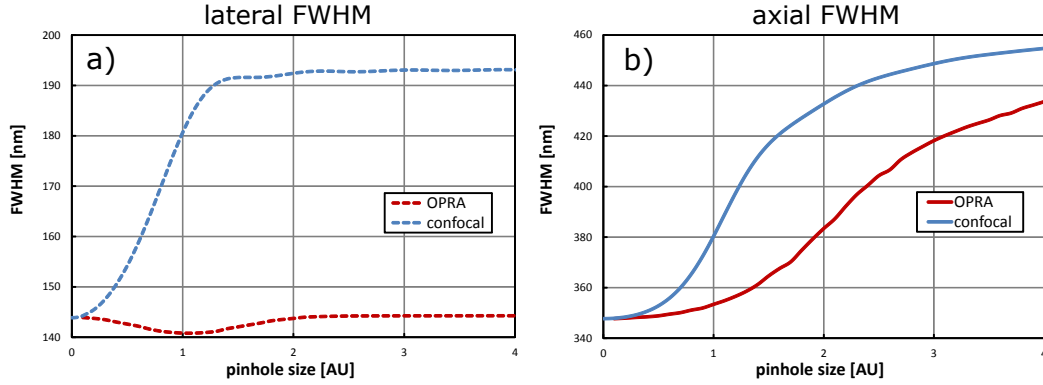


**Figure 5.13:** Numerical simulation of the full width at half maximum (FWHM) of the PSF of OPRA and confocal microscopy in the focal plane a) and along the optical axis b) in dependence on the pinhole diameter. The FWHM in OPRA is always improved in comparison to a confocal system. In the focal plane there is nearly no dependency of the lateral PSF width in OPRA, where the resolution of a confocal system decreases significantly as the pinhole size increases. Along the optical axis the size of the PSF width increases in OPRA for increasing pinhole diameter, but not as steep as in a confocal microscope. This is important, as the signal level is strongly linked to the pinhole diameter and decreases massively for values smaller than 1 AU (see figure 5.12). The values for this simulation were set to: NA=1.4; excitation wavelength: 488nm; emission wavelength: 525nm;  $n=1.518$ . This figure is reprinted with permission and can be found in [SR3].

Even though the reassignment principle is in general a two-dimensional effect it has also impact on the imaging properties along the axial dimension. Especially as OPRA is a laser scanning technique with the ability to insert a detection pinhole in the beam path it is possible to connect the high peak intensity of OPRA in the imaging plane with sectioning properties of confocal microscopy along the optical axis. As known from confocal microscopy, the signal level decreases with decreasing size of the pinhole [63]. In figure 5.12 the signal intensity of  $\text{PSF}_{\text{OPRA}}$  is shown as a function of the pinhole diameter visualizing the negative effect of small pinhole diameters (diameter smaller than 1AU) on the signal level. For pinholes bigger than 1.5AU the signal decrease can be neglected, making a combination of OPRA and large pinhole diameters reasonable. Figure 5.13 underlines this assumption, showing that OPRA with pinhole diameter above 1AU still shows very good results regarding the FWHM of the PSF in the image plane and along the optical axis. This is relevant, as the lateral resolution improvement of a confocal microscope in the ideal case (pinhole  $\hat{=}$   $\delta$  - function), nearly vanishes for a pinhole diameter larger as 1AU. For the axial direction the resolution of a confocal microscope drops dramatically for larger pinholes, where OPRA still achieves high

resolution even for pinhole diameter  $\approx 1.5$  AU.

### 5.3.2 Resolution enhancement by structured illumination

As outlined in the previous section, the use of a small detection pinhole is linked with loss in intensity. On the other hand, the axial resolution deteriorates if a large pinhole is used. Therefore the integration of a relatively large pinhole in combination with structured illumination to improve the sectioning ability seems a promising method to optimize sensitivity, contrast and resolution. This section gives a summary about the analysis presented in [SR3] and some further information on the sectioning behaviour of OPRA combined with structured illumination.

The presence of structured illumination gives the ability to achieve an improvement in sectioning via post-processing the data. It is important to notice, that the discussed structured illumination is not high-resolution SIM (HR-SIM) as only one direction of the illumination pattern is generated and the pattern is relatively coarse compared to the Abbe limit.

To generate the illumination pattern in [SR3] a piezo controlled 2D beam scanner (S-334.2SL with E-517 controller, Physik Instrumente GmbH, Germany) is used. The fast scan axis moves in a sinusoidal curve while the slow axis steps precisely, generating a striped pattern with a period of approximately 312nm. The whole sample is illuminated while moving the pattern by  $1/N$  of the period for each of the  $N$  acquired images. This structured data can be used to further improve the out-of-focus suppression even if it is not possible to insert a detection pinhole into the beam path.

The simplest way of processing is a simple summation of all phase images per slice. This calculation is always performed as reference because the resulting image should be equivalent to a normal OPRA image. The mean of all images is represented by:

$$\text{Mean}(\mathbf{r}) = \frac{1}{N} \sum_{n=1}^N I_n(\mathbf{r}). \quad (5.15)$$

Here  $(\mathbf{r})$  represents the three dimensional image coordinate,  $I_n$  the image of phase  $n$  of  $N$  phases in total. A relatively easy approach achieving reasonable sectioning results, is the MaxMin approach [86]:

$$\text{MaxMin}(\mathbf{r}) = \max_{n=1\dots N} I_n(\mathbf{r}) - \min_{n=1\dots N} I_n(\mathbf{r}). \quad (5.16)$$

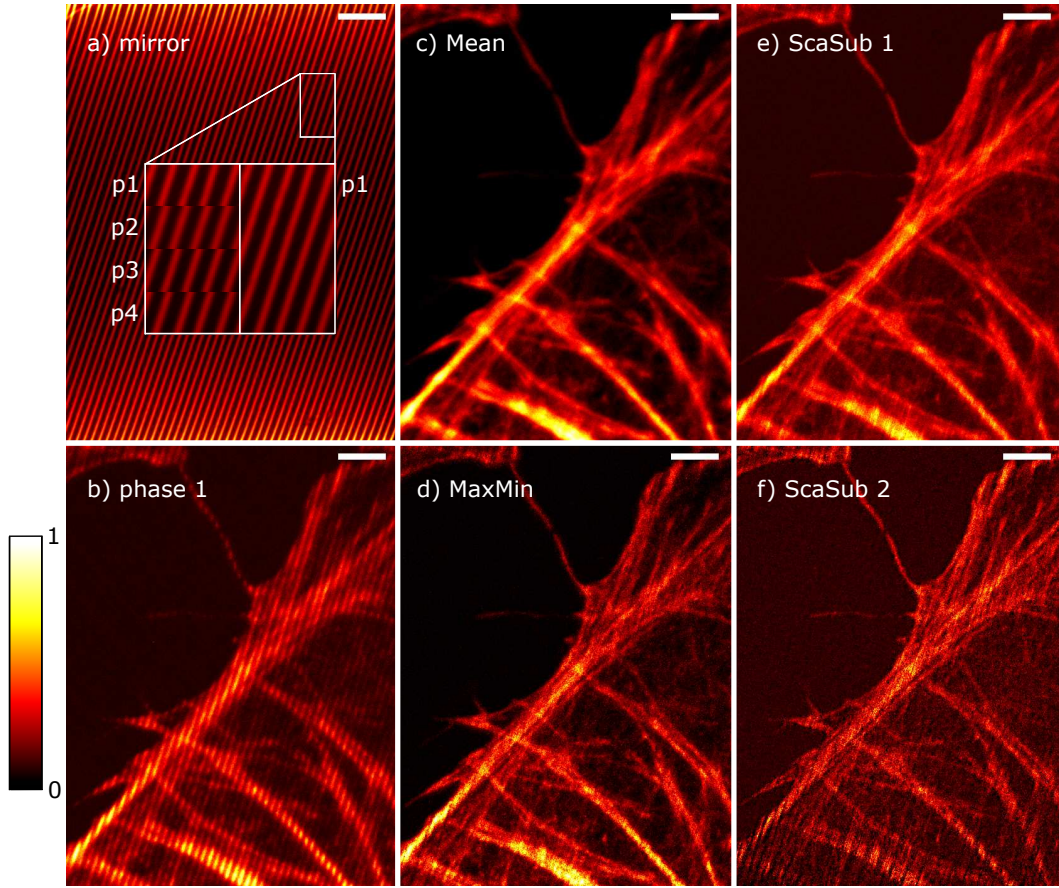


**Figure 5.14:** Principle of OPRA with structured illumination. In a) the measurement principle of OPRA with combined structured illumination is illustrated while showing the four different illumination phases (p1 to p4) on a mirror sample. In b) the pattern of phase 1 is visible while illuminating actin filaments of a BPAE cell. In c) the Mean-image of all 4 phase steps, which was calculated according to equation (5.15), is shown. The MaxMin-image 5.14d) (see equation (5.16)) gives already more crispy images and enhanced resolution. The ScaSub 1 image in e) was calculated with equation (5.20) ( $\alpha = 1/5$ ) and gives even finer details than d). In f) the ScaSub 2 was calculated while setting  $\alpha$  to  $1/3$ , achieving a better sectioning effect and making finer details visible. On the other hand, this image is affected by noise and illumination artefacts. Imaging parameters:  $NA=1.4$ ,  $\lambda_{ex}=488nm$ , scalebar:  $2\mu m$ . This figure is reprinted with permission and submitted in [SR3].

To further improve the ability to suppress the out-of-focus light Neil et al. suggested to use the images of opposing phases to determine and subtract the out-of-focus contribution [87–89]:

$$Neil(\mathbf{r}) = \sqrt{\sum_{n=1}^N (I_n(\mathbf{r}) - I_{(n+N \text{ div } 2) \bmod N}(\mathbf{r}))^2}. \quad (5.17)$$

Here *mod* is the modulo (giving the remainder after division) and *div* the integer

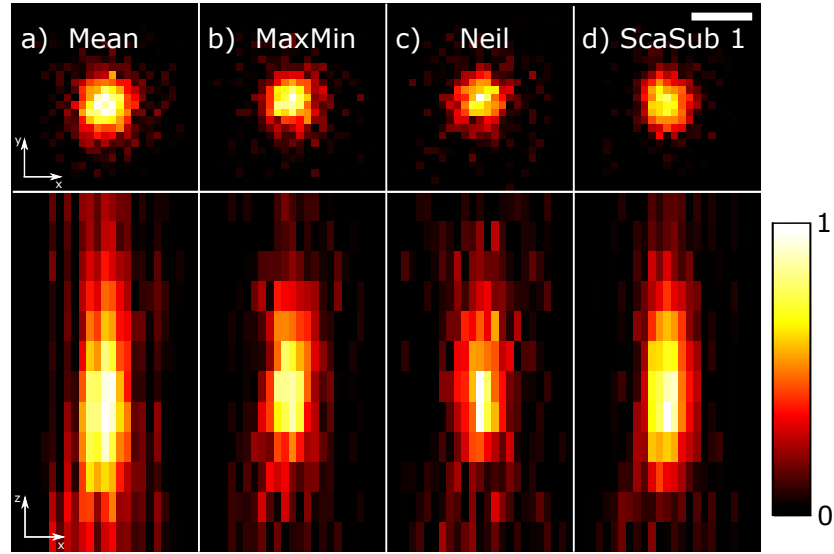


**Figure 5.15:** Three dimensional PSF for OPRA with structured illumination for different reconstruction methods when no detection pinhole is added to the detection beam path. It shows the measured 3D PSF for different reconstruction algorithms according to equations (5.15) - (5.20) showing a resolution enhancement along the optical axis and in the image plane. The corresponding width of the PSF are listed in the table in [SR3]. The scale bar is  $2\mu\text{m}$ .

division operator (finding the quotient) in Euclidean division. For this algorithm an even number of phase steps has the advantage that illuminated and not illuminated areas are equally distant to each other. In the setup in [SR3] the total number  $N$  of phase steps was set to four, thus equation (5.17) becomes

$$\text{Neil}(\mathbf{r}) = \sqrt{(I_1 - I_3)^2 + (I_2 - I_4)^2 + (I_3 - I_1)^2 + (I_4 - I_2)^2}. \quad (5.18)$$

This approach yielded good results regarding sectioning but the images suffer from noise (see figure 5.15). As OPRA uses a camera for imaging, it can easily be used to record the illumination pattern by illuminating a fluorescent plane. This pattern is described by the mask $_n(\mathbf{r})$  (5.19). As the mask can be either binary or smooth, there is also the possibility to account for different illumination intensities over the FOV and imperfections in the illumination pattern. Here a mask was used which fulfils the condition [88]:

$$\sum_{n=1}^N \text{mask}_n(\mathbf{r}) = 1; \forall(\mathbf{r}), \quad (5.19)$$

$$\text{ScaSub}(\mathbf{r}) = \sum_{n=1}^N I_n(\mathbf{r})\text{mask}_n(\mathbf{r}) - \alpha \sum_{n=1}^N I_n(\mathbf{r})(1 - \text{mask}_n(\mathbf{r})). \quad (5.20)$$

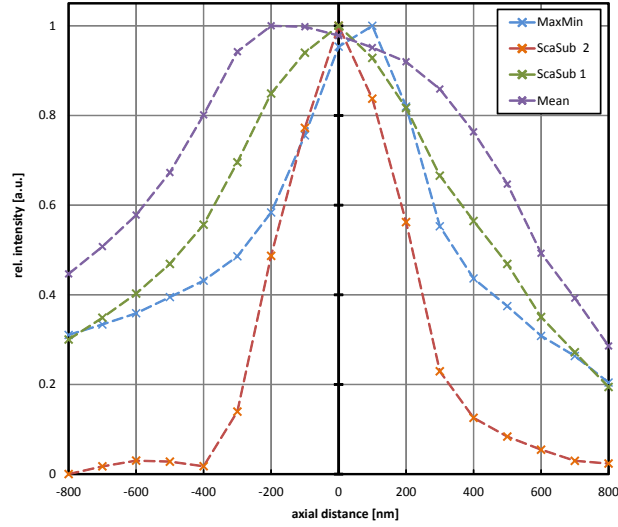


**Figure 5.16:** Mean intensity as function of the distance along the optical axis for OPRA with structured illumination. This figure compares the mean intensity along the optical axis of the data presented in figure 5.14 for different analysis methods in OPRA with structured illumination. To compare the different methods an out-of-focus offset was subtracted and the data was normalized to its modulation depth. This figure visualizes the enhanced sectioning performance of OPRA with structured illumination depending on the analysis method. It can be clearly seen, that the processing improves the sectioning performance. Also it has to be noted, that the image with the best sectioning performance (processed with the ScaSub 2 algorithm (see equation (5.20) and figure 5.14f)) is affected by noise and therefore is not the best image for a human observer.

To achieve a good compromise between background-signal-suppression and increase in SNR, the scaling factor  $\alpha$  should be adapted to the imaged sample properties. For ScaSub 1,  $\alpha$  is set to  $\alpha = 0.2$  and for ScaSub 2,  $\alpha$  is set to  $1/3$ . In figure 5.16 it can be seen, that ScaSub 2 achieves nicely sectioned data but with noisier images (see figure 5.14f). This trade-off can be adapted while setting the scaling factor  $\alpha$  accordingly. In figure 5.14e) the background is still very prominent, as in figure 5.14f) the sectioning is clearly enhanced as the image is simultaneously affected by noise.

Measured PSFs using OPRA with structured illumination pattern and subsequent image reconstruction is displayed in figure 5.15. Here a sample with fluorescent beads (FluoSpheres® Carboxylate-Modified Microspheres,  $0.11 \mu\text{m}$ , Yellow-Green Fluorescent 505/515) was imaged with a striped pattern and processed with the discussed algorithms. To generate the three dimensional PSF, the images of 22 beads were analysed. Therefore the single bead-images were cut, overlaid and the sum was fitted with

a three dimensional Gaussian function. Even if no detection pinhole is included, the improved resolution in the image plane and along the axial axis is apparent. To visualize the imaging principle, figure 5.14a) shows the illumination mask for each of the four phase steps. Figure 5.14b) shows a raw image of one illumination phase exciting the sample of a BPAE cell (Bovine Pulmonary Artery Endothelial Cells, stained with Alexa Fluor 488 Phalloidin, FluoCells Prepared Slides 1, Molecular Probes Inc.). In the figures 5.14c) to f) different processing algorithms were applied.

Figure 5.16 shows the mean intensity  $I(z)$  of the data presented in figure 5.14 per slice plotted along the optical axis. It has to be noted, that these curves were normalized to their modulation depth. Here  $z$  is the actual  $z$ -position and  $Z$  is the total number of slices.

$$I(z) = \frac{I(z) - \min_{z=0\dots Z} I(z)}{\max_{z=0\dots Z} I(z) - \min_{z=0\dots Z} I(z)} \quad (5.21)$$

As the FWHM of this curves can be reduced significantly for different processing procedures, the out-of-focus fluorescence suppression can be increased.

In this section we presented a detailed analysis of the 3D performance of OPRA. We further developed a measurement regime of combining pinholed OPRA data acquisition with pattern illumination to enhance imaging properties like background suppression. This scheme for data acquisition combines the most promising properties of OPRA like high sensitivity with the high sectioning performance of confocal or structured illumination microscopy. As the theoretical simulation in figure 5.13, the measurements results in [SR3] and the data in figure 5.14 show, the microscopy methods related to the reassignment principle in general and OPRA in particular have the potential to replace confocal microscopy as the standard tool in biological imaging.

## 5.4 Conclusion and outlook

In this thesis a promising new superresolution technique called Optical Photon Reassignment microscopy (OPRA) was introduced, analysed and applied to the field of fluorescence microscopy. The microscopy concept, together with proof-of-principle experiments and a mathematical framework, was published and patented in 2013 [24, SR1]. The method combines several important properties of fluorescent imaging in a unique way. This combination is very important for the development towards non invasive live-cell imaging. The key properties of OPRA are:

- Two-fold resolution enhancement to widefield microscopy, if compared to the cut-off frequency described by Abbe (equation (3.3)) in the focal plane. If resolution is described as region of support in frequency space, OPRA achieves a doubling of the cut-off frequency in the lateral directions. Therefore the FWHM of  $\text{PSF}_{\text{OPRA}}$  decreases by a factor of  $\sqrt{2}$ , if Gaussian PSF are assumed in the focal plane.
- Superresolution which is suitable for extremely fast imaging. As the photon reassignment happens during the de- and re-scan process, the achieved resolution is not limited to any processing time or needs the acquisition of several images. The imaging speed of the method is therefore mostly limited to the scan speed. This is a system inherent advantage to other superresolution techniques as SIM or the pointillistic methods as PALM or STORM.
- Superconcentration of light, meaning extremely sensitive detection with an increase in peak-intensity compared to widefield microscopy. The superconcentration effect describes the increase in light concentration beyond classical limits. In other superresolution techniques the light is usually not concentrated better than the classical limits predicts, as the resolution enhancement is achieved via multiple image frames (e.g. SIM and pointillistic methods), with the loss of fluorescent light during the process by stimulated emission (e.g. STED) or the use of diaphragms (e.g. confocal microscopy). This unique feature of optical reassignment methods has the ability to revolutionise the field of fluorescent microscopy, as it is possible to be less affected by the trade-off of resolution and illumination dose. Therefore the optical reassignment methods have the ability to replace confocal microscopy as the standard technique in biological imaging. This property is described in detail and supported by a quantitative measurements and published 2016 in Optics Letters [SR2]. The theoretical background of this measurement concept was used for a general comparison of the microscopes OTF [SR4].
- Improved axial resolution by combination with structured illumination. We presented a method to enhance the resolution along the optical axis by more than 10% over a confocal microscope preserving the superconcentration properties of OPRA. There is a classical trade-off in confocal laser scanning microscopy between sectioning performance and signal intensity as the detection pinhole

suppresses parts of the signal. It could be shown that this relation doesn't apply to OPRA in combination with structured illumination as the axial resolution could be improved while using large pinholes essentially maintaining the signal intensity. This illumination concept and measurement results on fluorescent beads and biological data are presented in [SR3].

- Versatility of the general concept of the reassignment principle. It is possible to adapt OPRA to the specific requirements of the biological experiment. For example, it is possible to parallelize the concept [27, 55] and to expand the method to pulsed excitation and work with multi-photon absorption fluorescence [80, 81]. There are no specific requirements to the sample preparation and therefore the method is suitable for imaging almost every fluorophore or fluorescent protein. This is an advantage over the single molecule methods such as STORM and PALM and over STED microscopy where the development of specific fluorophores is a challenge and field of ongoing research [40, 43].

As the resolution of optical reassignment methods is limited, other non-linear superresolution methods have advantage regarding resolution. But the combination of the listed properties make the optical reassignment methods promising fluorescent microscopy techniques with the potential to replace the confocal microscope as standard technique for biomedical imaging. Especially because of the instantaneous superresolution behaviour, OPRA in the parallelized realization is suitable for imaging of fast processes in living cells and is therefore a promising technique to help solving important biomedical questions in the coming decades of research. These properties of the optical reassignment methods lead to the development of several commercial products as the Re-Scan Confocal [25, 26], the spinning-disk variant (SD-OPR) by Yokogawa Electric Corporation [27, 28] or the multi-beam realisation called Vt-Sim by Visitech Int. [29].



## 6 Publications

### 6.1 Optical Photon Reassignment Microscopy (OPRA) [SR1]

Stephan Roth, Colin J.R. Sheppard, Kai Wicker and Rainer Heintzmann

*Optical Nanoscopy*, 2:5, (2013)

Stephan Roth	Designing, developing and building the microscopy setup, data acquisition and analysis, preparation of the manuscript
Colin J.R. Sheppard	Discussion of general aspects of the basic concept
Kai Wicker	Discussion of general aspects of the basic concept and developing of mathematical formalism
Rainer Heintzmann	Supervision of the project and discussion of the microscopic setup.

All authors revised, edited and proof read the manuscript and contributed to the general concept of reassignment microscopy.

Stephan Roth, Colin JR Sheppard, Kai Wicker, and Rainer Heintzmann. Optical photon reassignment microscopy (OPRA). *Optical Nanoscopy*, 2(1):5, 2013. ISSN 2192-2853. doi: 10.1186/2192-2853-2-5. URL <http://www.optnano.com/content/2/1/5>

**ORIGINAL ARTICLE****Open Access**

# Optical photon reassignment microscopy (OPRA)

Stephan Roth<sup>1,2</sup>, Colin JR Sheppard<sup>3</sup>, Kai Wicker<sup>1,2</sup> and Rainer Heintzmann<sup>1,2,4\*</sup>

**Abstract**

To enhance the resolution of a confocal laser scanning microscope the additional information of a pinhole plane image taken at every excitation scan position can be used (Sheppard 1988). This photon reassignment principle is based on the fact that the most probable position of an emitter is at half way between the nominal focus of the excitation laser and the position corresponding to the (off centre) detection position. Therefore, by reassigning the detected photons to this place, an image with enhanced detection efficiency and resolution is obtained. Here we present optical photon reassignment microscopy (OPRA) which realizes this concept in an all-optical way obviating the need for image-processing. With the help of an additional intermediate optical beam expansion between descanning and a further rescanning of the detected light, an image with the advantages of photon reassignment can be acquired. However, just as in computational photon reassignment, a loss in confocal sectioning performance is caused by working with relatively open pinholes. The OPRA system shares properties such as flexibility and ease of use with a confocal laser scanning microscope, and is therefore expected to be of use for future biomedical routine research.

**Keywords:** Photon reassignment; Image scanning microscopy; Confocal laser scanning microscopy

**Introduction**

Confocal laser scanning microscopy (CLSM) is an established tool in fluorescence microscopy and well-known for its optical sectioning ability and high contrast (Pawley 2006; Minsky 1961). These characteristics are achieved by using detectors with a high dynamic range and collecting the emitted light through a pinhole, which is usually aligned to the position of the excitation focus (thus the name “confocal”). The resulting image is constructed by assigning the detected intensity to the corresponding excitation scan position. In 1982 it was shown that it is possible to achieve enhanced resolution by applying an off-axis pinhole (Cox et al. 1982). In 1988 pinhole plane image detection and computational reassignment to a position half way between nominal excitation and detection position was proposed (Sheppard 1988), to improve detection efficiency and resolution. Note that for identical excitation and emission point spread functions (PSF) this reassigned position corresponds to the most probable position of an emitter in the sample. Recent work applied this principle in single

(Müller & Enderlein 2010) and multispot excitation (York et al. 2012) to the imaging of biological samples.

Here we present optical photon reassignment microscopy (OPRA). It is an optical realization of these computer based methods which avoids the need for data processing. Furthermore at a different scaling ratio, our method is applicable to the direct visualisation of high-resolution imaging methods like STED.

**Background**

In normal CLSM the detected intensity values of every scanning position are recorded with an integrating detector such as a photo-multiplier-tube (PMT) or an avalanche photo-diode. If a whole image of the pinhole plane is recorded at each scan position the acquired data-set of a single focal slice can be viewed as a 4 dimensional set of data (intensity values in dependency of xy scan and xy pinhole-plane image-position). Such data can be processed in several ways, for example allowing for a retroactive choice of the pinhole diameter and/or applying multi-view deconvolution (Brakenhoff & Visscher 1992, Heintzmann et al. 2003). Photon reassignment microscopy (Sheppard 1988; Müller & Enderlein 2010) is based on the insight that the most probable origin of the detected photons is at maximum of the joint probability

\* Correspondence: heintzmann@gmail.com

<sup>1</sup>Institute of Photonic Technology, Albert-Einstein-Str.9, 07745, Jena, Germany

<sup>2</sup>Institute of Physical Chemistry, Abbe Center of Photonics,

Friedrich-Schiller-University Jena, Helmholtzweg 4, 07743, Jena, Germany

Full list of author information is available at the end of the article

function (i.e. the product of the individual probability functions) of excitation and (off-centre) detection. This is contrary to a CLSM where all detected photons are assigned to the nominal excitation position  $s$ .

In OPRA a similar reassignment to the optimal emission location is achieved optically. For example by an intermediate beam expansion between descanning and a subsequent rescanning. This is illustrated in Figure 1 at 3 successive time points. The upper row (1a) depicts the situation in the sample, where a scanned excitation beam (blue) together with a fixed emitter (green) at the origin is shown. The lower row (1b) refers to the final image plane. Due to the intermediate beam expansion, the emission PSF is reduced in size. As a further consequence the image of the emitter is now found at  $s(1-m)$ , with  $s$  being the nominal image position of the centre of the excitation focus and  $m$  being the intermediate magnification. At non-uniform intermediate magnification ( $m \neq 1$ ) the image of the emitter now performs a small scan on the final image plane, changing its brightness (not shown in Figure 1) under the influence of the excitation spot.

To aid understanding, a movie of a simulated scan process depicting the sample plane, the pinhole plane and the camera- (or display screen-) plane is given in Additional file 1, for the confocal case and OPRA at  $m=1$  and  $m=0.5$ .

We now aim to find an analytical description of the PSF of the overall system. The emission PSF has also

undergone the intermediate beam expansion  $m$  and can therefore be written as  $h(x/m)$ , positioned at  $s(1-m)$ . Thus, the current image generated by the point source at the point of origin is  $h_{em}\left(\frac{x-s(1-m)}{m}\right)$ , where  $s$  is the nominal scan position and  $x$  the image coordinate (measured in sample coordinates).

The total image of our point emitter is formed by integrating over all scan positions  $s$ :

$$h_{total}(x) = \int h_{ex}(-s)h_{em}\left(\frac{x-s(1-m)}{m}\right)ds. \quad (1)$$

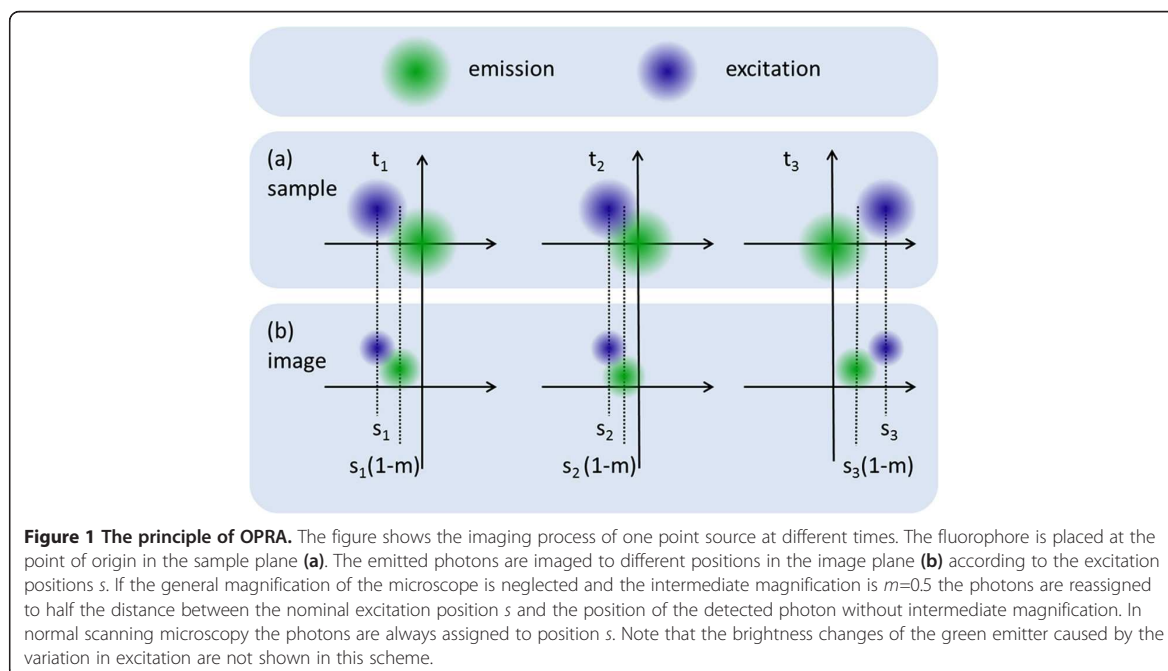
This can be written using the convolution operator  $\otimes$  as

$$h_{total}(x) = \left[ h'_{ex} \otimes h'_{em} \right] \left( \frac{x}{1-m} \right), \quad (2)$$

where  $h'_{em}(x) := h_{em}\left(\frac{x(1-m)}{m}\right)$  and the symmetrical excitation PSF  $h'_{ex}(x) := h_{ex}(-x)$  are used.

If we assume a Gaussian shaped excitation and emission PSF  $f(x) = \exp\left(-\frac{1}{2}\left(\frac{x}{\sigma}\right)^2\right)$  (standard deviation  $\sigma_{ex}$  for the excitation and corresponding  $\sigma_{em}$  for the emission function) the integral can be solved analytically. The final PSF is found to have the standard deviation.

$$\sigma_{OPRA}^2 = \sigma_{em}^2 m^2 + \sigma_{ex}^2 (1-m)^2. \quad (3)$$



The minimal total extent is found at:

$$m = \frac{\sigma_{ex}^2}{\sigma_{ex}^2 + \sigma_{em}^2}. \quad (4)$$

Thus the additional expansion  $m$  should be adjusted to the different width of the excitation and emission PSFs. This difference can be induced by the Stokes shift of the used fluorophores or is a feature of the microscopy technique itself, to which OPRA is applied (e.g. STED microscopy, where  $\sigma_{ex}$  is significantly smaller than  $\sigma_{em}$ ).

If we assume a beam expansion value of  $m=0.5$  (which makes a wider beam and therefore produces a smaller spot when focussed) we get a rough estimate for the resolution ability of OPRA

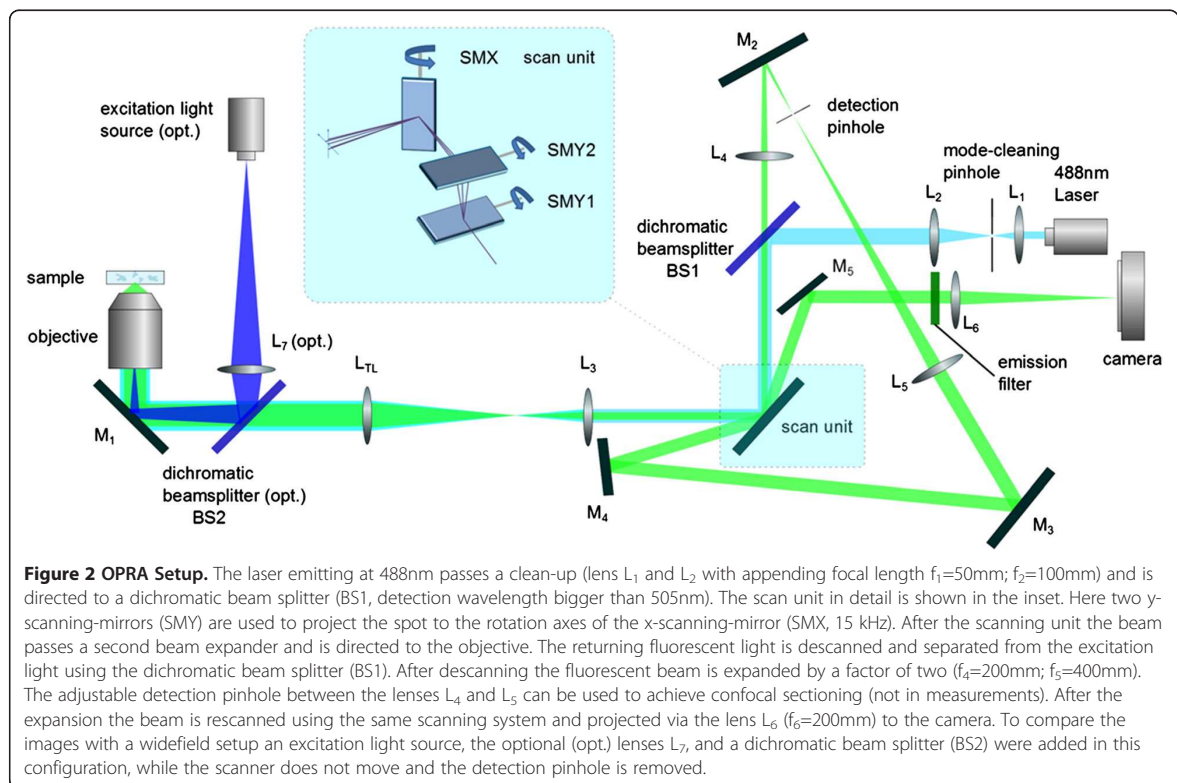
$$\sigma_{OPRA} = 0.5 \cdot \sqrt{\sigma_{ex}^2 + \sigma_{em}^2}. \quad (5)$$

If no Stokes shift is considered ( $\sigma_{ex} = \sigma_{em}$ ) we obtain a resolution improvement of  $\sqrt{2}$  over what we would expect for confocal detection with a closed pinhole. This shows that reassignment microscopy realizes high resolution at the theoretical overall detection efficiency of a widefield microscope. OPRA attains the same characteristics as computational reassignment without the need

for high-speed pinhole cameras and without the increased read-noise of multiple fast readouts. This raises the acquisition speed as the whole image is acquired in only one exposure frame. An additional pinhole can also be integrated in OPRA (before rescanning) to achieve confocal sectioning. Note that all emitted light of a scan from a planar fluorescent sample would otherwise reach the detector and thus prevent optical sectioning. For a detailed discussion of the sectioning ability see (Sheppard et al. 2013).

## Methods

Figure 2 shows the experimental setup. The illumination part is a normal laser scanning setup, which creates a moving illumination spot in the sample plane. The beam of the excitation laser (Coherent, Sapphire LP 488 nm) is sent through a beam expander ( $L_1$  and  $L_2$ ) to a dichromatic beam splitter (BS1, AHF Analysetechnik Tübingen, ZT488RDC) where it is reflected towards the scanning unit. Here, two scanning mirrors SMY1 and SMY2 (Cambridge Technologies, CT6800HPL with CTI CB6580 driver) achieve the scan along the  $y$ -axis while keeping the pupil plane stable at the position of the resonant  $x$ -scan mirror SMX (EOPC, SC-30, resonant optical scanner, 15 kHz, USA). Another beam expander consisting of the tube lens ( $f_{TL}=400$  mm) and an achromatic doublet



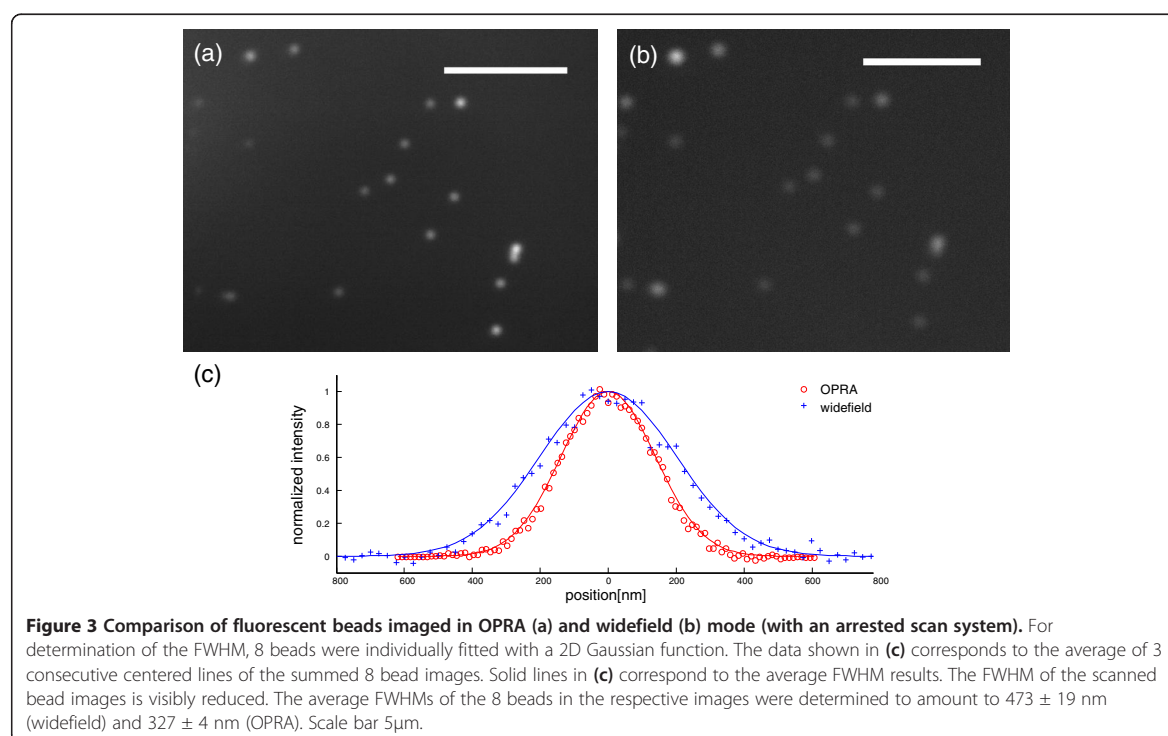
( $f_3=60$  mm) provides a slight over-illumination of the back focal plane of the objective (Carl Zeiss, Plan-Apochromat 63 $\times$ /0.7 Oil). On the detection side, the returning light is descanned using scan mirrors SMX, SMY1 and SMY2. Fluorescent and back-scattered illumination light are separated by the dichromatic beam splitter (BS1) and the fluorescent light is expanded by lenses  $L_4$  and  $L_5$  – this is the additional intermediate beam expansion. To achieve confocal sectioning a pinhole can be placed between these lenses, as this is a conjugate plane of the sample plane. Since the ideal intermediate beam expansion depends on the Stokes shift of the imaged fluorophores, the magnification can be adjusted by choosing the focal lengths of the lenses  $L_4$  and  $L_5$ . After this intermediate magnifying step, the emission light is guided to the same scanning unit to be rescanned. The concept of using the same mirror(s) for de- and rescanning is similar to the description in (Brakenhoff & Visscher 1992) and was part of a commercial system as it was sold by the company Meridian. Lens  $L_6$  finally directs the emission light to a camera (Andor Technology Inc., Neo sCMOS, Belfast) where a super-resolved image is captured by integrating (5s for the widefield case and 10s for the rescanned case in Figure 3) over a full scan process.

To compare theory with measurements, point spread functions were calculated using vectorial theory (here

assuming random polarisation) for the respective experimental wavelengths. The excitation PSF was then convolved with the emission PSF and the scale changed by a factor of 2 according to eqn. (2) with  $m=0.5$ . To finally account for the size of the beads, this resulting PSF was then convolved in 3D with a three-dimensional spherical volume of 200 nm diameter and the width of the resulting function was fitted with a Gaussian and measured.

## Results

To demonstrate the OPRA principle, fluorescent coated beads (FluoSpheres<sup>®</sup> Carboxylate-Modified Microspheres, 0.2  $\mu$ m, Yellow-Green Fluorescent (505/515)) with a diameter of 200 nm were imaged. For comparison a widefield excitation lamp (EXFO photonics solutions Inc., X-Cite series 120 Q) was coupled into the setup with an optional dichromatic beam splitter (Carl Zeiss Microscopy GmbH, FT 510), such that the same sample position could be imaged with both methods as shown in Figure 3. For comparison 8 bead-images were analysed and the full-widths at half maxima (FWHM) of fitted 2D Gaussian functions were determined. The mean FWHM of measured 200 nm beads in the widefield image (Figure 3b) is determined to be  $(473 \pm 19)$ nm and in the OPRA-image  $(327 \pm 4)$ nm (Figure 3a), without using a pinhole. Accounting for the 200nm diameter of the beads, equation (2) predicts a



FWHM of 297 nm (256 nm as Gaussian fit without accounting for the bead size) for the bead images acquired with OPRA, and 428nm for the widefield case, with the PSFs generated for the parameters as given above using vectorial diffraction theory. Thus theory and experiment agree to within about 10%. For the OPRA mode and 11% for the widefield detection. As the OPRA image theoretically contains the same number of photons as the widefield image but distributed to a sharper image, it is expected that the OPRA image also looks significantly brighter than the corresponding widefield (or confocal) image. However, since we used a separate illumination source to generate the widefield image, we could not do an appropriate comparison in this study.

### Discussion

In the presented paper a new method in fluorescence microscopy was introduced - OPRA microscopy. It realizes super-resolved images with high detection efficiency. Similar to computational photon reassignment (Cox et al. 1982; Müller & Enderlein 2010; York et al. 2012), the lateral resolution enhancement goes beyond the performance of a confocal microscope, even when compared to the limiting case of a confocal microscope with a completely closed pinhole. Note that approximating the PSF of a Gaussian and neglecting the Stokes shift, would predict identical PSFs for the fully closed pinhole confocal and the OPRA case. Also its optical transfer function has a significantly enhanced transfer strength at frequencies higher than 10% beyond the detection Abbe limit. Note also that this calculation was done with a demagnification of  $m=0.5$  which was not optimized to account for the slight change in wavelength (Sheppard et al. 2013).

Compared to computational photon reassignment no post-processing is required as the summation and photon reassignment is a system inherent property of OPRA. This prevents artefacts (e.g. pixilation artefacts, additional read noise) and is even insensitive to small variations in the scanning process, as those will mostly lead to small brightness changes in the resulting image. This makes it useful for very fast imaging with the scanning-speed and the camera frame-rate as the only limiting factors. We showed that the principle improves the resolution in comparison

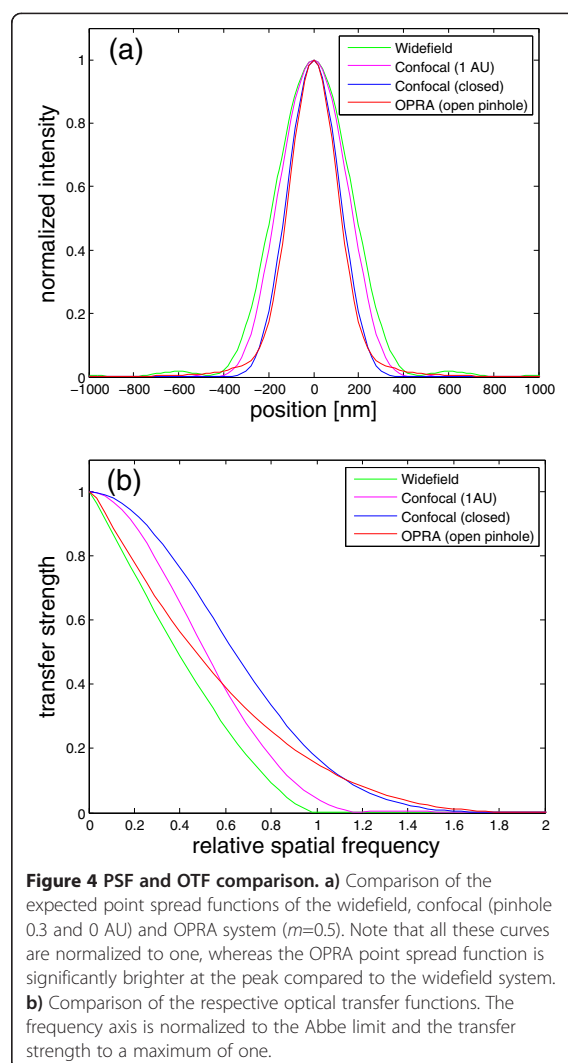


**Figure 4 PSF and OTF comparison.** a) Comparison of the expected point spread functions of the widefield, confocal (pinhole 0.3 and 0 AU) and OPRA system ( $m=0.5$ ). Note that all these curves are normalized to one, whereas the OPRA point spread function is significantly brighter at the peak compared to the widefield system. b) Comparison of the respective optical transfer functions. The frequency axis is normalized to the Abbe limit and the transfer strength to a maximum of one.

to classical widefield microscopy and we derived the basic theory for OPRA performance. It should be noted that the required OPRA properties are also achievable with realization methods other than intermediate magnification, such as the use of separate scan-units for illumination and detection light running at different speeds. OPRA can be adapted to various ratios of the sizes of excitation and emission PSF. Therefore the OPRA principle can also be used to optically realize versions of super-resolution modes such as STED, GSD and RESOLFT (Hell 2003). At large transition saturation factors, these methods would profit only marginally from an additional resolution gain but such a setup would, however, enable these modes for the first time to directly generate a highly resolved optical image without even the need for any data acquisition. Even a multi-spot STED, GSD or RESOLFT microscope

should be feasible with the OPRA approach, where the super-resolved image is built up during the integration time of a single frame. When using a periodic multi-spot excitation array, a single scan mirror can suffice. This was demonstrated in (York et al. 2013) which appeared after our manuscript was accepted for publication. Rescanning can also be performed with an electronically synchronised second scan mirror (or system of mirrors) or especially in the case of multi-spot illumination the rear side of the scan mirror can be used for rescanning. The camera can also be replaced by the human eye, realizing direct-view versions of STED or RESOLFT microscopy. Due to the simplicity and flexibility of the realizations, OPRA can enhance the performance of nearly every laser scanning microscope.

Currently our system does not use an appropriate tube lens to be free of chromatic aberrations. Future refinements of the imaging and scan optics are expected to push the performance of the system in both modes closer to the theoretical limit, especially for larger numerical apertures and low magnification.

Especially noteworthy is that OPRA achieves a theoretical image brightness superseding the performance of a widefield microscope under the same illumination dose. More photons are concentrated onto the same image pixel area. In this respect it differs from many alternative high-resolution methods which often only “shave” the PSF.

Even though OPRA improves photon reassignment in its all-optical realization, it should be noted that a full pinhole plane scan dataset of images with full dependency of scan and image coordinates is richer, and allows for better ways of image processing. These range from the ability retroactively to select the pinhole size, to optimization strategies such as weighted averaging in Fourier space and combined deconvolution (Heintzmann et al. 2003). As pinhole plane array data does not require a physical pinhole it can avoid the compromise between lateral resolution and optical sectioning performance of OPRA. Nevertheless, OPRA avoids generating large amount of data, along with the additional associated readout noise, with the additional benefit (even over a classical confocal microscope) of an inherent stability against scan imprecisions even when caused by mechanical vibrations influencing the scanners.

### Additional file

**Additional file 1: Simulation of the OPRA principle.** Top row (left to right): object and illumination intensity; pinhole plane; rescanned ( $m=1$ ); rescanned sum ( $m=1$ ). Bottom row (left to right): sum confocal (0.3 AU pinhole); pinhole plane ( $m=0.5$ ); rescanned ( $m=0.5$ ); rescanned sum ( $m=0.5$ ).

### Abbreviations

CLSM: Confocal laser scanning microscope; FWHM: Full width at half maximum; GSD: Ground state depletion; ISM: Images scanning microscopy; LSM: Laser scanning microscope; OPRA: Optical photon reassignment;

OTF: Optical transfer function; PSF: Point spread function; RESOLFT: Reversible saturable optical fluorescence transitions; sCMOS: Scientific complementary metal-oxide-semiconductor; STED: Stimulated emission depletion.

### Competing interests

The authors have jointly submitted a patent application.

### Authors' contributions

SR designed and performed the experiments, analysed the data and contributed to the concept. CJRS contributed to the concept and the theoretical understanding. KW contributed to the concept and helped with the data analysis. RH conceptualized OPRA and contributed to the experiment and data analysis. All authors read and approved the final manuscript.

### Author details

<sup>1</sup>Institute of Photonic Technology, Albert-Einstein-Str.9, 07745, Jena, Germany.

<sup>2</sup>Institute of Physical Chemistry, Abbe Center of Photonics, Friedrich-Schiller-University Jena, Helmholtzweg 4, 07743, Jena, Germany.

<sup>3</sup>Nanophysics, Instituto Italiano di Tecnologia, via Morego 30, 16163, Genoa, Italy. <sup>4</sup>King's College London, Randall Division, NHH, SE1 1UL, London, UK.

Received: 21 June 2013 Accepted: 4 October 2013

Published: 18 October 2013

### References

- Brakenhoff GJ, Visscher K (1992) Confocal imaging with bilateral scanning and array detectors. *J Microsc* 165:139–146
- Cox IJ, Sheppard CJR, Wilson T (1982) Improvement in resolution by nearly confocal microscopy. *Appl Opt* 21(5):778–781
- Heintzmann R, Sarafis V, Munroe P, Nailon J, Hanley QS, Jovin TM (2003) Resolution enhancement by subtraction of confocal signals taken at different pinhole sizes. *Micron* 34(6–7):293–300
- Hell S (2003) Toward fluorescence nanoscopy. *Nat Biotechnol* 21:1347–1355
- Minsky M (1961) Microscopy apparatus. U.S. patent 3,013,467. <http://www.freepatentsonline.com/3013467.html>
- Müller CB, Enderlein J (2010) Image scanning microscopy. *Phys Rev Lett* 104(198101):1–4
- Pawley JB (ed) (2006) *Handbook of Biological Confocal Microscopy*, 3rd edition. Springer, New York
- Sheppard CJR (1988) Super-resolution in confocal imaging. *Optik (Stuttgart)* 80:53–54
- Sheppard CJR, Mehta S, Heintzmann R (2013) Superresolution by image scanning microscopy using pixel reassignment. *Optics Lett* 38:2889–2892
- York AG, Parekh SH, Nogare DD, Fischer RS, Tempirne K, Mione M, Chitnis AB, Combs CA, Shroff H (2012) Resolution doubling in live, multicellular organisms via multifocal structured illumination microscopy. *Nat Methods* 9(7):749–754
- York AG, Chandris P, Nogare DD, Head J, Wawrzusin P, Fischer RS, Chitnis A, Shroff H (2013) Instant super-resolution imaging in live cells and embryos via analog image processing. *Nat Methods*. doi:10.1038/nmeth.2687

doi:10.1186/2192-2853-2-5

**Cite this article as:** Roth et al.: Optical photon reassignment microscopy (OPRA). *Optical Nanoscopy* 2013 **2**:5.

Submit your manuscript to a SpringerOpen® journal and benefit from:

- Convenient online submission
- Rigorous peer review
- Immediate publication on acceptance
- Open access: articles freely available online
- High visibility within the field
- Retaining the copyright to your article

Submit your next manuscript at ► [springeropen.com](http://springeropen.com)

## 6.2 Superconcentration of light: Circumventing the classical limit to achievable irradiance [SR2]

Stephan Roth, Colin J.R. Sheppard and Rainer Heintzmann

*Optics Letters* 41,Nr. 9, 2109, (2016)

Stephan Roth	Designing, developing and building the microscopy setup, data acquisition and analysis, preparation of the manuscript.
Colin J.R. Sheppard	Discussion of general aspects of superconcentration, contributing to the manuscript.
Rainer Heintzmann	Supervision of the project and discussion of the results.

All authors revised, edited and proof read the manuscript.

Stephan Roth, Colin J. R. Sheppard, and Rainer Heintzmann. Superconcentration of light: circumventing the classical limit to achievable irradiance. *Optics Letters*, 41(9):2109, may 2016. ISSN 0146-9592. doi: 10.1364/OL.41.002109. URL <https://www.osapublishing.org/abstract.cfm?URI=ol-41-9-2109>



# Optics Letters

## Superconcentration of light: circumventing the classical limit to achievable irradiance

STEPHAN ROTH,<sup>1</sup> COLIN J. R. SHEPPARD,<sup>2</sup> AND RAINER HEINTZMANN<sup>1,3,\*</sup>

<sup>1</sup>Leibniz Institute of Photonic Technology, Albert-Einstein-Str.9, 07745 Jena, Germany

<sup>2</sup>Nanophysics, Istituto Italiano di Tecnologia, via Morego 30, 16163 Genoa, Italy

<sup>3</sup>Institute of Physical Chemistry, Abbe Center of Photonics, Friedrich-Schiller-University Jena, Helmholtzweg 4, 07743 Jena, Germany

\*Corresponding author: heintzmann@gmail.com

Received 23 February 2016; accepted 8 March 2016; posted 5 April 2016 (Doc. ID 258595); published 29 April 2016

**Concentration of light is limited by a fundamental physical principle, which ensures that étendue, the product of area and solid angle, can never decrease in an optical system. In microscopy, many superresolving methods, which can overcome the classical resolution limit, have recently emerged. We propose, and demonstrate experimentally, that it is also possible to circumvent the classical light concentration limit. Actually, most superresolution methods exhibit a common drawback: with respect to the total number of emitted photons, they are less efficient than standard widefield microscopy. Most methods “shave” the point spread function (PSF) by discarding the disturbing signal from its edge. We show, that in contrast to PSF-shaving, methods related to reassignment microscopy (image scanning microscopy, optical photon reassignment, rescanned confocal, instant structured illumination microscopy) concentrate all detected photons in their superresolving images and thereby increase the detected signal per sample area compared to widefield microscopy. We term this behavior superconcentration, as it breaks the classical light concentration limit.** © 2016 Optical Society of America

**OCIS codes:** (180.0180) Microscopy; (180.1790) Confocal microscopy; (180.2520) Fluorescence microscopy; (180.5810) Scanning microscopy; (110.2990) Image formation theory; (100.6640) Superresolution.

<http://dx.doi.org/10.1364/OL.41.002109>

There is a well-known fundamental physical limit to how efficiently light can be concentrated. This is important in many applications where the number of photons per time interval is crucial. The basic invariant is named the étendue or the Lagrange invariant, also called throughput or accepting power, defined as the product of area and solid angle. This limits the irradiance that can be achieved using any optical system. The conservation of étendue can be established from several different basic concepts, including thermodynamic arguments [1], Hamiltonian optics, wave optics [2,3], or quantum optics [4]. Optimal concentration of scalar waves was studied by Kowarz [5], and by Sheppard and Gu [6]. They showed that

the maximum focal irradiance for a given input power into a finite angular aperture is achieved for a uniform converging spherical wave. This is seen to be in agreement with Fermat's principle: optimum concentration is achieved when all rays arrive at the focus in phase.

Bassett proved that the maximum possible total energy density  $W$  that can be achieved using a general electromagnetic concentrator (i.e., not necessarily an imaging system) is  $W = Pk^2/3\pi c$ , where  $P$  is the power,  $k = 2\pi/\lambda$  is the wave number with the wavelength  $\lambda$ , and  $c$  is the velocity of light [3].

Sheppard and Larkin showed that it is indeed possible to attain this upper bound, using a focusing system with a plane-polarized input producing a so-called mixed dipole field, exhibiting the same polarization and amplitude variation as the far field of crossed electric and magnetic dipoles [7]. This solution also provides the optimum concentration for a finite-sized circular aperture. The energy density is then equally divided between electric and magnetic energy densities. Later, Stamnes and Dhayalan [8], and Sheppard and Török [9] showed that an electric dipole field can also attain this upper bound, with the energy density at the focus all being of the electric type. This distinction is important, as most practical detectors and excitation processes such as fluorophore excitation are sensitive to the electric energy density. For a system of finite aperture smaller than a hemisphere (as is assumed throughout below), the optimum case gives a transversely oriented electric field at the focus, stronger than for the mixed dipole case. Another practically important geometry results in a longitudinally oriented electric dipole at the focus, corresponding to focusing of radially polarized light, but note that the concentration, for a finite aperture smaller than a hemisphere, is then lower than for the transverse dipole case [9].

These results establish a connection between concentration and focusing of light. As there is known to be a close connection between the processes of focusing and imaging, there is thus a relationship between the limit of concentration and the classical resolution limit in imaging [10]. As it has recently been established that overcoming the classical resolution limit is a reality [11], the physical limit to light concentration needs to be re-examined.

It is known that the resolution of a confocal laser scanning microscope can be increased by closing the pinhole [12].

However, it is plain to see that this would only discard more emitted photons, even at the ideal scan position, and thus would prohibit any superconcentration. The very successful superresolution method of stimulated emission depletion (STED) microscopy prevents, by stimulated emission, a fluorophore from spontaneously emitting, if it is not exactly at the nominal focus position [11]. Therefore the point spread function (PSF) will at best be identical in intensity to ordinary laser-scanning imaging at the nominal focus, but signal is removed (“PSF shaving”) at other positions. STED therefore shows no superconcentration effect compared to standard laser scanning microscopy.

However, in the technique of image scanning microscopy, which is basically confocal microscopy with a detector array coupled with pixel reassignment, the PSF can be narrowed without loss of photons [13,14]. This method is based on the principle that signals from different points of the detector array are neither attributed to the current scan position (i.e., excitation peak position), nor to their own position geometrically traced back to the sample (i.e., the most probable emitter position under widefield illumination). They are accumulated instead to the coordinate corresponding to the most probable overall emitter position, which is halfway between the excitation and detection points. This reassignment can be performed digitally or even optically [15–19]. We found theoretically that, without a limiting pinhole (corresponding to a large detector array), neglecting the Stokes shift, the peak intensity at the focus for a point object and circular pupils is 1.84 times the classical concentration limit [20]. We call this ratio the superconcentration factor (SCF). This intensity enhancement occurs because the PSF is narrowed while the energy in the image is conserved; hence, the light is effectively more concentrated than in classical widefield imaging. To perform optical sectioning a comparatively large pinhole can be used [larger than about 1 Airy unit (AU)]. As this pinhole discards some energy, the SCF will be below 1.84 in practice, but superconcentration can still be achieved.

In the following, we analyze the superconcentration behavior in reassignment microscopy more deeply, and present experimental results that demonstrate the effect in the implementation called optical photon reassignment (OPRA) microscopy. The aim of our Letter is not to present a new superresolution scheme, but to demonstrate experimentally that the classical physical limit to the concentration of light can be overcome. This demonstration is not trivial, as we need to compare quantitatively and absolutely the signal detected in two different optical schemes. As the reassignment of photons occurs within the area of the PSF, the superconcentration of light is only prominent for small objects, whereas a fluorescent plane maintains its brightness as a result of conservation of energy. This correlation with the object size is illustrated in the simulation in Fig. 1. There, the relative peak intensity of uniform fluorescent objects, imaged with the OPRA principle with respect to normal widefield microscopy, is shown as a function of the object diameter. Therefore, normalized images of different objects were calculated and the peak intensities compared. The PSF of OPRA in two dimensions is given by

$$\text{PSF}_{\text{OPRA}} = [\text{PSF}_{\text{ex}} \otimes \text{PSF}_{\text{em}}] \left( \frac{x}{1-m} \right) \quad (1)$$

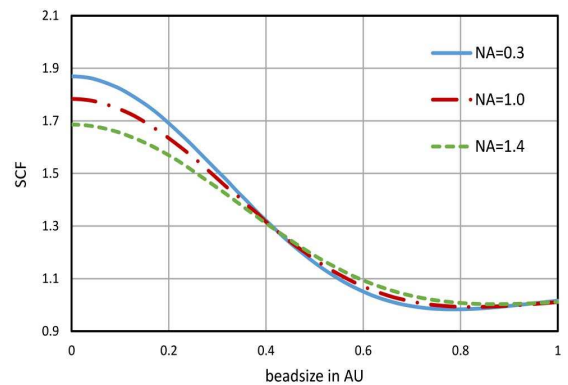


**Fig. 1.** Intensity enhancement of OPRA as a function of the object diameter for uniform fluorescent objects. The SCF gives the ratio of the peak intensity achieved with OPRA compared to that in widefield microscopy. The effect vanishes for objects bigger than 0.8 AU. In this numerical simulation no Stokes shift was considered.

with the PSF of excitation and emission light ( $\text{PSF}_{\text{ex}}$  and  $\text{PSF}_{\text{em}}$ ), the convolution operator  $\otimes$  and the intermediate magnification factor  $m$  [15]. While for small objects, an increase of the peak intensity is exhibited, large objects are not affected by the peak intensity enhancement. This fact can be utilized to compare images taken with different microscopy methods quantitatively, and an extended object (e.g., a fluorescent plane) can be used for calibration to determine the intensity enhancement of small objects.

For the measurements, an OPRA setup was modified such that it is also capable of operating in a widefield imaging mode (Fig. 2). The illumination side consists of a classical laser scanning setup with a 2D beam scanner (Sapphire LP 488 nm,

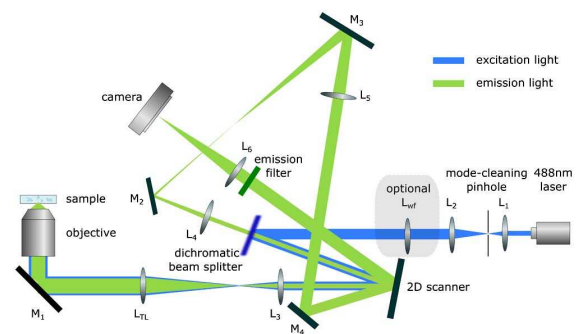


**Fig. 2.** OPRA setup. After passing a clean-up (lenses  $L_1$  and  $L_2$  with respective focal lengths  $f_1 = 50$  mm and  $f_2 = 100$  mm), the laser is directed to a dichromatic beam splitter. For sample illumination, a 2D scanner is used in a plane conjugate to the objective BFP. To overilluminate the BFP of the objective, the illumination beam passes through a second beam expander ( $f_3 = 60$  mm,  $f_{\text{TL}} = 400$  mm). The returning fluorescent light is descanned and separated from the excitation light using the aforementioned dichromatic beam splitter. After descanning, the fluorescent beam is expanded by a factor of 2 ( $f_4 = 200$  mm,  $f_5 = 400$  mm) and rescanned using the 2D scanner, and finally projected via the lens  $L_6$  ( $f_6 = 200$  mm) to the camera.

## Letter

Vol. 41, No. 9 / May 1 2016 / Optics Letters 2111

Coherent Inc. and S-334.2SL with E-517 controller, Physik Instrumente GmbH, Germany). The beam expander, consisting of lenses  $L_3$  ( $f_3 = 60$  mm) and  $f_{TL}$  ( $f_{TL} = 400$  mm), provides a required overillumination of the objective's (Plan-Apochromat Oil, Carl Zeiss, Germany) back focal plane (BFP) to create a small excitation spot in the sample. The fluorescent light is captured by the illumination objective, descanned and separated from the excitation laser light with a dichromatic beam splitter (zt488DC, Chroma Technology Corporation, USA). The reassignment of the photons occurs while magnifying the descanned beam by a factor of 2 as a result of lenses  $L_4$  ( $f_4 = 200$  mm) and  $L_5$  ( $f_5 = 400$  mm). To link the collected reassigned photons to the scan position, the descanned beam is directed to the 2D scanner again and focused by lens  $L_6$  ( $f_6 = 200$  mm) onto the camera (Neo sCMOS, Andor Technology, UK). To generate a widefield illumination, lens  $L_{wf}$  is inserted ( $f_{wf} = 150$  mm) in the illumination path and the 2D scanning unit is stopped. This small modification guarantees that the influence of changed optical parts in the setup is minimized and the same sample position is imaged.

For the analysis, images of fluorescent beads (FluoSpheres® Carboxylate-Modified Microspheres,  $0.11 \mu\text{m}$ , Yellow-Green Fluorescent 505/515) and a fluorescent plane consisting of a tightly packed layer of these beads were recorded under identical illumination conditions. The captured fluorescent plane is used for relative brightness calibration and locally accounts for the different illumination field and therefore the different power density in the two microscopy modes. To avoid nonlinear photoresponse of the fluorophores, only very moderate laser powers (around  $10 \mu\text{W}$  beam power) and long integration times (1–10 s) were used during scanning. Images of the same 32 beads in OPRA and the widefield mode were fitted with a 2D Gaussian function, as this function leads to a robust estimation of peak intensity and FWHM. After locally normalizing each image to its corresponding fluorescent plane value, the ratio of the peak intensities of OPRA to widefield mode (SCF) was found to be  $1.76 \pm 0.45$ . The error refers to the standard error of the individual measurement. Even with the high standard deviation error, caused by inhomogeneities in the illumination pattern and the bead size, this measurement agrees well with the theoretical calculation shown in Fig. 1 (for Gaussian pupils). For the parameter used in the experiment ( $\text{NA} = 0.7$ ;  $\lambda_{\text{ex}} = 488$  nm;  $\lambda_{\text{em}} = 520$  nm;  $m = 0.5$ ; refractive index  $n = 1.518$ ; bead diameter =  $110$  nm corresponding to  $0.12$  AU), the calculated SCF value is  $1.77$ . The FWHM of the fitted function was determined as  $(275 \pm 15)$  nm for OPRA and  $(411 \pm 40)$  nm for the widefield mode, and correlates well with the expected resolution of the OPRA mode [15]:

$$d_{\text{OPRA}}^2 = d_{\text{em}}^2 m^2 + d_{\text{ex}}^2 (1 - m)^2 \quad (2)$$

with  $d_{\text{OPRA}}$ ,  $d_{\text{em}}$ , and  $d_{\text{ex}}$  the widths of the OPRA, the emission, and the excitation PSF respectively, and the intermediate magnification  $m$  (in this setup the magnification is set to  $m = 0.5$ ). Note that for this simplified equation Gaussian PSFs are assumed. To visualize the intensity enhancement, the bead images in Figs. 3(a) and 3(b) were locally normalized to the corresponding fluorescent plane image. For better comparison and due to the different magnifications, affine image registration [21] was applied to the images. The line plots in Fig. 3(c) through the center of a single bead in Figs. 3(a) (red dashed line) and 3(b) (blue dashed line) exemplify the increased peak intensity

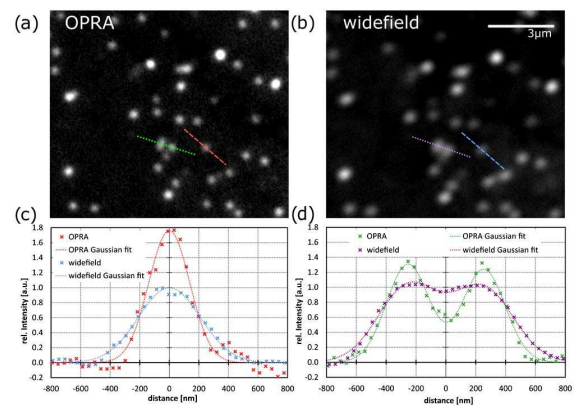


**Fig. 3.** Comparison of images of beads recorded with (a) OPRA and (b) widefield mode using an objective with a numerical aperture (NA) of 0.7. The relative intensity is normalized to its reference. In (c), the plot along the red dashed line [(a) OPRA] and the blue dashed line [(b) widefield] demonstrates the improved resolution and the apparent superconcentration behavior (the plotted data is clipped to the offset of the shown Gaussian fit). Also, the good approximation of peak intensity and FWHM of the Gaussian fit function is clearly visible. In (d) it is shown that the beads inseparable in (b) (purple dotted line) can clearly be discerned in (a) (green dotted line).

and the narrowed width of the imaged particles. Figure 3(d) shows that nearly unresolved beads in the widefield image [Fig. 3(b), purple dotted line] are clearly separable in Fig. 3(a) (green dotted line).

Figure 4 presents a plot along the ratio of  $\text{PSF}_{\text{OPRA}}$  and  $\text{PSF}_{\text{wf}}$ , which was calculated as the sum of all individual bead images. In the center of the bead, the image taken with the OPRA system is  $1.77$  times brighter than the widefield image ( $\text{SCF} = 1.77$ ). On the other hand, the center of the bead

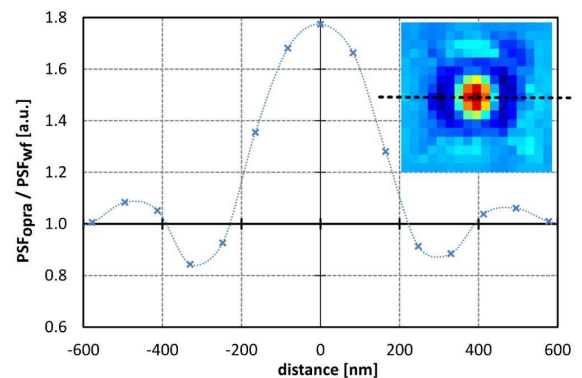


**Fig. 4.** Ratio of the measured OPRA and widefield PSF (calculated as sum of all imaged beads in each mode). The graph represents a plot along the dashed line shown in the inset (for better visualization, a spline function was added). The intensity in the center of the bead image in OPRA is enhanced by a factor of  $\text{SCF} = 1.77$ . The center is surrounded by a ring of an intensity ratio smaller than 1, showing that the photons in OPRA were reassigned from the border (fewer photons than widefield) to the center of the PSF (more photons than widefield).

image is surrounded by a ring with an intensity ratio smaller than 1, meaning that here the widefield image is brighter than the OPRA image. This shows convincingly that OPRA reassigns photons from the boundary to the center of the imaged bead object.

We have shown that the reassignment microscopy methods collect the same number of photons as ordinary widefield microscopes, but concentrate them on a smaller area. This leads to enhanced resolution, with increased peak intensity for small objects. We term this effect superconcentration of light, as it concentrates light better than it is possible with just a lens. We showed experimental results, comparing images taken with a widefield and an OPRA microscope. These images show clearly the enhanced peak intensity in the OPRA images. Thus we have demonstrated that the classical limit to light concentration can be overcome. The fundamental limit is still valid at every single time point, but overall it is circumvented, as our system, by design, integrates knowledge about localized sequential illumination and detection into a single scheme. The reason that the fundamental limit can be overcome in this case is time sequential scanning. Whereas Bassett specifically considered passive systems, the superconcentration approach in OPRA is based on an active system. There may be other ways of overcoming the limit, which could be of importance in other, different, applications. Similar to superresolution limits exploiting the time or other channels to transmit information through the limited passband [22], it seems that such channels can also be exploited to achieve superconcentration.

## REFERENCES

1. H. Ries, *J. Opt. Soc. Am.* **72**, 380 (1982).
2. R. Winston and W. T. Welford, *J. Opt. Soc. Am.* **72**, 1564 (1982).
3. I. M. Bassett, *Opt. Acta* **33**, 279 (1986).
4. I. M. Bassett, *Phys. Rev. Lett.* **54**, 2014 (1985).
5. M. W. Kowarz, *Opt. Commun.* **110**, 274 (1994).
6. C. J. R. Sheppard and M. Gu, *J. Mod. Opt.* **40**, 1631 (1993).
7. C. Sheppard and K. Larkin, *J. Mod. Opt.* **41**, 1495 (1994).
8. J. J. Stamnes and V. Dhayalan, *Pure Appl. Opt.* **5**, 195 (1996).
9. C. J. R. Sheppard and P. Török, *Optik* **104**, 175 (1997).
10. A. Walther, *J. Opt. Soc. Am.* **57**, 639 (1967).
11. S. W. Hell, *Nat. Biotechnol.* **21**, 1347 (2003).
12. I. Cox, C. Sheppard, and T. Wilson, *Optik* **60**, 391 (1982).
13. C. J. R. Sheppard, *Optik* **80**, 53 (1988).
14. C. B. Müller and J. Enderlein, *Phys. Rev. Lett.* **104**, 198101 (2010).
15. S. Roth, C. J. Sheppard, K. Wicker, and R. Heintzmann, *Opt. Nanoscopy* **2**, 5 (2013).
16. G. M. De Luca, R. M. Breedijk, R. A. J. Brandt, C. H. Zeelenberg, B. E. de Jong, W. Timmermans, L. N. Azar, R. A. Hoebe, S. Stallinga, and E. M. Manders, *Biomed. Opt. Express* **4**, 2644 (2013).
17. A. G. York, P. Chandris, D. D. Nogare, J. Head, P. Wawrzusin, R. S. Fischer, A. Chitnis, and H. Shroff, *Nat. Methods* **10**, 1122 (2013).
18. P. W. Winter, A. G. York, D. D. Nogare, M. Ingaramo, R. Christensen, A. Chitnis, G. H. Patterson, and H. Shroff, *Optica* **1**, 181 (2014).
19. T. Azuma and T. Kei, *Opt. Express* **23**, 15003 (2015).
20. C. J. R. Sheppard, S. B. Mehta, and R. Heintzmann, *Opt. Lett.* **38**, 2889 (2013).
21. P. Thévenaz, U. E. Ruttimann, and M. Unser, *IEEE Trans. Image Proc.* **7**, 27 (1998).
22. W. Lukosz, *J. Opt. Soc. Am.* **56**, 1463 (1966).

### 6.3 Optical Photon Reassignment with increased axial resolution by structured illumination [SR3]

Stephan Roth and Rainer Heintzmann

submitted to *Methods and Applications in Fluorescence* in may 2016

Stephan Roth	Creation of the publication idea. Designing, developing and building the microscopy setup, data acquisition and analysis, preparation of the manuscript.
Rainer Heintzmann	Supervision of the project and discussion of the manuscript and the results.

Both authors revised, edited and proof read the manuscript.

Stephan Roth and Rainer Heintzmann. Optical Photon Reassignment with increased axial resolution by structured illumination. *Methods and Applications in Fluorescence*, 2016

**Optical Photon Reassignment with increased axial resolution by structured illumination**Stephan Roth<sup>1</sup> and Rainer Heintzmann<sup>1,2</sup><sup>1</sup>Leibniz Institute of Photonic Technology, Albert-Einstein-Str.9, 07745 Jena, Germany<sup>2</sup>Institute of Physical Chemistry, Abbe Center of Photonics, Friedrich-Schiller-University Jena, Helmholtzweg 4, 07743 Jena, Germany

## ABSTRACT

Fluorescent microscopy methods linked to the reassignment principle as Image Scanning Microscopy (ISM), re-scan confocal (RSC), Optical Photon Reassignment (OPRA) and instant Structured Illumination Microscopy (iSIM) have the potential to replace confocal microscopy as the standard microscopy technique. Photon reassignment methods are known to link the most important properties in biological imaging as resolution, sensitivity, imaging speed and combinability with fluorophores in an elegant way. On the example of OPRA, we show how this method could be easily extended to the third dimension. If OPRA is used in combination with a structured illumination pattern the sectioning ability can be improved while maintaining the very high signal intensity. We present a detailed analysis about the imaging properties of OPRA in three dimensions and show experimental results on biological samples.

## INTRODUCTION

In the past decades many improvements in superresolution microscopy were made [1]. But as high resolution is normally linked to high illumination dose, the practically achievable resolution is set by the illumination acceptance of the sample. This is very important in live cell imaging, as the acceptable illumination dose of living cells is significantly lower than in fixed cells [2]. In this point of view the methods linked to the reassignment principle provide a completely new approach combining high detection sensitivity and moderate high resolution [3-8]. Especially the fact, that for fine details these methods deliver the same amount of photons as widefield microscopy but concentrated them on a smaller volume, leads to higher light concentration than proposed by classical theory. This property is called superconcentration of light [9] and illustrates the high detection sensitivity of reassignment methods. This manuscript investigates specifically the imaging properties along the optical axis in optical photon reassignment microscopy (OPRA) [7]. It further discusses the influence of the size of the detection pinhole in terms of resolution and detection sensitivity and investigates the combination of OPRA with a structured illumination scan mode.

Methods linked to the reassignment principle are laser scanning techniques that use the spatial information in the pinhole plane to enhance the imaging properties. If the pinhole plane image is

demagnified for every scan position, it is possible to improve lateral resolution and simultaneously enhance the detected peak intensity. This demagnification can be done computationally (for example in ISM, MSIM or Zeiss AiryScan) or optically (as in OPRA, RSC and iSIM) and leads to a reassignment of the pixels (in case of the computational methods) or photons (in case of the optical methods respectively). In the optical realizations of this concept, the descanned and demagnified fluorescent light has to be rescanned. This can be done, while using the same scanning device again [7, 8] or using a second re-scanner [6]. Also an implementation in a spinning-disk image scanning device is possible [10]. The all-optical methods have the advantage, that they deliver instantaneous super-resolved images without the need of further processing. This property is very important towards fast imaging of biological samples. The computationally methods have to record one pinhole plane image for every scan position. The additional necessary rendering makes these methods more time consuming than the optical realizations. On the other hand, the collected information content in the computational methods is bigger and can be exploited for different imaging modes and processing algorithms with a better signal-to-noise performance.

The demagnification in the pinhole plane giving the best results regarding resolution improvement depends on the different width of excitation and emission PSF. As for most commonly used fluorophores this shift in wavelength is negligible, the intermediate demagnification factor is set in most of the literature to  $m=0.5$  and is therefore also used here.

For this demagnification factor, the equation

$$PSF_{OPRA}(\mathbf{r}) = (PSF_{ex} \otimes PSF_{em})(2\mathbf{r}) \quad (1)$$

with  $PSF_{OPRA}$ ,  $PSF_{ex}$  and  $PSF_{em}$  being the point spread function of OPRA, the excitation and the emission light and  $\otimes$  the convolution operator respectively, describes OPRA analytically in two dimensions as  $\mathbf{r}$  represents the image coordinates  $\mathbf{r} = (x, y)$ . Compared to normal widefield microscopy, the resolution in the focal plane and along the optical axis is enhanced in OPRA. Nevertheless, for thick samples, images acquired with OPRA appear noisy, as the same amount of out-of-plane fluorescence as in common widefield approaches is generated.

The presence of out-of-focus light legitimates the usage of background suppressing methods in OPRA. If a detection pinhole for sectioning is used, the superconcentration properties are reduced for small pinhole diameters. We suggest the combination of OPRA and structured illumination as it links high detection efficiency and sectioning performance compromised by only a minor loss in imaging speed.

### OPRA in three dimensions

To investigate the sectioning performance of OPRA in three dimensions, a comparison with widefield microscopy seems not to be sufficient. Therefore, in Fig. 1 a numerical simulation of the resolution of confocal microscopy and OPRA is shown. The full width at half maximum (FWHM) of the point spread function (PSF) in the focal plane and along the optical axis are presented as a function of the pinhole

diameter. Compared to normal confocal microscopy, OPRA yields a smaller width for both directions. This is even more significant for bigger pinhole diameters which are preferred considering the relevant light losses for pinhole diameters below 1 Airy unit (AU).

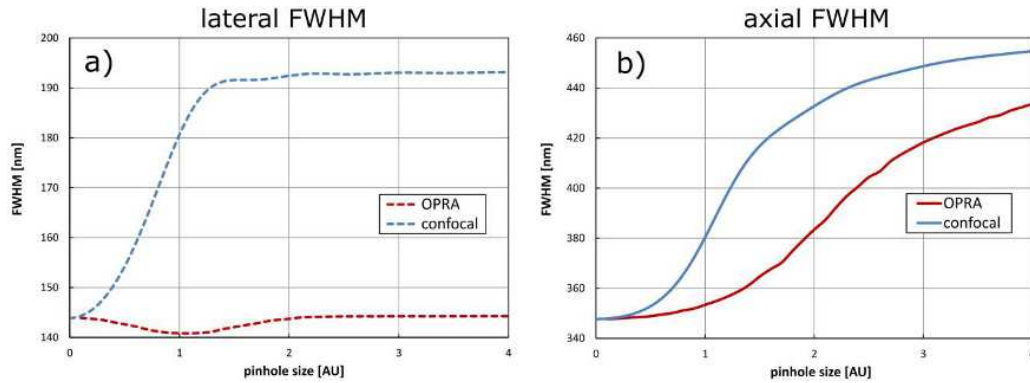


Fig. 1 Numerical simulation of the full width at half maximum (FWHM) of the PSF of OPRA and confocal in the focal plane (Fig. 1a) and along the optical axis (Fig. 1b) in dependency of the pinhole diameter. The FWHM in OPRA is always improved in comparison to a confocal system. In the focal plane (Fig. 1a) there is nearly no dependency of the PSF-width in OPRA, but the resolution of a confocal system decreases significantly as the pinhole size increases. Along the optical axis (Fig. 1b) the size of the PSF increases in OPRA for increasing pinhole diameter as well, but not as dramatic as in a confocal microscope. This is important, as the signal level is strongly linked to the pinhole diameter and decreases massively for values below 1 AU. The values for this simulation were set to:  $NA=1.4$ ;  $\lambda_{ex}=488\text{nm}$ ;  $\lambda_{em}=525\text{nm}$ ;  $n=1.518$ .

For confocal microscopy it is already known that there is a trade-off between sectioning performance and a good signal-to-noise ratio (SNR) [11]. As the sectioning performance is theoretically best for the smallest pinhole diameter, the SNR gets worse for small pinhole sizes as nearly all the light is blocked by the pinhole. A pinhole diameter of 0.68 AU yields the best compromise between SNR and sectioning performance [12]. To further improve the out-of-focus suppression in OPRA we propose to scan the illumination spot in that way, that it generates a structured illumination pattern in the sample which than can be used to computationally identify and subtract the out-of-focus contributions [13, 14]. The structured illumination pattern should not be confused with the full-field technique of high resolution structured illumination microscopy (HR-SIM) [13]. In HR-SIM the sample information is modulated with a very fine illumination pattern, where here, in OPRA with increased axial sectioning, the sample is illuminated with a scanned excitation spot forming a relatively coarse pattern. Such scanning pattern is only useful to improve the optical sectioning and axial resolution but has little influence on lateral resolution. With this method it is even possible to achieve a proper sectioning ability if no pinhole could be added to the beam-path. For pattern illumination the overall illumination time of the field of view (FOV) and the illumination dose stays the same, as only the number of frames per resulting image is increased. Since the read-noise of modern scientific cameras is usually negligible the image quality is enhanced and therefore pattern illumination seems reasonable.



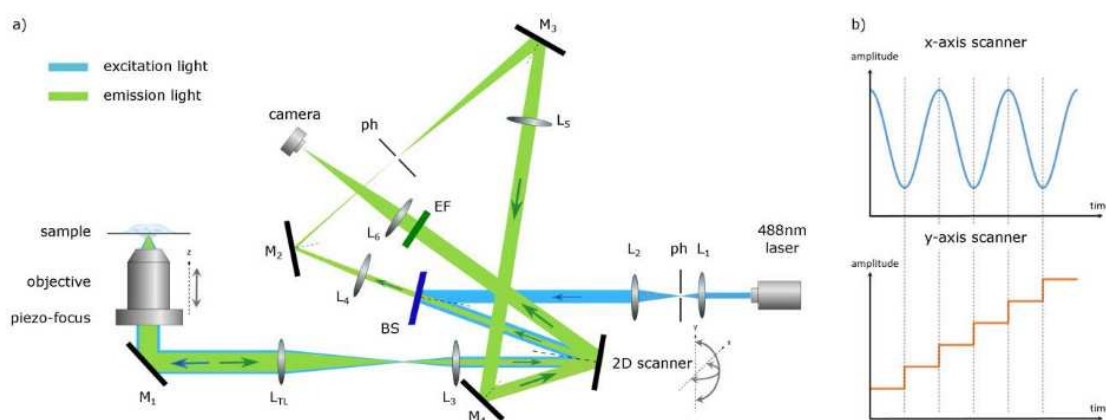


Fig. 2 Optical setup of OPRA with enhanced axial resolution by structured scanning pattern. a) shows the optical setup consisting of a laser scanning illumination and a fluorescent detection part with optical reassignment. For illumination, the sample is excited by 488nm laser light. For the three scan-steps (scanning, de- and rescanning) a piezo-driven beam scanner with two scan-axes is used (S-334.2SL with E-517 controller, Physik Instrumente GmbH). The fluorescent light from the sample is descanned and directed via passing the dichromatic beamsplitter (BS) to the pinhole plane (ph). This image plane is demagnified via lenses  $L_4$  and  $L_5$  to perform the optical reassignment process. After reassignment, the fluorescent light beam is rescanned and directed to the camera via lens  $L_6$ . To generate three dimensional stacks, a piezo-driven objective mount is used (Nano-F200W, Mad City Labs Inc.). In b) a schematic representation of the scan behavior is shown. Where the fast x-axis of the 2-scan-axes beam-scanner runs in sinusoidal scan-shape, the slow y-axis is stepped precisely every half period to generate the line-wise illumination pattern. The step height is chosen that way, that a pattern period of approximately 312nm is generated in the sample plane. Other abbreviations: mirror (M),  $L_{TL}$  (tubelens), emission filter (EF).

## METHODS

The optical setup presented in figure 2a) was used to demonstrate the imaging performance of OPRA using structured scanning. The beam-scanning was driven by a scan mirror with the ability to scan along two orthogonal axes (S-334.2SL with E-517 controller, Physik Instrumente GmbH). For reproducible placement, the pinhole was mounted on a magnetic base. To generate a structured illumination pattern, the fast axis of the beam scanner was running at the fastest speed with a 50Hz sine generator function whether the slow axis was stepped precisely every half period. The overlay of both movements generates the illumination scan pattern as explained in Fig. 2b) and shown in Fig. 3a). The pattern has a period of 312nm in the focal plane and each of the four phase steps has a value of  $312\text{nm} \times 0.25 = 78\text{nm}$ . The 3D data sets with images refocused by 100nm steps along the optical axis were acquired using a piezo-focus drive (Nano-F200W, Mad City Labs Inc.).

## IMAGE RECONSTRUCTION

Several well-known sectioning algorithms were used to reconstruct the recorded images, and the image properties of the so acquired images was compared [13, 14]. The normal image without any structured pattern illumination is obtained by the mean of all acquired phase-shifted images per slice and is used as reference.

$$Mean(\mathbf{r}) = \frac{1}{N} \sum_{n=1}^N I_n(\mathbf{r}) \quad (2)$$

Where  $I_n$  is the image of phase  $n$  of total  $N$  phase steps and  $\mathbf{r}$  is now the image coordinate in three dimensions. To achieve a sectioning enhancement, already a very good estimate is given by the MaxMin equation (3) [15]. This approach determines the maximum  $\max_{n=1\dots N}$  and the minimum  $\min_{n=1\dots N}$  value for every pixel  $\mathbf{r}$  in all images  $I_n$  in one focal plane and subtracts them. As for out-of-focus light the modulation is decreased and averaged over multiple emitters, the minimum is a reasonable and simple estimate of the out-of-focus contribution. For this approach it is beneficial to have an even number of phase steps.

$$MaxMin(\mathbf{r}) = \max_{n=1\dots N} I_n(\mathbf{r}) - \min_{n=1\dots N} I_n(\mathbf{r}) \quad (3)$$

As OPRA uses a camera for imaging, one can record the illumination scan pattern while using a thin fluorescent plane or a mirror sample. This mask describes the illuminated and non-illuminated areas for each phase step and can be used to process a scaled subtraction of out-of-plane fluorescence in the acquired images given by eq. (4) [13, 14].

$$ScaSub(\mathbf{r}) = \sum_{n=1}^N I_n(\mathbf{r}) mask_n(\mathbf{r}) - \alpha \sum_{n=1}^N I_n(\mathbf{r}) (1 - mask_n(\mathbf{r})) \quad (4)$$

Here  $\alpha$  is a subtraction scaling factor which influences the sectioning performance and SNR in the resulting image. For the ScaSub 1 method according to [14] the scaling factor is set to  $\alpha = 1/(N + 1)$  and for ScaSub 2 to  $\alpha = 1/(N - 1)$ . Here we use a smooth mask, where  $(1 - mask_n(\mathbf{r}))$  represents the inverse mask describing the non-illuminated areas in every acquisition frame. We further force the mask to be homogenous.

$$\sum_{n=1}^N mask_n(\mathbf{r}) = 1 ; \quad \forall(\mathbf{r}) \quad (5)$$

This image reconstruction is straight forward and therefore can easily be applied to the acquired images.

## RESULTS

To validate the method, thick samples with 110nm fluorescent beads (FluoSpheres® Carboxylate-Modified Microspheres, 0.11  $\mu\text{m}$ , Yellow-Green Fluorescent 505/515) in a 3D volume (embedded in Prolong Antifade, Molecular Probes, Invitrogen Inc.) were measured. The table 1 shows the FWHM of

the measured beads within and perpendicular to the focal plane for different OPRA modes (with and without a pinhole) and compares different image processing algorithms. This survey shows that the patterned illumination improves the imaging performance in OPRA. The FWHM along the optical axis is decreased by over 19% if a large detection pinhole (approximately 2 AU) is inserted and by 29% if no pinhole is present. The table also shows that a large sectioning pinhole is useful as the processed data of the setup with pinhole achieves better resolution along the optical axis compared to the data acquired with no pinhole. For the in-plane resolution, the processed data reaches the expected limit. A possible explanation is that the patterned illumination in combination with the sectioning algorithms helps to minimize the influence of imperfections by optical aberrations in the setup.

	pinhole with 2.4 AU diameter			no pinhole		
	Mean	MaxMin	ScaSub 1	Mean	MaxMin	ScaSub 1
FWHM lateral [nm]	174	142	145	191	162	154
FWHM axial [nm]	584	487	472	866	620	615

Table 1 Resolution comparison of a 3D volume bead sample (bead-diameter is 110nm) for different processing types. The table shows that illumination with a striped pattern followed by processing, improves the resolution in OPRA. It is preferable to include a fairly large pinhole as disturbing out-of-focus light doesn't reach the detector. But also for data without detection pinhole the processing leads to improved resolution.

A visualization of the imaging method and results for a biological sample are presented in Fig. 3. The inset of the illumination pattern in Fig. 3a shows a magnified part of the FOV and the overlay of images of the 4 phase pattern (p1...p4) visualizes the phase steps. Figure 3b shows one single frame of excited fluorophores labelling actin filaments of a BPAE cell (FluoCells Prepared Slides #1, BPAE cell stained with AlexaFluor 488 with Phalloidin, Molecular Probes Inc.). In Fig. 3d to Fig. 3g different computational methods according to eq. (2) - (5) illustrate the image quality improvement due to structured illumination in OPRA. Note that a pinhole of approximately 2 AU diameter was present in the beam path. Even for this relatively thin sample and with a pinhole already suppressing a lot of the out-of-plane fluorescence, the resolution enhancement and sectioning improvement is apparent and can be seen in Fig. 3c. The simple MaxMin approach in Fig. 3e (eq. 3) gives clearly sharper images. For the scaled subtraction (eq. 4) the imaging performance depends on the scaling factor  $\alpha$ . With increasing  $\alpha$ , the background suppression and sectioning ability improves but the image appears noisier and is affected by artefacts caused by the illumination pattern (Fig. 3f and 3g). These more subjective parameters can be supported with the measurement of the overall intensity of the FOV per z-slice, as given in figure 3c. This curve shows the obvious improvement of the sectioning performance in dependency of the used algorithm and compared to the normal OPRA mode.

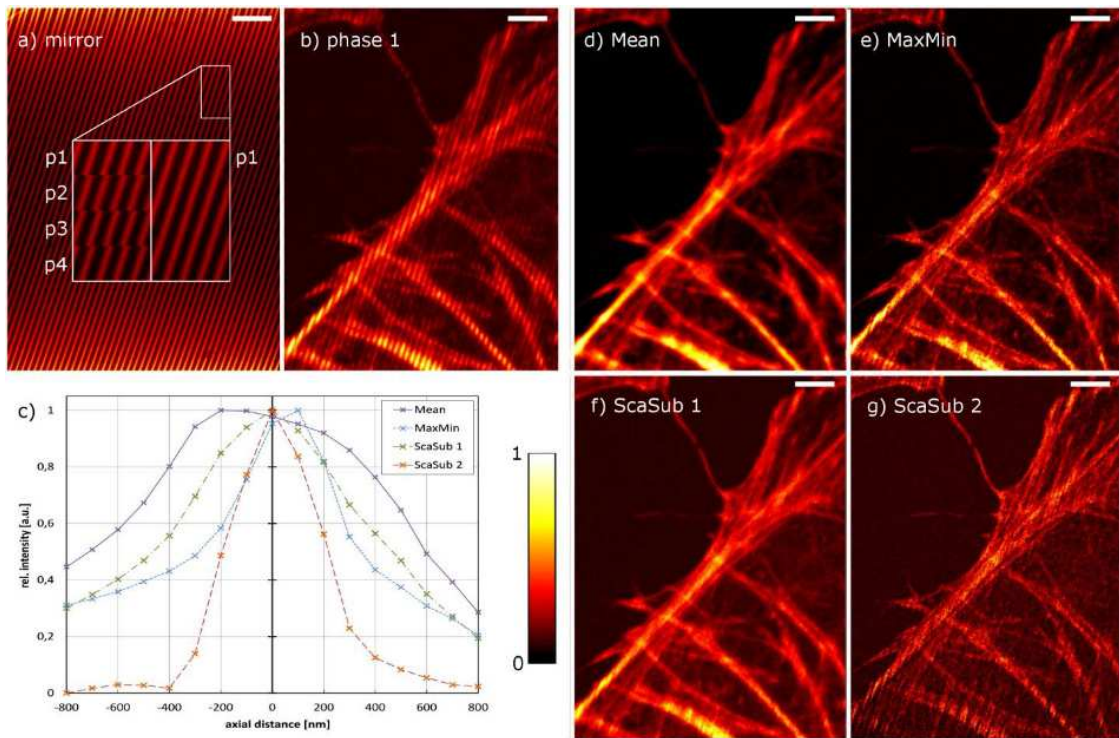


Fig. 3 Resolution enhancement in OPRA through structured illumination. Figure 3a) shows an image of a mirror illuminated with the pattern of phase 1 (p1) (for this purpose, the excitation filter was unmounted). In the inset one region of the FOV is magnified and the 4 phase steps (p1...p4) are visualized. In 3b) the pattern of phase 1 is visible while illuminating actin filaments of a BPAE cell (Bovine Pulmonary Artery Endothelial Cells, stained with Alexa Fluor 488 Phalloidin). In 3d) the Mean-image of all 4 phase steps, which was calculated according to equation (2), is shown. The MaxMin-image (see eq. (3)) in 3e) gives already more crispy images and enhanced resolution. The ScaSub 1 in 3f) was calculated with eq. (4) ( $\alpha = 1/5$ ) and gives even finer details than 3e). In ScaSub 2 (see Fig. 3g)  $\alpha$  was set to  $1/3$  achieving a better sectioning effect and therefore making finer details visible but the image is affected by noise and illumination artefacts. The mean intensity of the images 3d) to 3g) as function of the axial distance can be found in 3c). Here the intensity of the FOV is normalised and an offset from an out-of-focus plane is subtracted. The improvement of the sectioning performance for the different sectioning algorithm compared to the normal OPRA image is clearly visible. Imaging parameters:  $NA=1.4$   $\lambda_{ex}=488nm$ ; scalebar:  $2\mu m$ .

To further demonstrate the sectioning ability in OPRA we also imaged a relatively thick sample of HELA cells (Human Cervical Adenocarcinoma Cells) expressing the Kohinoor protein (Fig. 4). In the OPRA image without a pinhole (Fig. 4a to 4d), the out of focus light deteriorates the image quality, where this light could be partially suppressed in the processed data (Fig. 4c). Nevertheless, inserting a large pinhole for background elimination in combination with patterned illumination seems to give the best results as the signal is still at high level and the out-of-focus signal doesn't pass the pinhole. For thick samples, the MaxMin algorithm (Fig. 4b and 4f) doesn't work as well as for thin samples, but the scaled subtraction (Fig. 4c and 4g) benefits from the used mask and generates nicely sectioned data. Therefore the combination of OPRA with a relatively large pinhole and structured illumination seems to merge most of the important imaging properties as 3D resolution and signal-to-noise ratio.

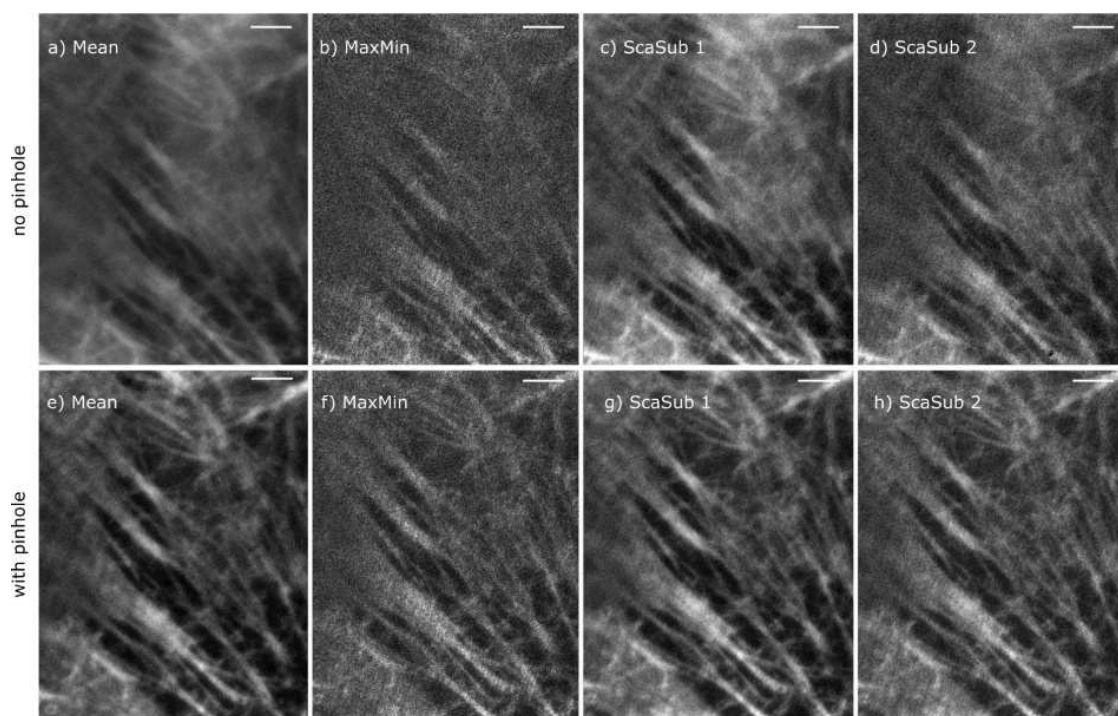


Fig. 4 HELA cells expressing fluorescent Kohinoor protein imaged without (top row: Fig. 4a) to Fig. 4d) and with a detection pinhole (bottom row: Fig. 4e) to Fig. 4h). In the upper right corner of subfigures 4a) to 4d), out-of-plane light is visible as the fluorescent structure is more than  $3\mu\text{m}$  along the optical axis apart from the focal plane. This light is suppressed by the detection pinhole in the figures 4e) to 4h). The MaxMin approach in 4b) and 4f) doesn't work as fine for thick samples. Here the use of a mask and scaled subtraction enhances the imaging quality (Fig. 4c) and 4g). Imaging parameters:  $\text{NA}=1.4$ ;  $\lambda_{\text{ex}}=488\text{nm}$ ; scalebar:  $2\mu\text{m}$ .

## CONCLUSION & DISCUSSION

We demonstrated that structured illumination for z-sectioning improves the imaging quality of OPRA. As the structured illumination mode can be implemented relatively easily to a given OPRA setup and also the image processing is straight-forward, this mode can be adapted to almost every optical reassignment setup. It gives the possibility to achieve the full performance of the optical reassignment techniques and gains from their high sensitivity and signal-to-noise ratio. The illumination pattern helps to achieve the full resolution of OPRA in the focal plane, as disturbing out-of-focus light can be suppressed. Compared to confocal microscopy, it is also possible to achieve enhanced resolution in the focal plane and along the optical axis even for relative large pinhole diameters. This leads to high imaging performance of OPRA as the resolution in all three directions is enhanced while only a little part of the emitted light is lost during the imaging acquisition.

## LITERATURE

1. Schermelleh, L., Heintzmann, R. & Leonhardt, H. A guide to super-resolution fluorescence microscopy. *J. Cell Biol.* **190**, 165–175 (2010).
2. Wagner, M. *et al.* Light Dose is a Limiting Factor to Maintain Cell Viability in Fluorescence Microscopy and Single Molecule Detection. *Int. J. Mol. Sci.* **11**, 956–966 (2010).
3. Sheppard, C. J. R. Superresolution in confocal Imaging. *Optik (Stuttg.)* **80**, 53 – 54 (1988).
4. Müller, C. B. & Enderlein, J. Image Scanning Microscopy. *Phys. Rev. Lett.* **104**, 198101 (2010).
5. York, A. G. *et al.* Resolution doubling in live, multicellular organisms via multifocal structured illumination microscopy. *Nat. Methods* **9**, 749–54 (2012).
6. De Luca, G. M. R. *et al.* Re-scan confocal microscopy: scanning twice for better resolution. *Biomed. Opt. Express* **4**, 2644 (2013).
7. Roth, S., Sheppard, C. J., Wicker, K. & Heintzmann, R. Optical photon reassignment microscopy (OPRA). *Opt. Nanoscopy* **2**, 5 (2013).
8. York, A. G. *et al.* Instant super-resolution imaging in live cells and embryos via analog image processing. *Nat. Methods* **10**, 1122–1126 (2013).
9. Roth, S., Sheppard, C. J. R. & Heintzmann, R. Superconcentration of light: circumventing the classical limit to achievable irradiance. *Opt. Lett.* **41**, 2109 (2016).
10. Azuma, T., & Kei, T. Super-resolution spinning-disk confocal microscopy using optical photon reassignment. *Optics Express*, 23(11), 15003 (2015).
11. Sheppard, C. J. R., Gan, X., Gu, M. & Roy, M. in *Handbook Of Biological Confocal Microscopy* (ed. Pawley) 442–452 (Springer Science, 2006).
12. X. S. Gan and C. J. R. Sheppard, "Detectability: A new criterion for evaluation of the confocal microscope," *Scanning* 15, 187-192 (1993)
13. Heintzmann, R. & Benedetti, P. A. High-resolution image reconstruction in fluorescence microscopy with patterned excitation. *Appl. Opt.* **45**, 5037–5045 (2006).
14. Heintzmann, R. in *Handbook of biological confocal microscopy* (ed. Pawley, J. B.) 265–279 (Springer Science, 2006).
15. Benedetti, P. A., Evangelista, V., Guidarini, D. and Vestri, S. (1994), Achieving confocal-point performance in confocal-line microscopy. *Bioimaging*, 2: 122–130.

## 6.4 Interpretation of the optical transfer function: Significance for image scanning microscopy [SR4]

Colin J. R. Sheppard, Stephan Roth, Rainer Heintzmann, Castello Marco, Giuseppe Vicidomini, Rui Chen, Xudong Chen and Alberto Diaspro  
submitted to *Optics Express* in sep 2016

Colin J. R. Sheppard	Idea for the article. Writing of the manuscript.
Stephan Roth	Contribution to the general concept of normalizing OTFs and also contribution to the importance of the low spatial frequency behaviour.
Rainer Heintzmann	Discussion of the manuscript and general results.
Castello Marco	Contribution to the importance of the low spatial frequency behaviour.
Giuseppe Vicidomini	Contribution to the importance of the low spatial frequency behaviour.
Rui Chen	Contribution to the importance of the low spatial frequency behaviour.
Xudong Chen	Discussion of the manuscript and general results.
Alberto Diaspro	Discussion of the manuscript and general results.

All the authors revised, edited and proof read the manuscript.

Colin J R Sheppard, Stephan Roth, Rainer Heintzmann, Castello Marco, Giuseppe Vicidomini, Rui Chen, Xudong Chen, and Alberto Diaspro. Interpretation of the optical transfer function : Significance for image scanning microscopy. *Optics Express*, 2016

# Interpretation of the optical transfer function: Significance for image scanning microscopy

Colin J. R. Sheppard<sup>1</sup>, Stephan Roth<sup>2,3</sup>, Rainer Heintzmann<sup>1,2</sup>, Marco Castello<sup>1,4</sup>,  
Giuseppe Vicidomini<sup>1</sup>, Rui Chen<sup>5</sup>, Xudong Chen<sup>5</sup>, Alberto Diaspro<sup>1,4,6</sup>

<sup>1</sup> Nanophysics, Istituto Italiano di Tecnologia, via Morego 30, 16163 Genova, Italy

<sup>2</sup> Leibniz Institute of Photonic Technology, Albert-Einstein-Str.9, 07745 Jena, Germany

<sup>3</sup> Institute of Physical Chemistry and Abbe Center of Photonics, Friedrich-Schiller-University Jena, Helmholtzweg 4,  
07743 Jena, Germany

<sup>4</sup> University of Genoa, 16145 Genoa, Italy

<sup>5</sup> Dept. ECE, National University of Singapore 117576, Singapore

<sup>6</sup> Nikon Imaging Center, Istituto Italiano di Tecnologia, via Morego 30, 16163 Genova, Italy

\* [colinjrshppard@gmail.com](mailto:colinjrshppard@gmail.com)

**Abstract:** The optical transfer function (OTF) is widely used to compare the performance of different optical systems. Conventionally, the OTF is normalized to unity for zero spatial frequency, but in some cases it is better to consider the unnormalized OTF. Examples are in confocal microscopy and image scanning microscopy, where the signal level increases with pinhole or array size. Comparison of the respective unnormalized OTFs gives useful insight into their relative performance. The significance of other properties of the general OTF is discussed.

©2016 Optical Society of America

**OCIS codes:** (070.2580) Fourier optics, (110.4850) Optical transfer functions, (110.0180) Microscopy, (170.1790) Confocal microscopy.

---

## References and links

1. H. H. Hopkins, "The frequency response of a defocused optical system," *Proc. R. Soc. London Ser. A* **231**, 91-103 (1955).
2. M. Gu and C. J. R. Sheppard, "Confocal fluorescent microscopy with a finite-sized circular detector," *J. Opt. Soc. Am. A* **9**, 151-153 (1992).
3. C. J. R. Sheppard and K. G. Larkin, "Vectorial pupil functions and vectorial transfer functions," *Optik* **107**, 79-87 (1997).
4. D. A. Tichenor and J. W. Goodman, "Coherent transfer function," *J. Opt. Soc. Am.* **62**, 293-295 (1972).
5. H. H. Hopkins, "On the diffraction theory of optical images," *Proc. R. Soc. London Ser. A* **217**, 408-432 (1953).
6. C. J. R. Sheppard, "Super-resolution in confocal imaging," *Optik* **80**, 53-54 (1988).
7. C. B. Müller and J. Enderlein, "Image scanning microscopy," *Phys. Rev. Letts.* **104**, 198101 (2010).
8. A. G. York, S. H. Parekh, D. D. Nogare, R. S. Fischer, K. Temprine, M. Mione, A. B. Chitnis, C. A. Combes, and H. Shroff, "Resolution doubling in live, multicellular organisms via multifocal structured illumination microscopy," *Nature Methods* **9**, 749-754 (2012).
9. C. J. R. Sheppard, S. B. Mehta, and R. Heintzmann, "Superresolution by image scanning microscopy using pixel reassignment," *Optics Letters* **38**, 2889-2892 (2013).
10. G. M. R. De Luca, R. M. P. Breeding, R. A. J. Brandt, C. H. C. Zeelenberg, B. E. de Jong, W. Timmermans, L. Nahidi Azar, R. A. Hoebe, S. Stallinga, and E. M. Manders, "Re-scan confocal microscopy: scanning twice for better resolution," *Biomedical Optics Express* **4**, 2644-2656 (2013).
11. S. Roth, C. J. R. Sheppard, K. Wicker, and R. Heintzmann, "Optical photon reassignment microscopy (OPRA)," *Optical Nanoscopy* **2**, 5 (2013).
12. Y. Li and E. Wolf, "Three-dimensional intensity distribution near the focus in systems of different Fresnel numbers," *J. Opt. Soc. Am. A* **1**, 801-808 (1984).
13. C. J. R. Sheppard, "Imaging in optical systems of finite Fresnel number," *J. Opt. Soc. Am. A* **3**, 1428-1432 (1986).
14. R. N. Bracewell, *The Fourier Transform and its Applications*, McGraw-Hill Electrical and Electronic Engineering Series (McGraw Hill, New York, 1978).
15. C. J. R. Sheppard and M. Gu, "The significance of 3-D transfer functions in confocal scanning microscopy," *J. Microsc.* **165**, 377-390 (1992).



16. X. S. Gan and C. J. R. Sheppard, "Detectability: A new criterion for evaluation of the confocal microscope," *Scanning* **15**, 187-192 (1993).
17. T. Wilson and D. K. Hamilton, "Difference confocal scanning microscopy," *Optica Acta* **31**, 452-465 (1984).
18. V. Sarafis, C. Johnson, and G. Boyer, "Confocal microscopy with pinhole super-resolution," *Cell Vision* **4**, 264 (1997).
19. R. Heintzmann, V. Sarafis, P. Munroe, J. Nailon, Q. S. Hanley, and T. M. Jovin, "Resolution enhancement by subtraction of confocal signals taken at different pinhole sizes," *Micron* **34**, 293-300 (2003).
20. H. Dehez, M. Pich', and Y. D. Koninck, "Resolution and contrast enhancement in laser scanning microscopy using dark beam imaging," *Optics Express* **21**, 11440-11445 (2013).
21. S. You, C. F. Kuang, Z. Rong, and X. Liu, "Eliminating deformations in fluorescence emission difference microscopy," *Optics Express* **22**, 3118-3121 (2014).
22. R. Gauderon and C. J. R. Sheppard, "Improvement in imaging in confocal fluorescent microscopes using detector arrays," *Bioimaging* **6**, 126-129 (1998).
23. S. Roth, C. J. R. Sheppard, and R. Heintzmann, "Superconcentration of light – Circumventing the classical limit to achievable irradiance," *Opt. Lett.* (2016).

## 1. Introduction

The optical transfer function (OTF) is a central concept in Fourier optics. The OTF is a property of the optical system only, and once calculated, can be used to model the image formation process for different objects. It can also be used to compare different optical systems, as in order to achieve high resolution we know that the cut-off spatial frequency must be as high as possible, and to achieve good contrast the OTF should also have a large magnitude. The concept of the OTF can be applied to three dimensional (3D) imaging, but here we restrict our attention to the 2D case.

The OTF is applicable to incoherent imaging systems. It is the Fourier transform of the (intensity) point spread function (PSF). As the PSF is real, the OTF must be Hermitian. For a symmetrical system, the OTF must therefore be real, but can be negative, thus resulting in artifacts in the form of contrast reversal. Negative values of OTF occur with defocus [1] (or in the presence of other aberrations), with confocal systems with finite confocal pinhole size [2], in vectorial (polarized) systems [3], and also with nonlinear effects such as fluorescence saturation. Often the magnitude of the OTF is plotted, which is very confusing as a negative value is shown as positive. The negative value is important when calculating an image from the object spectrum.

For coherent imaging systems, many of the properties of the OTF apply to the analogous coherent transfer function (CTF), which determines the strength and phase of the amplitude in the image for a component of spatial frequency in the amplitude object. There are stricter conditions (as compared with the case of the OTF) that need to be satisfied for the CTF to be space-invariant [4]. For partially coherent optical systems, the transfer function approach can be generalized to a bilinear transmission cross-coefficient (TCC) [5].

The OTF is conventionally normalized to unity at zero spatial frequency. This assumption is natural for conventional optical systems that do not absorb energy, as then a featureless object is imaged perfectly. As power is conserved, the value of the OTF for zero frequency is invariant under defocus, or in the presence of aberrations.

However, there are cases when normalization of the transfer function is not appropriate. One case is in a dark field system, when the transfer function is zero at the origin, so that normalization is not possible. A second case is when we consider an increase in the aperture of a system, resulting in better collection efficiency. Also, in a confocal system, as then the signal strength increases as the pinhole size is increased. And in a confocal microscope defocus reduces the signal, even for a featureless object, such as a thin fluorescent sheet for example. If the OTF is not normalized, spatial frequencies are only imaged efficiently if the value their strength in the image is above the noise floor of the optical system. For comparing the relative imaging performance of different optical systems it is thus important to compare the absolute values of the OTF.

This paper considers the general properties of OTFs, and unnormalized OTFs in particular. We then consider as practical examples the cases of confocal microscopy, and image scanning microscopy (ISM), which is basically a confocal microscope with a detector

array [6-11]. ISM allows the signal strength in a confocal microscope to be increased, while at the same time retaining, or even improving upon, the resolution of a true (pointlike detector) confocal microscope. In a confocal microscope, the object is illuminated with a scanned focused spot of light. In order to speed up the scanning process, the single illumination spot is sometimes replaced by an array of spots, as in a spinning disc microscope. A detector array can then be used to record a full-field image at each scan position. The similarity of ISM with structured illumination microscopy (SIM), which is a conventional microscope with a fringe pattern projected on to the object, is then apparent. We can consider confocal microscopes and SIMs as particular cases of a general patterned illumination microscope (PIM).

If light is focused through a circular aperture stop with radius  $a$ , on to a point a distance  $z$  away, with a Fresnel number  $N = a^2 / (\lambda z)$  not large compared with one, it is found that the axial maximum in intensity is displaced towards the aperture. This is called the focal shift effect [12]. It can be explained by the properties of the OTF [13]. For points closer to the aperture, the effective numerical aperture of the system is increased, so that the spatial frequency cutoff is also increased. But there is also defocus: the defocused OTF is rescaled because of the increased numerical aperture (NA). A property of the Fourier transform is that the integral (2D for the present case of a system with circular symmetry) under the OTF gives the on-axis intensity of the PSF. So the on-axis intensity reaches its maximum value when the integral under the OTF is a maximum.

Because of the reciprocal nature of the Fourier transform, the integral under the PSF gives the magnitude of the OTF for zero spatial frequency. As a result of conservation of energy, the value of the OTF at the origin is independent of defocus, and is conventionally set to unity. The relationship between an integral and a central value, in the two domains, is a special case of the projection/slice theorem of tomography.

This result can also be generalized to higher order moments, the integral being just the zero order moment. The cusp (discontinuity in the first derivative) in the OTF at zero spatial frequency (the second derivative is infinite) is related to the  $1/\rho^3$  decay in PSF intensity (where  $\rho$  is cylindrical radius) [14]. This results in the fact that the second moment of the PSF is infinite for a hard-edged aperture, and cannot therefore be used as a measure of resolution in this case.

Next we consider some general properties of unnormalized OTFs. A simple example to illustrate the behavior is that of changing the diameter  $2a$  of an ideal lens of fixed focal length  $f$ , obeying the sine condition. Taking  $f$  to be the radius of the Gaussian reference sphere, the NA is just  $NA = na / f$ , where  $n$  is the refractive index of the immersion medium. The intensity at the focal point is proportional to  $a^4$ . The power of four comes from a power 2 from the stronger focusing with change in NA, and another power of 2 from the increase in area, and therefore focused power.

The effect of increasing the NA, by a factor of  $\sqrt{2}$  (corresponding to a change of aperture of one stop), on the unnormalized OTF is that the value of the OTF at zero spatial frequency, which is proportional to the power in the focused light, is doubled, while the cut-off frequency is increased by a factor of  $\sqrt{2}$ , so that the intensity at the focal point is increased by a factor of 4. If we consider the noise floor to be at a constant value of say 0.1 relative to the peak in the original OTF, the effective cut-off frequency is increased by a factor of 1.54. This example stresses the importance of not normalizing the OTF when considering the performance in the presence of noise.

Fig. 1 shows the normalized in-focus OTF for a confocal fluorescence microscope for different pinhole sizes, calculated using a scalar paraxial theory [2]. The pinhole radius is measured in Airy units. It is seen that the strength of the high spatial frequency components is increased, relative to the zero frequency, as the pinhole size is decreased. The normalized cut-off frequency is 4, where the normalized frequency is  $l = l_t (NA / \lambda)$ , and  $l_t$  is the true frequency. As the pinhole size tends to infinity, the response for normalized frequencies

greater than 2 tends to zero, so the cut-off frequency becomes 2, and the OTF becomes identical to that in a conventional fluorescence microscope.

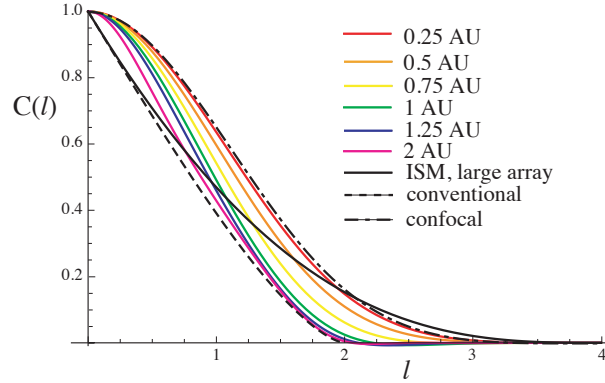


Fig. 1. The normalized OTF for a confocal microscope with different pinhole sizes in Airy units. The OTF for ISM with a large array is also shown.

But this does not tell the whole story, because as the pinhole size becomes smaller the signal measured from a thin, featureless, planar fluorescent object decreases. The unnormalized OTF has already been presented [15], and is replotted in Airy units in Fig. 2 (a). The OTF was calculated from the two dimensional convolution:

$$C(l) = v_d \int_0^{2\pi} \int_0^{2\pi} C_1 C_2 \frac{J_1(l_2 v_d)}{l_2} l_1 d\theta_1 d\theta_2, \quad (1)$$

where  $C_{1,2}$  are the OTFs for the two lenses,

$$C_{1,2} = \text{Re} \left\{ \frac{2}{\pi} \arccos \left[ \frac{l_{1,2}}{2} \sqrt{1 - \frac{l_{1,2}^2}{4}} \right] \right\}, \quad (2)$$

$$l_{1,2} = \sqrt{l^2 + \frac{1}{4} l^2 - l \cos \theta},$$

and  $v_d$  is the radius of the pinhole in optical units, so that  $v_d = 3.83$  AU with AU the pinhole size in Airy units. The integral is evaluated over the region of overlap of  $C_1 C_2$ . The normalized OTF can then be calculated using the signal level from a uniform fluorescent plane [2], given by putting  $l = 0$  in Eq. 2.

It is seen that the magnitude of the OTF for  $l > 2$  is weak if the pinhole size is larger than 0.75 AU. This behavior is shown in more detail in Fig. 3 (a). The OTF exhibits negative values for pinhole sizes greater than 0.5 AU, which degrade the imaging performance. The frequency at which the OTF first becomes zero drops from 4 to 2.2 as the pinhole size increases from 0.5 to 1 AU, as shown in Fig. 4. Interestingly, the negative values of the OTF are strongest for a pinhole size of around 1AU, which is a commonly used size in experimental confocal microscopy. There is therefore some advantage in limiting the size of the pinhole to a smaller value. Actually, a pinhole size of 0.68 AU has been shown to optimize the ratio of signal to noise from background [16]. Alternatively, if a larger pinhole size is used, digital filtering should be employed to suppress or invert the negative parts of the OTF. If the image is low-pass filtered, a modest resolution improvement is attainable for a pinhole size in the range 0.75-1 AU. Note that simple high-frequency enhanced filtering is not a good strategy, as it enhances the negative parts of the OTF. It should be combined with

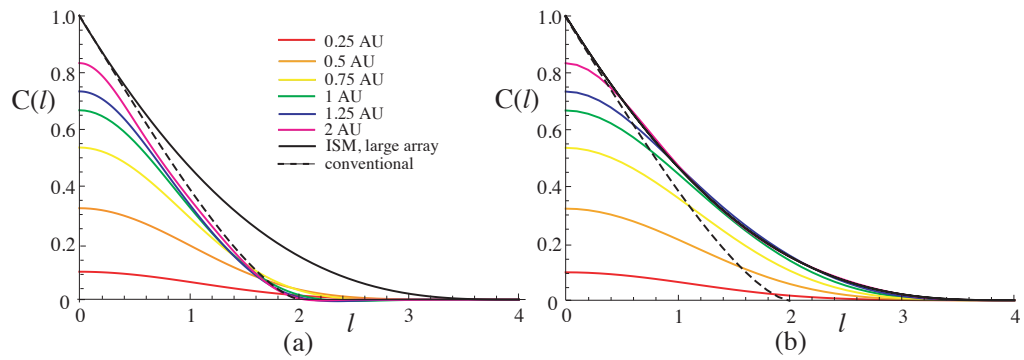


Fig. 2. The unnormalized OTF for (a) confocal microscopes and (b) ISM with different pinhole/array sizes.

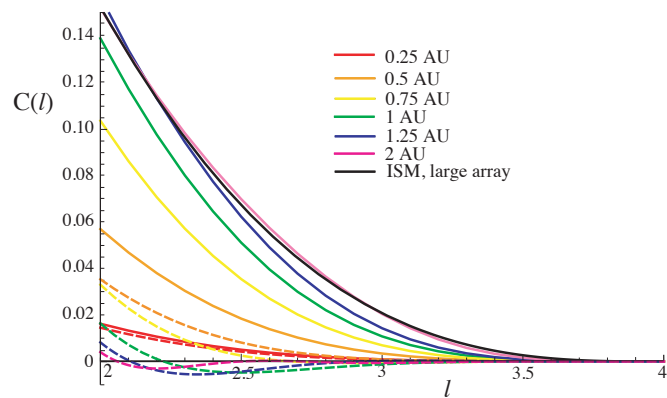


Fig. 3. A close up of the unnormalized OTF at high spatial frequency for a confocal microscope with different pinhole sizes (dashed lines) and ISM with different array sizes (solid lines). The behavior of ISM with a large array is also shown for comparison.

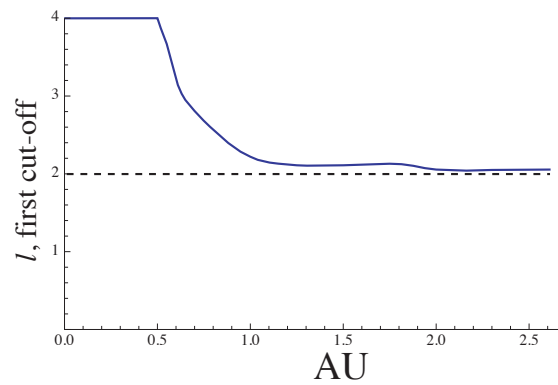


Fig. 4. The normalized spatial frequency for the first zero of the OTF, for confocal imaging with pinhole size in Airy units.

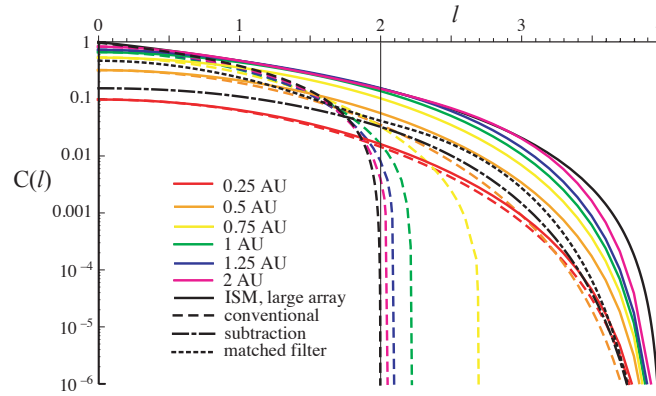


Fig. 5. A logarithmic plot of the unnormalized OTFs for a confocal microscope (dashed lines) and ISM (solid lines) with different pinhole/array sizes. The first positive lobe only of the confocal OTF is shown. The behavior for subtracting images from two pinhole sizes, or using a matched filter with two ring detectors is also shown.

apodization or sign reversal of the high spatial frequencies. A popular imaging technique at present is the general class of methods based on subtractive imaging, where a lower resolution image is subtracted from a high resolution image [17-22]. If a multi-element detector array is used, then images from two different pinhole sizes can be acquired simultaneously. Usually, subtraction reduces the signal and amplifies the noise. But if the subtracted image is recorded with a system with negative components in the OTF, subtraction actually reinforces these components in the final image [22]. Fig. 2 (a) suggests that pinhole radii of about 0.5 AU and 1 AU would be suitable. The multiplication factor of the subtracted signal can be chosen to give a resolution improvement while avoiding strong negative intensities in the final image: subtracting a quarter of the second image from the first gives empirically a good compromise between frequency response and signal level, as shown in the logarithmic plot of Fig. 5, where the first positive lobe only of the confocal OTF is shown. Of course, combining these two images using multi-image deconvolution (e.g. using Richardson-Lucy) or weighted averaging [19] would be even better, but with more computational effort and the need to know the original OTFs. Fig. 5 also shows the result of using a simple matched filter, which combines the OTFs from a 0.5 AU pinhole and a 0.5-1 AU ring. The processed OTF is taken as  $C = (C_1^2 + C_2^2)^{1/2}$ . The performance is quite good, but to implement this approach the signs of the OTFs must be known *a priori*.

In ISM, a 4D data set is acquired by scanning a laser spot in 2D as in confocal, and detecting an image from a detector array at each scan position. The image can be processed using the concept of pixel reassignment, where it is recognized that a combination of illumination point and detection point effectively produces an image of the object point midway between them. These signals can then be integrated over a detector array, which then gives an optical sectioning effect very similar to that in a confocal system with pinhole size equal to the array size. The resulting OTF is shown in Fig. 2 (b), which when compared with Fig. 2 (a) sums up the comparison in the imaging behavior for ISM and confocal microscopy. The OTF was calculated from the Hankel transform

$$C(l) = \frac{1}{2} \int_0^{v_d/2} \int_0^{v_d/2} h_1 h_2 J_0(lv) v v' d v' dv, \quad (3)$$

where the offset intensity point spread functions for illumination and detection after reassignment are

$$h_{1,2} = \frac{4J_1^2(\sqrt{v^2 + \frac{1}{4}v'^2 \pm vv' \cos\theta})}{v^2 + \frac{1}{4}v'^2 \pm vv' \cos\theta}. \quad (4)$$

Again the signal level can be calculated, by putting  $l=0$  in Eq 3. For a small array (e.g. 0.25 AU), the OTF is almost identical to that in confocal, but for larger arrays the high spatial frequency response is much increased (see Fig. 2 (b)). The value of the OTF never exhibits negative values (Fig. 3), as are observed with confocal microscopy with a finite pinhole size. The difference between the OTFs for confocal and ISM is illustrated dramatically in the logarithmic plot in Fig. 5. Note that the OTF for a finite array can have a value slightly greater than that for an infinite array, labelled ISM in Figs. 2, 3 and 5. The performance of ISM with an array bigger than 0.5 AU is better than the matched filter strategy without pixel reassignment.

The peak in the PSF is given by the integral under the OTF. As it is apparent that this is greater for ISM than for confocal, the peak PSF intensity is higher. For large arrays and simple integration with reassignment, the peak intensity is 1.84 times that of conventional fluorescence [8]. The mechanism is that most light is detected, but squeezed into a smaller PSF. This effect has been called superconcentration [23].

ISM with simple integration over a large array exhibits a cusp in the OTF. The PSF is sharper (by a factor 1.53) than in conventional fluorescence, but decays as  $1/\rho^3$  as does conventional fluorescence. For low spatial frequencies, the OTF for ISM and confocal microscopy for the same size of array/pinhole are very similar. For a large array, ISM thus behaves similarly to conventional fluorescence for low frequencies. A large, featureless object contains only low spatial frequencies, so that the superconcentration effect is not observed in this case, but only for small objects.

We have discussed several properties of the general OTF. We have stressed the merits in calculating unnormalized OTFs, and in retaining the sign rather than the magnitude only. Phase is also important, including the case of a phase of  $180^\circ$ . In addition we have discussed the significance of the area under the OTF, the value for zero spatial frequency, and the low frequency behavior, including the presence of a cusp.

These principles were applied to the performance of confocal microscopy and image scanning microscopy, and their comparison. The OTF of image scanning microscopy for different array sizes was presented.

The combination of improvement in signal strength and resolution of ISM will mean that it is likely that eventually this general approach will replace confocal microscopy with a pinhole for most applications.

## 7 Appendix

### 7.1 Peer reviewed publications

- [SR1] Stephan Roth, Colin JR Sheppard, Kai Wicker, and Rainer Heintzmann. Optical photon reassignment microscopy (OPRA). *Optical Nanoscopy*, 2(1):5, 2013. ISSN 2192-2853. doi: 10.1186/2192-2853-2-5. URL <http://www.optnano.com/content/2/1/5>
- [SR2] Stephan Roth, Colin J. R. Sheppard, and Rainer Heintzmann. Superconcentration of light: circumventing the classical limit to achievable irradiance. *Optics Letters*, 41(9):2109, may 2016. ISSN 0146-9592. doi: 10.1364/OL.41.002109. URL <https://www.osapublishing.org/abstract.cfm?URI=ol-41-9-2109>
- [SR3] Stephan Roth and Rainer Heintzmann. Optical Photon Reassignment with increased axial resolution by structured illumination. *Methods and Applications in Fluorescence*, 2016, submitted
- [SR4] Colin J R Sheppard, Stephan Roth, Rainer Heintzmann, Castello Marco, Giuseppe Vicidomini, Rui Chen, Xudong Chen, and Alberto Diaspro. Interpretation of the optical transfer function : Significance for image scanning microscopy. *Optics Express*, 2016, submitted

### Patents

1. Rainer Heintzmann, Stephan Roth, Colin J. R. Sheppard, and Kai Wicker. Verfahren zum optisch hochaufgelösten Raster-scanning eines Objekts, 2014, DE102013005927A. URL <http://www.freepatentsonline.com/DE102013005927A1.html>

## 7.2 Oral presentations

1. Rainer Heintzmann [invited], Kai Wicker, Stephan Roth, Shalin B. Metha and Colin J. R. Sheppard. Optical Photon Reassignment Microscopy. *ELMI conference*, Bordeaux, may 2013.
2. Rainer Heintzmann [invited], Kai Wicker, Stephan Roth, Shalin B. Metha and Colin J. R. Sheppard. Optical Photon Reassignment Microscopy. *Topical Problems of Biophotonics*, Nishni Nowgorod, jul 2013.
3. Rainer Heintzmann [invited], Kai Wicker, Stephan Roth, Shalin B. Metha and Colin J. R. Sheppard. Optical Photon Reassignment Microscopy. *Methods and Applications in Fluorescence conference*, Genua, aug 2013.
4. Stephan Roth, Kai Wicker, Colin J. R. Sheppard and Rainer Heintzmann. Optical Photon Reassignment Microscopy. *Doktorandenseminar*, Dornburg, mar 2014.
5. Stephan Roth and Rainer Heintzmann. Optical Photon Reassignment Microscopy. *DokDok*, Eisenach, oct 2015.
6. Stephan Roth and Rainer Heintzmann. Superconcentration of light in Optical Photon Reassignment Microscopy. *Doktorandenseminar*, Dornburg, feb 2016.
7. Colin J. R. Sheppard [invited], Stephan Roth, Rainer Heintzmann, Marco Castello, Giuseppe Vicidomini, Chen Chen, Xudong Chen and Alberto Diaspro. Interpretation of the optical transfer function: Implications for confocal and image scanning microscopy. *Focus on microscopy*, Taipei, mar 2016.
8. Stephan Roth and Rainer Heintzmann. Optical Photon Reassignment Microscopy. *Workshop for microscopy methods*, Innsbruck, sep 2016.



### 7.3 Poster presentations

1. Stephan Roth, Colin J. R. Sheppard and Rainer Heintzmann. Optical Photon Reassignment Microscopy. *49th Klosters Winterseminar*, Klosters, jan 2014.
2. Stephan Roth and Rainer Heintzmann. Superconcentration of light in Optical Photon Reassignment Microscopy. *Doktorandenseminar*, Dornburg, jan 2015.
3. Stephan Roth, Colin J. R. Sheppard and Rainer Heintzmann. Superconcentration of light: circumventing the classical limit to achievable irradiance. *Focus on microscopy*, Göttingen, mar 2015.
4. Stephan Roth and Rainer Heintzmann. Optical Photon Reassignment Microscopy. *DokDok*, Eisenach, oct 2015.

## 7.4 Curriculum vitae

Name: Stephan Roth  
Address: Jansonstraße 2, 07745 Jena, Germany  
Date of birth: 29.02.1984  
Phone: +49 (0) 151 592 15 272  
Mail: stephan.roth@uni-jena.de

1994 – 2002 Gymnasium “Friedrich-Schiller” in Weimar, Abitur  
2002 – 2003 civilian service in the hospital „Sophien-Hufeland“ in Weimar  
2003 – 2009 studying physics at the “Friedrich-Schiller-University” in Jena, very good graded diploma, photonics certification  
2006 – 2010 scientific assistant and diploma thesis about the characterisation of organic light emitters at the “Fraunhofer Institute for Applied Optics and Precision Engineering, IOF” in Jena  
11/2010 - 2016 PhD at the Biomedical imaging department of Prof. Heintzmann at the “Leibniz Institute of Photonic Technologies, IPHT” in Jena

## 7.5 Acknowledgement

I feel really pleased and honoured to have the ability to work on such an interesting topic in this field of research. Also it is a pleasure to be part of an interdisciplinary institute as the IPHT. The interaction with different research areas and disciplines helps to not get lost in small details, while still have the chance to get a different perspective on challenges and needs.

First I want to thank my supervisor Prof. Rainer Heintzmann for given me the opportunity to work on the topic of superresolution fluorescent microscopy. It is a pleasure to work together with a pioneer in superresolution microscopy. I'm honestly impressed by his way of "out-of-the-box" thinking. I'm now even more convinced, that, if you really love what you do, it is way easier to accept the stress and work load that is often connected with work in research. Without failure there is no success. What sounds obvious is with no doubt true for research, as the risks of failure are definitely high, if something new is tried. Rainer always encouraged and motivated me to try something new and keep pushing.

I also want to acknowledge Dr. Kai Wicker who really contributed a lot in the first years to the project. Of course I'm pleased to collaborate with one of the pioneers in confocal microscopy - Prof. Colin Sheppard. He impressed me not only because of his huge knowledge and mathematical skills but also in his way to act with people and to motivate them. I want to thank Dr. Thomas Bocklitz for his help regarding the structure and the language of this thesis and for all the mountain adventures we had together. I also want to thank my second evaluator Prof. Michael Schmitt for his willingness to appraise my thesis.

Of course the most important support in daily work comes from my dear colleagues and office mates. I'm sure that in this regard I was extremely lucky, because this friendly and at the same time also productive working atmosphere is far from being the normal case.

In the end, I want to thank my family. They gave me everything I needed to get here and become what I am today. Without their support, nothing would be possible. Thank you for everything!

Stephan Roth

## Selbstständigkeitserklärung

Hiermit erkläre ich,

dass ich die vorliegende Arbeit selbstständig und unter Verwendung der angegebenen Hilfsmittel, persönlichen Mitteilungen und Quellen angefertigt habe.

Jena, 13. Oktober 2016

---

Stephan Roth

## Erklärung über die Eigenanteile

Erklärung zu den Eigenanteilen des Promovenden sowie der weiteren Doktoranden als Koautoren an den Publikationen und Zweitpublikationsrechten bei einer kumulativen Dissertation.

Für alle in dieser kumulativen Dissertation verwendeten Manuskripte liegen die notwendigen Genehmigungen der Verlage („Reprint permissions“) für die Zweitpublikation vor. Die Co-Autoren der in dieser kumulativen Dissertation verwendeten Manuskripte sind sowohl über die Nutzung, als auch über die oben angegebenen Eigenanteile informiert und stimmen dem zu.

Die Anteile der Co-Autoren an den Publikationen sind im Kapitel 6 aufgeführt. Ich bin mit der Abfassung der Dissertation als publikationsbasiert, d.h. kumulativ, einverstanden und bestätige die vorstehenden Angaben. Eine entsprechend begründete Befürwortung mit Angabe des wissenschaftlichen Anteils des Doktoranden an den verwendeten Publikationen werde ich parallel an den Rat der Fakultät der Chemisch-Geowissenschaftlichen Fakultät richten.

Jena, 13. Oktober 2016

---

Stephan Roth

Jena,      Oktober 2016

---

Rainer Heintzmann (Erstbetreuer)

## References

- [1] Ernst Abbe. Beiträge zur Theorie des Mikroskops und der mikroskopischen Wahrnehmung. *Archiv für Mikroskopische Anatomie*, 9(1):413–418, dec 1873. ISSN 0176-7364. doi: 10.1007/BF02956173. URL <http://link.springer.com/10.1007/BF02956173>.
- [2] Stefan Hell and Ernst H. K. Stelzer. Properties of a 4Pi confocal fluorescence microscope. *Journal of the Optical Society of America A*, 9(12):2159, dec 1992. ISSN 1084-7529. doi: 10.1364/JOSAA.9.002159. URL <https://www.osapublishing.org/abstract.cfm?URI=josaa-9-12-2159>.
- [3] Nobelprize.org. The Nobel Prize in Chemistry 2014 - Advanced Information, 2014. URL [http://www.nobelprize.org/nobel\\_prizes/chemistry/laureates/2014/advanced.html](http://www.nobelprize.org/nobel_prizes/chemistry/laureates/2014/advanced.html).
- [4] Stefan W Hell and Jan Wichmann. Breaking the diffraction resolution limit by stimulated emission: stimulated-emission-depletion fluorescence microscopy. *Opt. Lett.*, 19(11):780–782, jun 1994. doi: 10.1364/OL.19.000780. URL <http://ol.osa.org/abstract.cfm?URI=ol-19-11-780>.
- [5] Stefan W Hell. Far-Field Optical Nanoscopy. *Science*, 316(5828):1153–1158, may 2007. ISSN 0036-8075. doi: 10.1126/science.1137395. URL <http://www.sciencemag.org/cgi/doi/10.1126/science.1137395>.
- [6] Katrin I Willig, Benjamin Harke, Rebecca Medda, and Stefan W Hell. STED microscopy with continuous wave beams. *Nature Methods*, 4(11):3–5, nov 2007. ISSN 1548-7091. doi: 10.1038/NMETH1108. URL <http://www.ncbi.nlm.nih.gov/pubmed/17952088>.
- [7] Andriy Chmyrov, Jan Keller, Tim Grotjohann, Michael Ratz, Elisa D’Este, Stefan Jakobs, Christian Eggeling, and Stefan W Hell. Nanoscopy with more than 100,000 ‘doughnuts’. *Nature methods*, 10(8):737–40, aug 2013. ISSN 1548-7105. doi: 10.1038/nmeth.2556. URL <http://www.ncbi.nlm.nih.gov/pubmed/23832150>.
- [8] Fabian Bergermann, Lucas Alber, Steffen J. Sahl, Johann Engelhardt, and Stefan W. Hell. 2000-fold parallelized dual-color STED fluorescence nanoscopy. *Optics Express*, 23(1):211, 2015. ISSN 1094-4087. doi: 10.1364/OE.23.000211. URL <http://www.opticsexpress.org/abstract.cfm?URI=oe-23-1-211>.
- [9] Eric Betzig. Proposed method for molecular optical imaging. *Optics letters*, 20(3):237–9, 1995. ISSN 0146-9592. doi: 10.1364/OL.20.000237. URL <http://www.ncbi.nlm.nih.gov/pubmed/19859146>.
- [10] R M Dickson, a B Cubitt, R Y Tsien, and W E Moerner. On/off blinking and switching behaviour of single molecules of green fluorescent protein. *Nature*, 388(6640):355–8, jul 1997. ISSN 0028-0836. doi: 10.1038/41048. URL <http://www.ncbi.nlm.nih.gov/pubmed/9237752>.
- [11] Eric Betzig, George H Patterson, Rachid Sougrat, O Wolf Lindwasser, Scott Olenych, Juan S Bonifacino, Michael W Davidson, Jennifer Lippincott-Schwartz, and Harald F Hess. Imaging Intracellular Fluorescent Proteins at Nanometer Resolution. *Science*, 313(5793):1642–1645, sep 2006. ISSN 0036-8075.

- doi: 10.1126/science.1127344. URL <http://www.sciencemag.org/cgi/doi/10.1126/science.1127344>.
- [12] Rainer Heintzmann, Thomas M. Jovin, and Christoph Cremer. Saturated patterned excitation microscopy—a concept for optical resolution improvement. *J. Opt. Soc. Am. A*, 19(8):1599–1609, aug 2002. doi: 10.1364/JOSAA.19.001599. URL <http://josaa.osa.org/abstract.cfm?URI=josaa-19-8-1599>.
- [13] M. G L Gustafsson. Surpassing the lateral resolution limit by a factor of two using structured illumination microscopy. SHORT COMMUNICATION. *Journal of Microscopy*, 198(2):82–87, may 2000. ISSN 0022-2720. doi: 10.1046/j.1365-2818.2000.00710.x. URL <http://doi.wiley.com/10.1046/j.1365-2818.2000.00710.x>.
- [14] Aurélie Jost and Rainer Heintzmann. Superresolution Multidimensional Imaging with Structured Illumination Microscopy. *Annual Review of Materials Research*, 43(1):261–282, jul 2013. ISSN 1531-7331. doi: 10.1146/annurev-matsci-071312-121648. URL <http://www.annualreviews.org/doi/abs/10.1146/annurev-matsci-071312-121648>.
- [15] Kai Wicker and Rainer Heintzmann. Resolving a misconception about structured illumination. *Nature Photonics*, 8(May):342–344, 2014. ISSN 1749-4885. doi: 10.1038/nphoton.2014.88. URL <http://www.nature.com/nphoton/journal/v8/n5/full/nphoton.2014.88.html>.
- [16] Ronny Förster, Hui-Wen Lu-Walther, Aurélie Jost, Martin Kielhorn, Kai Wicker, and Rainer Heintzmann. Simple structured illumination microscope setup with high acquisition speed by using a spatial light modulator. *Optics Express*, 22(17):20663, aug 2014. ISSN 1094-4087. doi: 10.1364/OE.22.020663. URL <http://www.opticsinfobase.org/abstract.cfm?URI=oe-22-17-20663>.
- [17] Colin J. R. Sheppard. Superresolution in confocal Imaging. *Optik*, 80(2):53 – 54, 1988.
- [18] Lana Lau, Yin Loon Lee, Steffen J. Sahl, Tim Stearns, and W. E. Moerner. STED microscopy with optimized labeling density reveals 9-fold arrangement of a centriole protein. *Biophysical Journal*, 102(12):2926–2935, 2012. ISSN 00063495. doi: 10.1016/j.bpj.2012.05.015. URL <http://dx.doi.org/10.1016/j.bpj.2012.05.015>.
- [19] Michael J Rust, Mark Bates, and Xiaowei Zhuang. Sub-diffraction-limit imaging by stochastic optical reconstruction microscopy (STORM). *Nature Methods*, 3(10):793–796, oct 2006. ISSN 1548-7091. doi: 10.1038/nmeth929. URL <http://www.nature.com/doi/10.1038/nmeth929>.
- [20] Clemens Roider, Monika Ritsch-Martel, and Alexander Jesacher. High-resolution confocal Raman microscopy using pixel reassignment. *Optics Letters*, 41(16):3825, aug 2016. ISSN 0146-9592. doi: 10.1364/OL.41.003825. URL <https://www.osapublishing.org/abstract.cfm?URI=ol-41-16-3825>.
- [21] A. Chodon. Circa 1590: Invention of the microscope. *APS News*, 13(3):2004, 2004. URL <http://www.aps.org/publications/apsnews/200403/history.cfm>.
- [22] J R Porter. Antony van Leeuwenhoek: tercentenary of his discovery of bacteria. *Bacteriological reviews*, 40(2):260–9, jun 1976. ISSN 0005-3678. URL <http://www.pubmedcentral.nih.gov/articlerender.fcgi?artid=PMC413956>.

- [23] Claus B. Müller and Jörg Enderlein. Image Scanning Microscopy. *Physical Review Letters*, 104(19):198101, may 2010. ISSN 0031-9007. doi: 10.1103/PhysRevLett.104.198101. URL <http://link.aps.org/doi/10.1103/PhysRevLett.104.198101>.
- [24] Rainer Heintzmann, Stephan Roth, Colin J. R. Sheppard, and Kai Wicker. Verfahren zum optisch hochaufgelösten Raster-scanning eines Objekts, 2014, DE102013005927A. URL <http://www.freepatentsonline.com/DE102013005927A1.html>.
- [25] Giulia M.R. De Luca, Ronald M.P. Breedijk, Rick a.J. Brandt, Christiaan H.C. Zeelenberg, Babette E. de Jong, Wendy Timmermans, Leila Nahidi Azar, Ron a. Hoebe, Sjoerd Stallinga, and Erik M.M. Manders. Re-scan confocal microscopy: scanning twice for better resolution. *Biomedical Optics Express*, 4(11):2644, oct 2013. ISSN 2156-7085. doi: 10.1364/BOE.4.002644. URL <http://www.opticsinfobase.org/abstract.cfm?URI=boe-4-11-2644>.
- [26] De Luca Giulia, Breedijk Ronald, and Manders Erik. Re-Scan Confocal, 2016. URL <http://re-scan.nl/>.
- [27] Takuya Azuma and Takayuki Kei. Super-resolution spinning-disk confocal microscopy using optical photon reassignment. *Optics Express*, 23(11):15003, jun 2015. ISSN 1094-4087. doi: 10.1364/OE.23.015003. URL <https://www.osapublishing.org/oe/abstract.cfm?uri=oe-23-11-15003>.
- [28] Yokogawa. Yokogawa - CSU-SR, 2016. URL <http://www.yokogawa.com/pr/news/2016/pr-news-2016-0610-en.htm>.
- [29] VisiTech International Ltd. vt-iSIM, 2016. URL <http://www.visitech.co.uk/vt-isim.html>.
- [30] Jeff W Lichtman and José-Angel Conchello. Fluorescence microscopy. *Nature Methods*, 2(12):910–919, 2005. ISSN 1548-7091. doi: 10.1038/nmeth817. URL <http://www.nature.com/doifinder/10.1038/nmeth817>.
- [31] Marta Fernández-Suárez and AY Ting. Fluorescent probes for super-resolution imaging in living cells. *Nature Reviews Molecular Cell Biology*, 9(12):929–943, 2008. ISSN 1471-0080. doi: 10.1038/nrm2531. URL <http://www.nature.com/nrm/journal/v9/n12/abs/nrm2531.html>.
- [32] Michael Eisenstein. Super-resolve me: from micro to nano. *Nature*, 526(7573):459–462, oct 2015. ISSN 0028-0836. doi: 10.1038/526459a. URL <http://www.nature.com/doifinder/10.1038/526459a>.
- [33] Florian Ströhl and Clemens F Kaminski. Frontiers in structured illumination microscopy. *Optica*, 3(6):667, jun 2016. ISSN 2334-2536. doi: 10.1364/OPTICA.3.000667. URL <https://www.osapublishing.org/abstract.cfm?URI=optica-3-6-667>.
- [34] Stefan W Hell, Steffen J Sahl, Mark Bates, Xiaowei Zhuang, Rainer Heintzmann, Martin J Booth, Joerg Bewersdorf, Gleb Shtengel, Harald Hess, Philip Tinnefeld, Alf Honigmann, Stefan Jakobs, Ilaria Testa, Laurent Cognet, Brahim Lounis, Helge Ewers, Simon J Davis, Christian Eggeling, David Klenerman, Katrin I Willig, Giuseppe Vicidomini, Marco Castello, Alberto Diaspro, and Thorben Cordes. The 2015 super-resolution microscopy roadmap. *Journal*



- of Physics D: Applied Physics*, 48(44):443001, 2015. ISSN 0022-3727. doi: 10.1088/0022-3727/48/44/443001. URL <http://stacks.iop.org/0022-3727/48/i=44/a=443001?key=crossref.64b10c5e92be3dbad6191dbfa3f07386>.
- [35] Elen Tolstik, Sapna Shukla, and Rainer Heintzmann. High-resolution Far-field Microscopy. In *The Optics Encyclopedia*, volume 49, pages 1–31. Wiley-VCH Verlag GmbH & Co. KGaA, Weinheim, Germany, jun 2015. ISBN 9783527600441. doi: 10.1002/9783527600441.oel1007. URL <http://doi.wiley.com/10.1002/9783527600441.oel1007>.
- [36] Lothar Schermelleh, Rainer Heintzmann, and Heinrich Leonhardt. A guide to super-resolution fluorescence microscopy. *The Journal of Cell Biology*, 190(2): 165–175, 2010. doi: 10.1083/jcb.201002018. URL <http://jcb.rupress.org/content/190/2/165.abstract>.
- [37] Stefan W Hell. Microscopy and its focal switch. *Nat Meth*, 6(1):24–32, 2009. ISSN 1548-7091. URL <http://dx.doi.org/10.1038/nmeth.1291>.
- [38] Rainer Heintzmann and Christoph G Cremer. Laterally modulated excitation microscopy: improvement of resolution by using a diffraction grating. In *BiOS Europe'98*, pages 185–196. International Society for Optics and Photonics, 1999.
- [39] Eva Rittweger, Kyu Young Han, Scott E Irvine, Christian Eggeling, and Stefan W Hell. STED microscopy reveals crystal colour centres with nanometric resolution. *Nature Photonics*, 3(March):1–4, 2009. doi: 10.1038/NPHOTON.2009.2.
- [40] Christian a Wurm, Kirill Kolmakov, Fabian Göttfert, Haisen Ta, Mariano Bossi, Heiko Schill, Sebastian Berning, Stefan Jakobs, Gerald Donnert, Vladimir N Belov, and Stefan W Hell. Novel red fluorophores with superior performance in STED microscopy. *Optical Nanoscopy*, 1(1):7, 2012. ISSN 2192-2853. doi: 10.1186/2192-2853-1-7. URL <http://www.optnano.com/content/1/1/7>.
- [41] Hui-Wen Lu-Walther. *Fast SLM-based linear and nonlinear structured illumination microscopy Kumulative Dissertation*. PhD thesis, FSU, 2016.
- [42] Sebastian van de Linde, Ivan Krstić, Thomas Prisner, Sören Doose, Mike Heilemann, and Markus Sauer. Photoinduced formation of reversible dye radicals and their impact on super-resolution imaging. *Photochemical & photobiological sciences : Official journal of the European Photochemistry Association and the European Society for Photobiology*, 10(4):499–506, apr 2011. ISSN 1474-9092. doi: 10.1039/c0pp00317d. URL <http://www.ncbi.nlm.nih.gov/pubmed/21152594>.
- [43] Joshua C Vaughan, Shu Jia, and Xiaowei Zhuang. Ultrabright photoactivatable fluorophores created by reductive caging. *Nature Methods*, 9(october):1–7, 2012. ISSN 1548-7091. doi: 10.1038/nmeth.2214. URL <http://dx.doi.org/10.1038/nmeth.2214>.
- [44] M Minsky. Microscopy Apparatus, 1957. URL <http://www.freepatentsonline.com/3013467.html>.
- [45] Guy Cox and Colin J. R. Sheppard. Practical limits of resolution in confocal and non-linear microscopy. *Microscopy research and technique*, 63(1):18–22, jan 2004. ISSN 1059-910X. doi: 10.1002/jemt.10423. URL <http://www.ncbi.nlm.nih.gov/pubmed/14677129>.

- [46] XS Gan and C.J.R. Sheppard. Detectability: a new criterion for evaluation of the confocal microscope. *Scanning*, 15(January 1993):187–192, 1993. ISSN 01610457. doi: 10.1002/sca.4950150402. URL <http://onlinelibrary.wiley.com/doi/10.1002/sca.4950150402/abstract>.
- [47] T. R. Corle and G. S. Kino. *Confocal scanning optical microscopy and related systems*. Academic Press, Inc., San Diegp, USA, 1996. ISBN 9780124087507. URL <http://www.sciencedirect.com/science/book/9780124087507>.
- [48] I. J. Cox. Scanning optical fluorescence microscopy. *Journal of Microscopy*, 133(2):149–154, feb 1984. ISSN 00222720. doi: 10.1111/j.1365-2818.1984.tb00480.x. URL <http://doi.wiley.com/10.1111/j.1365-2818.1984.tb00480.x>.
- [49] José-Angel Conchello and Jeff W Lichtman. Optical sectioning microscopy. *Nature methods*, 2(12):920–31, dec 2005. ISSN 1548-7091. doi: 10.1038/nmeth815. URL <http://www.ncbi.nlm.nih.gov/pubmed/16299477>.
- [50] Seth R. Goldstein, Thomas Hubin, Scott Rosenthal, and Clayton Washburn. A confocal video-rate laser-beam scanning reflected-light microscope with no moving parts. *Journal of Microscopy*, 157(1):29–38, jan 1990. ISSN 00222720. doi: 10.1111/j.1365-2818.1990.tb02944.x. URL <http://doi.wiley.com/10.1111/j.1365-2818.1990.tb02944.x>.
- [51] Wiliam B Amos. Achromatic scanning system, 1991. URL <http://www.google.com/patents/US4997242>.
- [52] Christin Bechtel, Jens Knobbe, Heinrich Grüger, and Hubert Lakner. Large field of view MEMS-based confocal laser scanning microscope for fluorescence imaging. *Optik - International Journal for Light and Electron Optics*, 125(2):876–882, 2014. ISSN 00304026. doi: 10.1016/j.ijleo.2013.07.091. URL <http://linkinghub.elsevier.com/retrieve/pii/S0030402613010851>.
- [53] G J Brakenhoff and K Visscher. Confocal imaging with bilateral scanning and array detectors. *Journal of Microscopy*, 165(1):139–146, jan 1992. ISSN 00222720. doi: 10.1111/j.1365-2818.1992.tb04311.x. URL <http://dx.doi.org/10.1111/j.1365-2818.1992.tb04311.x>.
- [54] Barry R Masters and Andreas A Thaer. Real-time scanning slit confocal microscopy of the in vivo human cornea. *Applied Optics*, 33(4):695–701, 1994. ISSN 0003-6935. doi: 10.1364/AO.33.000695. URL <http://www.ncbi.nlm.nih.gov/pubmed/20862066>.
- [55] Andrew G York, Panagiotis Chandris, Damian Dalle Nogare, Jeffrey Head, Peter Wawrzusin, Robert S Fischer, Ajay Chitnis, and Hari Shroff. Instant super-resolution imaging in live cells and embryos via analog image processing. *Nature Methods*, 10(11):1122–1126, oct 2013. ISSN 1548-7091. doi: 10.1038/nmeth.2687. URL <http://www.nature.com/doi/finder/10.1038/nmeth.2687>.
- [56] Alistair Curd, Alexa Cleasby, Katarzyna Makowska, Andrew York, Hari Shroff, and Michelle Peckham. Construction of an instant structured illumination microscope. *Methods*, 88(July):37–47, 2015. ISSN 10462023. doi: 10.1016/j.ymeth.2015.07.012. URL <http://linkinghub.elsevier.com/retrieve/pii/S1046202315300293>.
- [57] Andrew G York, Sapun H Parekh, Damian Dalle Nogare, Robert S Fischer, Kelsey

- Temprine, Marina Mione, Ajay B Chitnis, Christian a Combs, and Hari Shroff. Resolution doubling in live, multicellular organisms via multifocal structured illumination microscopy. *Nature methods*, 9(7):749–54, jul 2012. ISSN 1548-7105. doi: 10.1038/nmeth.2025. URL <http://www.ncbi.nlm.nih.gov/pubmed/22581372>.
- [58] Mojmír Petráň, Milan Hadravský, M David Egger, and Robert Galambos. Tandem-Scanning Reflected-Light Microscope\*. *Journal of the Optical Society of America*, 58(5):661, may 1968. ISSN 0030-3941. doi: 10.1364/JOSA.58.000661. URL <https://www.osapublishing.org/abstract.cfm?URI=josa-58-5-661>.
- [59] G. Q. Xiao, T. R. Corle, and G. S. Kino. Real-time confocal scanning optical microscope. *Applied Physics Letters*, 53(8):716, 1988. ISSN 00036951. doi: 10.1063/1.99814. URL <http://scitation.aip.org/content/aip/journal/apl/53/8/10.1063/1.99814>.
- [60] Zeiss. Zeiss LSM 800 mit AiryScan, 2016. URL [http://www.zeiss.de/microscopy/de\\_de/produkte/confocal-microscopes/lsm-800-with-airyscan.html](http://www.zeiss.de/microscopy/de_de/produkte/confocal-microscopes/lsm-800-with-airyscan.html).
- [61] C J R Sheppard and T Wilson. Image formation in confocal scanning microscopes. *Optik*, 55(4):331–342, 1980. ISSN 00304026.
- [62] G. J. Brakenhoff, P. Blom, and P. Barends. Confocal scanning light microscopy with high aperture immersion lenses. *Journal of Microscopy*, 117(2):219–232, nov 1979. ISSN 00222720. doi: 10.1111/j.1365-2818.1979.tb01178.x. URL <http://doi.wiley.com/10.1111/j.1365-2818.1979.tb01178.x>.
- [63] Colin J. R. Sheppard, Xiaosong Gan, Min Gu, and Maitreyee Roy. Signal-to-Noise Ratio in Confocal Microscopes. In Pawley, editor, *Handbook Of Biological Confocal Microscopy*, number April, chapter 22, pages 442–452. Springer US, Boston, MA, 2006. ISBN 978-0-387-25921-5 978-0-387-45524-2. doi: 10.1007/978-0-387-45524-2. URL [http://link.springer.com/chapter/10.1007/978-0-387-45524-2\\_22](http://link.springer.com/chapter/10.1007/978-0-387-45524-2_22).
- [64] Hans Blom and Jerker Widengren. Blurry vision belongs to history. *Physics*, 3: 40, may 2010. ISSN 1943-2879. doi: 10.1103/Physics.3.40. URL <http://link.aps.org/doi/10.1103/Physics.3.40>.
- [65] I J Cox, Colin J. R. Sheppard, and T Wilson. Improvement in resolution by nearly confocal microscopy. *Applied optics*, 21(5):778–81, mar 1982. ISSN 0003-6935. URL <http://www.ncbi.nlm.nih.gov/pubmed/20372538>.
- [66] C. J. R. Sheppard, I. J. Cox, and D. K. Hamilton. Edge detection in micrometrology with nearly confocal microscopy. *Applied Optics*, 23(5):657, mar 1984. ISSN 0003-6935. doi: 10.1364/AO.23.000657. URL <https://www.osapublishing.org/abstract.cfm?URI=ao-23-5-657>.
- [67] F Reinholz, W Schutt, G Grummer, F Kuhlmann, and S Kraeft. A new powerful mode of laser scanning microscopy. *Optik*, 4(4):165–168, 1989.
- [68] Fred Reinholz and T Wilson. Image enhancement by tracking and sampling in the detection plane. *Optik*, 1994.
- [69] Rainer Heintzmann and Pier A Benedetti. Space and frequency domain reconstruction strategies in a confocal microscope based on patterned illumination and wide-field image collection. In *FOM Genova 2003*, volume 1907, page 3568, 2003.

- [70] Colin J. R. Sheppard and C J Cogswell. Confocal Microscopy with Detector Arrays. *Journal of Modern Optics*, 37(2):267–279, 1990. doi: <http://www.tandfonline.com/doi/abs/10.1080/09500349014550331>. URL <http://www.tandfonline.com/doi/abs/10.1080/09500349014550331>.
- [71] Rainer Heintzmann, V. Sarafis, Paul Munroe, John Nailon, Quentin S. Hanley, and Thomas M. Jovin. Resolution enhancement by subtraction of confocal signals taken at different pinhole sizes. *Micron*, 34(6-7):293–300, oct 2003. ISSN 09684328. doi: 10.1016/S0968-4328(03)00054-4. URL <http://linkinghub.elsevier.com/retrieve/pii/S0968432803000544>.
- [72] Colin J. R. Sheppard, Shalin B Mehta, and Rainer Heintzmann. Superresolution by image scanning microscopy using pixel reassignment. *Optics Letters*, 38(15):2889, aug 2013. ISSN 0146-9592. doi: 10.1364/OL.38.002889. URL <https://www.osapublishing.org/ol/abstract.cfm?uri=ol-38-15-2889>.
- [73] Olaf Schulz, Christoph Pieper, Michaela Clever, Janine Pfaff, Aike Ruhlandt, Ralph H Kehlenbach, Fred S Wouters, Jörg Großhans, Gertrude Bunt, and Jörg Enderlein. Resolution doubling in fluorescence microscopy with confocal spinning-disk image scanning microscopy. *Proceedings of the National Academy of Sciences of the United States of America*, 110(52):21000–5, dec 2013. ISSN 1091-6490. doi: 10.1073/pnas.1315858110. URL [www.pnas.org/lookup/suppl/doi:10.1073/pnas.1315858110/-/DCSupplemental](http://www.pnas.org/lookup/suppl/doi:10.1073/pnas.1315858110/-/DCSupplemental).
- [74] Joseph Huff. The Airyscan detector from ZEISS: confocal imaging with improved signal-to-noise ratio and super-resolution. *Nature Publishing Group*, 12, 2015. doi: 10.1038/nmeth.f.388. URL [http://www.nature.com/app\\_notes/nmeth/2015/150812/pdf/nmeth.f.388.pdf](http://www.nature.com/app_notes/nmeth/2015/150812/pdf/nmeth.f.388.pdf).
- [75] J.E. McGregor, C.a. Mitchell, and N.a. Hartell. Post-processing strategies in image scanning microscopy. *Methods*, (May):1–9, 2015. ISSN 10462023. doi: 10.1016/j.ymeth.2015.05.002. URL <http://linkinghub.elsevier.com/retrieve/pii/S1046202315001930>.
- [76] Cuifang Kuang, Shuai Li, Wei Liu, Xiang Hao, Zhaotai Gu, Yifan Wang, Jianhong Ge, Haifeng Li, and Xu Liu. Breaking the Diffraction Barrier Using Fluorescence Emission Difference Microscopy. *Scientific Reports*, 3:1441, 2013. ISSN 2045-2322. doi: 10.1038/srep01441. URL <http://www.nature.com/doi/10.1038/srep01441>.
- [77] Ye Ma, Cuifang Kuang, Yue Fang, Baoliang Ge, Dian Li, and Xu Liu. Virtual fluorescence emission difference microscopy based on photon reassignment. *Optics Letters*, 40(20):4627, oct 2015. ISSN 0146-9592. doi: 10.1364/OL.40.004627. URL <https://www.osapublishing.org/abstract.cfm?URI=ol-40-20-4627>.
- [78] Cuifang Kuang, Ye Ma, Renjie Zhou, Guoan Zheng, Yue Fang, Yingke Xu, Xu Liu, and Peter T. C. So. Virtual k -Space Modulation Optical Microscopy. *Physical Review Letters*, 117(2):028102, jul 2016. ISSN 0031-9007. doi: 10.1103/PhysRevLett.117.028102. URL <http://link.aps.org/doi/10.1103/PhysRevLett.117.028102>.
- [79] Florian Ströhl and Clemens F Kaminski. A joint Richardson—Lucy deconvolution algorithm for the reconstruction of multifocal structured il-

- lumination microscopy data. *Methods and Applications in Fluorescence*, 3(1):014002, 2015. ISSN 2050-6120. doi: 10.1088/2050-6120/3/1/014002. URL <http://stacks.iop.org/2050-6120/3/i=1/a=014002?key=crossref.2a14d9cec7125134c39268583744009b>.
- [80] Peter W Winter, Andrew G York, Damian Dalle Nogare, Maria Ingaramo, Ryan Christensen, Ajay Chitnis, George H Patterson, and Hari Shroff. Two-photon instant structured illumination microscopy improves the depth penetration of super-resolution imaging in thick scattering samples. *Optica*, 1(3):181, sep 2014. ISSN 2334-2536. doi: 10.1364/OPTICA.1.000181. URL <https://www.osapublishing.org/optica/abstract.cfm?uri=optica-1-3-181>.
- [81] Peter W Winter, Panagiotis Chandris, Robert S Fischer, Yicong Wu, Clare M Waterman, and Hari Shroff. Incoherent structured illumination improves optical sectioning and contrast in multiphoton super-resolution microscopy. *Optics Express*, 23(4):5327, feb 2015. ISSN 1094-4087. doi: 10.1364/OE.23.005327. URL <http://www.opticsexpress.org/abstract.cfm?URI=oe-23-4-5327>.
- [82] K. Thorn. A quick guide to light microscopy in cell biology. *Molecular Biology of the Cell*, 27(2):219–222, 2016. ISSN 1059-1524. doi: 10.1091/mbc.E15-02-0088. URL <http://www.molbiolcell.org/content/27/2/219.full>.
- [83] Winnok H. De Vos, Didier Beghuin, Christian J. Schwarz, David B. Jones, Jack J W A Van Loon, Juergen Bereiter-Hahn, and Ernst H K Stelzer. Invited Review Article: Advanced light microscopy for biological space research. *Review of Scientific Instruments*, 85(10), 2014. ISSN 10897623. doi: 10.1063/1.4898123. URL <http://dx.doi.org/10.1063/1.4898123>.
- [84] I M Bassett. Limits to Concentration by Passive Means. *Physical Review Letters*, 54(18):2014–2017, may 1985. ISSN 0031-9007. doi: 10.1103/PhysRevLett.54.2014. URL <http://link.aps.org/doi/10.1103/PhysRevLett.54.2014>.
- [85] I.M. Bassett. Limit to Concentration by Focusing. *Optica Acta: International Journal of Optics*, 33(3):279–286, mar 1986. ISSN 0030-3909. doi: 10.1080/713821943. URL <http://www.tandfonline.com/doi/abs/10.1080/713821943>.
- [86] Pier A Benedetti, Valtere Evangelista, Dante Guidarini, and Stefano Vestri. Method for the acquisition of images by confocal, 1997. URL <https://patentimages.storage.googleapis.com/pdfs/US6016367.pdf>.
- [87] M A A Neil, R. Juškaitis, and T Wilson. Method of obtaining optical sectioning by using structured light in a conventional microscope. *Optics Letters*, 22(24):1905, dec 1997. ISSN 0146-9592. doi: 10.1364/OL.22.001905. URL <https://www.osapublishing.org/abstract.cfm?URI=ol-22-24-1905>.
- [88] Rainer Heintzmann. *Handbook Of Biological Confocal Microscopy*. Springer US, Boston, MA, 3. edition, 2006. ISBN 978-0-387-25921-5. doi: 10.1007/978-0-387-45524-2. URL <http://link.springer.com/10.1007/978-0-387-45524-2>.
- [89] R. Heintzmann, Q. S. Hanley, D. Arndt-Jovin, and T. M. Jovin. A dual path programmable array microscope (PAM): Simultaneous acquisition of conjugate and non-conjugate images. *Journal of Microscopy*, 204(2):119–135, 2001. ISSN 00222720. doi: 10.1046/j.1365-2818.2001.00945.x.

- 
- [90] Stephan Roth, Colin JR Sheppard, Kai Wicker, and Rainer Heintzmann. Optical photon reassignment microscopy (OPRA). *Optical Nanoscopy*, 2(1):5, 2013. ISSN 2192-2853. doi: 10.1186/2192-2853-2-5. URL <http://www.optnano.com/content/2/1/5>.
- [91] Stephan Roth, Colin J. R. Sheppard, and Rainer Heintzmann. Superconcentration of light: circumventing the classical limit to achievable irradiance. *Optics Letters*, 41(9):2109, may 2016. ISSN 0146-9592. doi: 10.1364/OL.41.002109. URL <https://www.osapublishing.org/abstract.cfm?URI=ol-41-9-2109>.
- [92] Stephan Roth and Rainer Heintzmann. Optical Photon Reassignment with increased axial resolution by structured illumination. *Methods and Applications in Fluorescence*, 2016.
- [93] Colin J R Sheppard, Stephan Roth, Rainer Heintzmann, Castello Marco, Giuseppe Vicidomini, Rui Chen, Xudong Chen, and Alberto Diaspro. Interpretation of the optical transfer function : Significance for image scanning microscopy. *Optics Express*, 2016.